2023

Water-Soluble Palladium, Copper, and Nickel Catalysts and their Formation in Ligand-Free Suzuki-Miyaura Cross-Coupling Reactions

Priya Karna
University of Kentucky, priya.karna@uky.edu
Author ORCID Identifier:
https://orcid.org/0000-0002-6036-8638

Digital Object Identifier: https://doi.org/10.13023/etd.2023.129

Recommended Citation

Karna, Priya, "Water-Soluble Palladium, Copper, and Nickel Catalysts and their Formation in Ligand-Free Suzuki-Miyaura Cross-Coupling Reactions" (2023). *Theses and Dissertations--Chemistry*. 179.
https://uknowledge.uky.edu/chemistry_etds/179

STUDENT AGREEMENT:

I represent that my thesis or dissertation and abstract are my original work. Proper attribution has been given to all outside sources. I understand that I am solely responsible for obtaining any needed copyright permissions. I have obtained needed written permission statement(s) from the owner(s) of each third-party copyrighted matter to be included in my work, allowing electronic distribution (if such use is not permitted by the fair use doctrine) which will be submitted to UKnowledge as Additional File.

I hereby grant to The University of Kentucky and its agents the irrevocable, non-exclusive, and royalty-free license to archive and make accessible my work in whole or in part in all forms of media, now or hereafter known. I agree that the document mentioned above may be made available immediately for worldwide access unless an embargo applies.

I retain all other ownership rights to the copyright of my work. I also retain the right to use in future works (such as articles or books) all or part of my work. I understand that I am free to register the copyright to my work.

REVIEW, APPROVAL AND ACCEPTANCE

The document mentioned above has been reviewed and accepted by the student's advisor, on behalf of the advisory committee, and by the Director of Graduate Studies (DGS), on behalf of the program; we verify that this is the final, approved version of the student's thesis including all changes required by the advisory committee. The undersigned agree to abide by the statements above.

Priya Karna, Student

Dr. Dong-Sheng Yang, Major Professor

Dr. Dong-Sheng Yang, Director of Graduate Studies

WATER-SOLUBLE PALLADIUM, COPPER, AND NICKEL CATALYSTS AND THEIR FORMATION IN LIGAND-FREE SUZUKI-MIYAURA CROSS-COUPLING REACTIONS

DISSERTATION

A dissertation submitted in partial fulfillment of the
requirements for the degree of Doctor of Philosophy in the
College of Arts and Sciences
at the University of Kentucky

By
Priya Karna
Lexington, Kentucky
Director: Dr. Dong-Sheng Yang, Professor of Chemistry
Lexington, Kentucky
2023

https://orcid.org/ 0000-0002-6036-8638

ABSTRACT OF DISSERTATION

WATER-SOLUBLE PALLADIUM, COPPER, AND NICKEL CATALYSTS AND THEIR FORMATION IN LIGAND-FREE SUZUKI-MIYAURA CROSS-COUPLING REACTIONS

Transition-metal catalyzed Suzuki-Miyaura (SM) cross coupling is a powerful synthetic method for constructing carbon-carbon and carbon-heteroatom bonds in designing organic compounds, agrochemicals, pharmaceuticals, and precursors for materials. However, the nature of catalysis and identity of the transition metal catalysts used in these reactions remain under debate or unknown. This dissertation reports the studies of three metals: Pd, Cu, and Ni. Pd-nanocluster catalysts and their formation in ligand-free SM reactions with Pd(II) nitrate as a precatalyst was investigated. The catalysts are water-soluble neutral Pd tetramer and trimer in their singlet electronic states as identified by UV-Vis absorption spectroscopy and are formed by leaching of spherical Pd(0) nanoparticles with an average diameter of about three nanometers. The Pd(0) nanoparticles are produced by reducing Pd(II) nitrate and characterized with transmission electron microscopy (TEM) and Pd-K edge extended x-ray fine structure spectroscopy (EXAFS). The Pd(II) reduction is induced by ethanol and enhanced by potassium hydroxide and monitored with x-ray photoelectron spectroscopy (XPS). For the Cu-catalyzed SM coupling, a water-soluble active molecular catalyst, and its formation in the ligand-free SM cross-coupling reactions with copper iodide as the precatalyst in aqueous solutions has been reported. The SM coupling is also homogeneous in nature, and the molecular catalyst is Cu(OH) in its singlet electronic state also identified by experimental and computational UV-Vis absorption spectroscopy. The Cu(OH) catalyst is generated through the leaching of oval-shaped Cu_2O nanoparticles, which are characterized with X-ray Auger electron spectroscopy, X-ray absorption spectroscopy (XAS), and TEM. The soluble Cu(OH) species is stable for at least four weeks under ambient conditions. Similarly, for Ni-catalyzed ligand-free SM coupling, the active Ni catalyst is reported as Ni(0) species with Ni(0) powder as the precatalyst. The SM coupling is homogeneous in nature. The water-soluble active Ni(0) catalyst is generated through the leaching of Ni(0) nanoparticles, which are characterized with XPS. The water-soluble active Ni(0) catalyst species is stable for at least fourteen weeks under ambient conditions. Thus, this dissertation showcases the nature of catalysis and the identity of catalytically active species in ligand-free SM reactions catalyzed by Pd, Cu, and Ni transition metals.

KEYWORDS: cross-coupling, homogeneous catalysis, palladium nanoclusters, copper (I) hydroxide catalyst, nickel (0) catalyst

Priya Karna

05/01/2023

Date

WATER-SOLUBLE PALLADIUM, COPPER, AND NICKEL CATALYSTS AND THEIR FORMATION IN LIGAND-FREE SUZUKI-MIYAURA CROSS-COUPLING REACTIONS

By
Priya Karna

Dr. Dong-Sheng Yang
Director of Dissertation

Dr. Dong-Sheng Yang
Director of Graduate Studies

05/01/2023
Date

DEDICATION

To my parents, Dr. Sunil Karna and Mrs. Pushpa Karna. Thank you for always instilling in me the importance of higher education. This is to you. This is for you. This is because of you.

ACKNOWLEDGMENTS

First and foremost, I would like to thank my PhD advisor, Dr. Dong-Sheng Yang. I would like to thank him for always pushing me to understand the core fundamentals of the research rather than performing the basic bench work. I used to complain about it in the beginning, but I am glad to have done it all now. Thank you also to Dr. Mark Watson for his support in the GC-MS instrument and his advice on any organic chemistry related questions. I am not exaggerating when I say my graduate schoolwork could not be completed without his help.

I would also like to thank my committee members, Dr. Doo Young Kim, Dr. Kenneth Graham, and Dr. Fuqian Yang for their support and insight during the committee meetings and qualifying exams. I would especially like to thank Dr. Kim and Dr. Yuguang Cai for serving as my CHE 441G TA supervisors. It was their mentorship, recommendation letters, and advice that gave me a nudge to become a responsible educator for my future career.

I would also like to say thank you to my fellow group members who have played a critical role in my journey as a graduate student, for which I would like to especially thank Dr. Rosemary Calabro, Dr. Yuchen Zhang, Micheal Okeke, and Phoenix DuBravac. Similarly, Dr. Kim’s students have also always been helpful to me whether it was to use their lab instrument, discuss my research, or teaching activities. Moreover, I also want to thank the staff at Electron Microscopy Center at the University of Kentucky for their help with TEM, SEM, and XPS. Special thanks to Art Sebesta for his humbleness while assisting me with the repair of any instrument in my lab, and to Jeff Babbitt for the same with the service of specialty-made glassware.

I have to thank the entire staff of the Department of Chemistry for their assistance with any general questions about accommodation, deadlines, and logistics. Special thanks to the Graduate School, Student Government Association, and the Graduate Student Association at the University of Kentucky for giving me so many opportunities for public speaking competitions, monetary awards, honors, and fellowships. These were the kind of opportunities I doubt I would have received had I picked elsewhere to attend graduate school.

Finally, I would like to thank my family and friends who have provided moral support and encouragement throughout this whole process. My parents, Dr. Sunil Karna and Mrs. Pushpa Karna have sacrificed their own happiness by living apart from each other for years just so I could get a chance at proper education. My words of thanks to them will always be incomplete. I would also like to extend my thanks to my sister, Roma Karna who lived with me throughout my graduate school career and provided support when I could not do it on my own. I also want to thank my significant other, Dr. Ankit Pandeya who has provided nothing but support, encouragement, patience, and kindness to me for the past six years. I also want to thank all my friends in Lexington, especially Dr. Nabin Panth and his family.

Graduate school has been quite a whirlwind of uncertainty, but thank you to everyone who made me who I am today. The past six years have been so transformative and impactful both personally and professionally. I would not have traded any of the hardworking days and sleepless nights for the world.

TABLE OF CONTENTS

LIST OF TABLES

LIST OF FIGURES

LIST OF ABBREVIATIONS

SM	Suzuki-Miyaura
GC-MS	Gas Chromatography-Mass Spectrometry
EI	Electron Ionization
NMR	Nuclear Magnetic Resonance
RF	Radiofrequency
UV-Vis	Ultraviolet-Visible
XPS	X-ray Photoelectron Spectroscopy
KE	Kinetic Energy
BE	Binding Energy
XANES	X-ray Absorption Near Edge Structure
EXAFS	Extended X-ray Absorption Fine Structure
TEM	Transmission Electron Microscopy
DFT	Density Function Theory
AUG-CC-pVTZ	Augmented - Correlation Consistent - Polarization Valence-only Triple-Zeta

CHAPTER 1. INTRODUCTION

1.1 Carbon-Carbon Cross-Coupling Reactions

Among organic chemistry reactions, cross-coupling reactions are one type of the most important and widely used reactions for synthesizing natural, non-natural, and other bioactive compounds.[1-14] Their importance due to versatile applications, such as to synthesize nervous system agents, cancer drugs, and other natural products have been well documented in the literature.[15-21] The foundation of these kinds of reactions can be traced back to the 1940's, and several scientists have been fortunate enough to have their names associated with the reactions, such as R. F. Heck, A. Suzuki, S. L. Buchwald, J. F. Hartwig, and E. I. Negishi.[1, 22-23] Eventually, the Nobel Prize in Chemistry in 2010 was awarded to Heck[24], Suzuki[25], and Negishi[26] for their exceptional work in carbon-carbon cross-coupling reactions, and the award indicated the essence of such kinds of reactions.[1, 22]

Cross-coupling involves the reaction between an electrophile and an organometallic nucleophile catalyzed by a metal catalyst in a basic environment (Figure 1.1).[23, 27-30] Such reaction yields a hydrocarbon compound by the formation of a new carbon-carbon or carbon-heteroatom bond that joins the two organic fragments.[23, 31] The reaction is named after the type of nucleophile used. For example, an organomagnesium nucleophile is called a Kumada[32] reaction, organozinc nucleophile is called a Negishi[26] reaction, and organotin nucleophile is called a Stille[33] reaction.

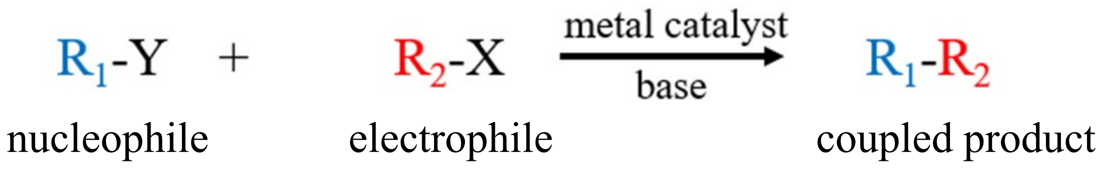

Figure 1.1. Generic cross-coupling reaction.

1.2 Suzuki-Miyaura (SM) Coupling Reactions

One type of coupling reactions that uses an organoborane nucleophile is called the SM coupling. [23, 25] The SM coupling involves the reaction between an organic halide and an organic boron compound catalyzed by a metal catalyst in a basic solution.[25] The SM coupling reactions have been used widely in the fields of pharmacy, medicine, and organic syntheses, such as in the production of biphenyl discussed in this dissertation and the production of losartan, a drug used to treat blood pressure.[23, 34] Moreover, such reactions are also famous for their inclination to the production of planar structures.[23, 35-36]

A typical Suzuki-coupling reaction employs phenylboronic acid and an aryl halide, such as chlorobenzene, bromobenzene, and iodobenzene with a base, a solvent, and a Pd catalyst. Phenylboronic acid is used because it is mild, non-toxic, thermally stable, and inert to water and air.[25] The purpose of the base is to convert the boronic acid into the borate anion in the transmetalation step of the reaction mechanism.[37] Similarly, the solvent also serves many purposes. The solvent influences the reaction equilibrium, selectivity, product isolation, the lifetime of the catalyst, the activity of the acid and base, and regulating the rate of the reaction.[38] The solvent dissolves all the precursors, making the reaction proceed smoothly. No solvent means doing the reaction in a solid state, which is not easy because of the small surface area of the reactants.

The first metal catalysts used for the S-M coupling reactions were first-row transition metal chloride salts, such as $FeCl_3$, $CoCl_2$, $NiCl_2$, and $CuCl_2$.[23] Even though earlier developments were made using these metals, further studies of Pd led to the observance that Pd is the best catalyst for cross-coupling reactions due to its operation in mild experimental conditions, compatibility with multiple functional groups, higher catalytic efficiency even in trace amounts, higher stability, high activity, and reusability.[1, 15, 23, 39-41] Due to such versatility, applications of Pd as a catalyst can be found in organic synthesis of different cross-coupling products (such as to form a C-N bond or to cause a

C-H bond activation) and in autocatalysts, hydrogen storage, biomedical research, environmental improvement, polymers, and inorganic materials.[40-46] Furthermore, Pd nanoparticles formed through the reduction of Pd salts can be fine-tuned in a way that can adsorb a huge amount of ligands because of their large surface areas and multiple low coordination sites.[46-47] Another way Pd has been exploited in catalysis is through a support system, such as a graphene oxide, CeO_2, or TiO_2.[45, 48-49] In the SM coupling reaction, Pd (0) couples with aryl halide to form aryl halide – Pd (II) complex, which yields the desired product after multiple steps as described later in this dissertation in the mechanism of the reaction.[25] It is because of the tendency of Pd to undergo the reduction from Pd(II) complexes to Pd(0), the "two electron"-based reduction, that makes Pd a useful component in activating many precatalysts and C-H activation processes.[44] Thus, there is no surprise as to why Pd is considered "the king of transition-metal catalysts."[44, 50]

However, growing concerns about its long-term sustainability arise due to the low nature abundance, prohibitive costs, and high toxicity of Pd metal; other metals have reemerged an alternative for metal-catalyzed cross-coupling reactions.[51-55] There has been increasing interest in the study of using copper catalysts to form carbon–carbon and carbon– heteroatom bonds in the recent years.[51, 56] Similarly, Ni has also been increasingly used in many organic reactions because of its ability to create products and intermediates with diverse functionalities.[55] In addition, as a transition metal, nickel can exhibit many redox states, such as Ni(0)/Ni(II) and Ni(I)/Ni(III), which is in contrast to Pd, which typically exists in the Pd(0)/Pd(II) redox state even though Pd(III) and Pd(IV) have been used in C–H functionalization.[55] As such, this dissertation presents the study of three of such metals: Pd, Cu, and Ni.

1.3 Reaction Mechanism of the Pd-catalyzed homogeneous SM reaction

The homogeneous mechanism of the SM coupling reaction occurs in three steps: oxidative addition, transmetalation, and reductive elimination (Figure 1.2).[57-63]

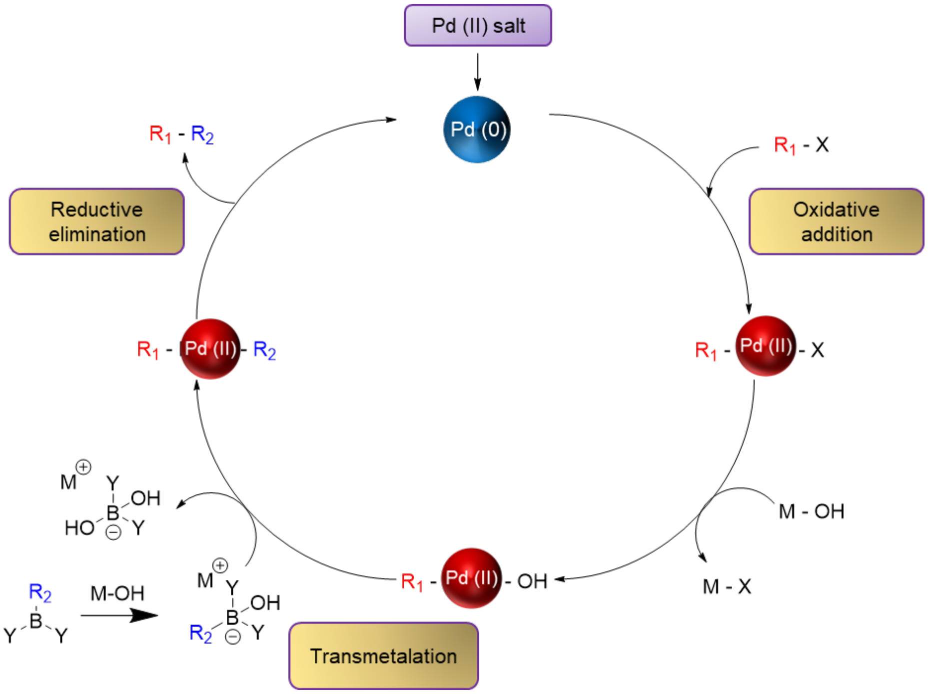

Figure 1.2. Overall mechanism of the Suzuki-Miyaura coupling reaction.

1.3.1 Oxidative addition

Oxidative addition is a class of organic reactions where the oxidation state and the coordination number of the metal center increases. It is the rate-determining step in the catalytic cycle because it is difficult to break the bond between the benzene ring and the halide in an aryl halide. Pd(0) reacts with the aryl halide to form a stable Pd(II) complex. Pd(II) induces its insertion between the benzene ring and the halide. The relative reactivity increases down the group, i.e., Cl < Br < I. This is because the C-X (X = Cl, Br, I) bond strength decreases from Cl to Br to I, and the weaker C-X bond should facilitate the Pd insertion into the C-X bond. Due to the larger size of iodine, it experiences a greater shielding effect and has a lower effective nuclear charge. As a result, electrons are pulled away from the iodine atom relatively easier than from bromine and chlorine. This makes the bond between benzene and iodine easier to break in iodobenzene. Hence, Pd (0) couples with the aryl halide to form the organopalladium complex by breaking the carbon-halide bond, and Pd(0) is oxidized to Pd(II).[57, 64-69]

1.3.2 Transmetalation

Transmetalation is a class of organic reactions where ligands transfer from one species to the other. This step is not yet well understood. Essentially, the Pd(II) complex formed during the oxidative addition reacts with a base to yield an intermediate, which is a Pd(II) – OH complex. Then, the OH group from KOH attacks the boron center in the organoborane compound in a step called nucleophilic addition. Eventually, Pd(II) is inserted between the two R_1 and R_2 groups. A base is necessary in this step. The purpose of the base is to convert the boronic acid into the borate anion in the transmetalation step of the reaction mechanism.[37] The base replaces the halide with the OH group to form R_2-Pd(II)-X.[58, 70-73]

1.3.3 Reductive elimination

Reductive elimination is a class of organic reaction where the oxidation state of the Pd center decreases from +2 to 0, while a new C-C bond is formed. This is the final step of the reaction mechanism where the Pd(0) catalyst is regenerated.[57, 59, 74-75]

1.4 Statement of Purpose

Even though the evidence of such reactions has been presented in the literature since the 1940s with emphasis on synthetic chemistry by creating novel catalysts and ligands to form new products in high yields, the identity of the active catalyst is under debate or remains unknown. Identifying the fundamental nature of catalysis and the catalytic species paves the path towards new designs of catalysts to synthesize crucial products. This dissertation presents the study of chemical identities of active catalysts and their formation in the homogeneous SM coupling reactions using ligand-free Pd, Cu, and Ni precatalysts.

CHAPTER 2. INSTRUMENTATION AND THEIR PRINCIPLES

2.1 Gas Chromatography – Mass Spectrometry (GC-MS)

GC-MS is an analytical technique used to identify components in a chemical mixture. It consists of two parts: GC and MS. The sample is injected into the GC inlet and vaporized. The vaporized sample is transferred to the chromatographic column by mixing with a carrier gas, such as helium (mobile phase). The components of the sample mixture are separated by their relative interaction with the coating of the column, such as silicone (stationary phase) and the carrier gas. The column passes through a heated transfer line where the neutral sample molecules eluting from the column enter the MS. These neutral sample molecules are then converted to charged particles by the ion source using a technique called electron ionization (EI). In EI-MS, a beam of high-energy electrons (70 eV) is emitted from a filament. These high-energy electrons strike the stream of neutral sample molecules coming in from the column in GC. The electron beam knocks an electron out of the neutral molecule to create smaller ions. The mass analyzer then separates the ions based on their masses that are based on their m/z ratios, which are characteristic of the molecular components of the sample. The chromatogram and mass peaks can be seen on the computer for each data point.[76-77] A cartoon depicting the GC-MS principle is presented in Figure 2.1.

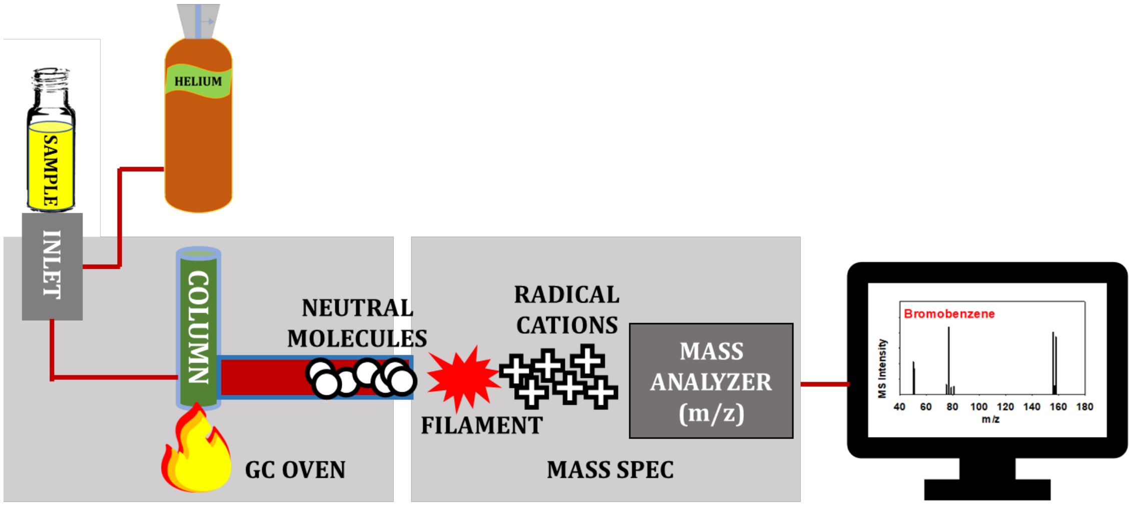

Figure 2.1. A diagram of a GC-MS instrument.

2.2 Nuclear Magnetic Resonance (NMR)

NMR is a spectroscopic method used to decipher molecular structure and purity of a compound. NMR is based on the principle that many atomic nuclei have spin. These are the nuclei that have either an odd number of protons or an odd number of neutrons, such as ${}^{1}_{1}H$, ${}^{13}_{6}C$, ${}^{14}_{7}N$, and ${}^{19}_{9}F$. Let us consider a hydrogen nucleus with one proton, which has a positive charge. If we place a sample of protons in an external magnetic field (B_o), the magnetic field of the protons can either align with the B_o or align against it. A hydrogen nucleus can either have a +1/2 or a -1/2 spin. The spin state of the nucleus that is aligned with the direction of B_o has a lower energy, whereas the spin state that is opposite to the B_o has a higher energy. The energy difference between these two spin states is ΔE, which is dependent on the strength of B_o. The higher the B_o, the greater the ΔE. For this hydrogen nucleus, to switch from the spin state of lower energy to higher energy, radiofrequency (RF) energy needs to be applied. If the nucleus again switches from the higher to the lower energy, it can emit RF. Hence, when the nucleus is constantly switching back and forth between the two states, it is called to be in “resonance.” Most of the protons will be at lower energy than higher energy. This excess of nuclei in the lower-energy spin state is what allows for the resonance. The higher the operating frequency of the NMR instrument, the better the resonance signals because more nuclei can undergo transition.[77] A cartoon depicting the NMR principle is presented in Figure 2.2.

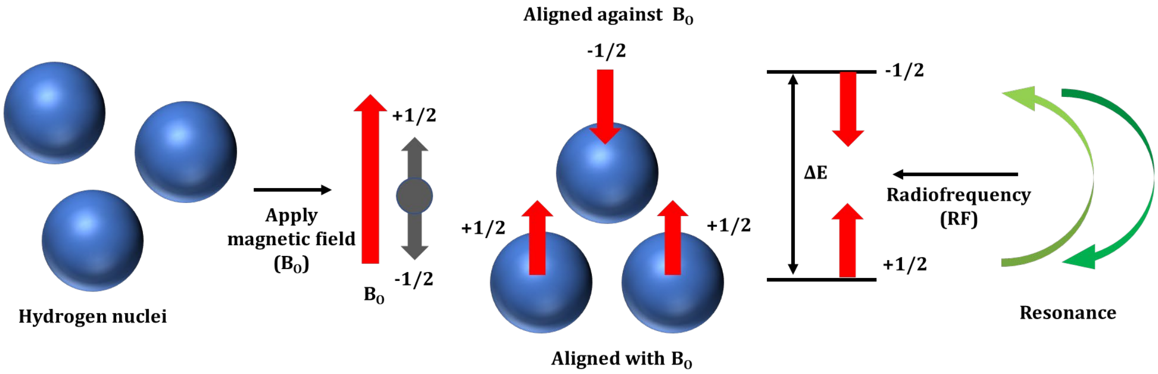

Figure 2.2. Basic principle of NMR.

2.2.1 Chemical shift

It is important to note that the protons in a molecule are shielded by the electrons that surround them. The exact resonance frequency of any proton is very difficult to measure. Hence, a reference compound called tetramethylsilane (TMS) (Figure 2.3) is added in the sample to be measured, and the resonance frequency of each proton in the sample is measured relative to the resonance frequency of the protons of TMS in parts per million (ppm). TMS was chosen because the protons of its methyl groups are well shielded. NMR spectrum goes from 0 to 14 ppm on the horizontal x-axis with 0 being on the right and 14 on the left. TMS is at 0 ppm. If the electron density around a nucleus decreases, the nucleus feels more external magnetic field, and is said to be deshielded. Because such proton experiences higher external magnetic field, it needs a higher frequency to achieve resonance, and therefore, the chemical shift shifts downfield (higher ppm). On the other hand, if the electron density around a nucleus increases, the nucleus feels less external magnetic field, and is said to be upshielded. Such proton does not experience much external magnetic field, and does not need a higher frequency to achieve resonance, and therefore, the chemical shift remains upfield (lower ppm). Peaks closer to 0.00 ppm (to the right of the NMR spectrum) are said to be upfield with highly-shielded protons, whereas the peaks farther from 0.00 ppm (to the left to the NMR spectrum) are said to be downfield with deshielded protons.[77]

.

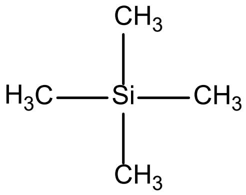

Figure 2.3. Tetramethylsilane (TMS) is the reference compound for NMR.

2.2.2 Chemical equivalence

If a molecule has protons that are equivalent by symmetry considerations, or in chemically identical environments, these protons are said to be chemically equivalent**.** They often exhibit the same chemical shift.[77] Figure 2.4 shows some examples of the chemically equivalent protons in a molecule; each chemically equivalent proton is depicted with the same color.

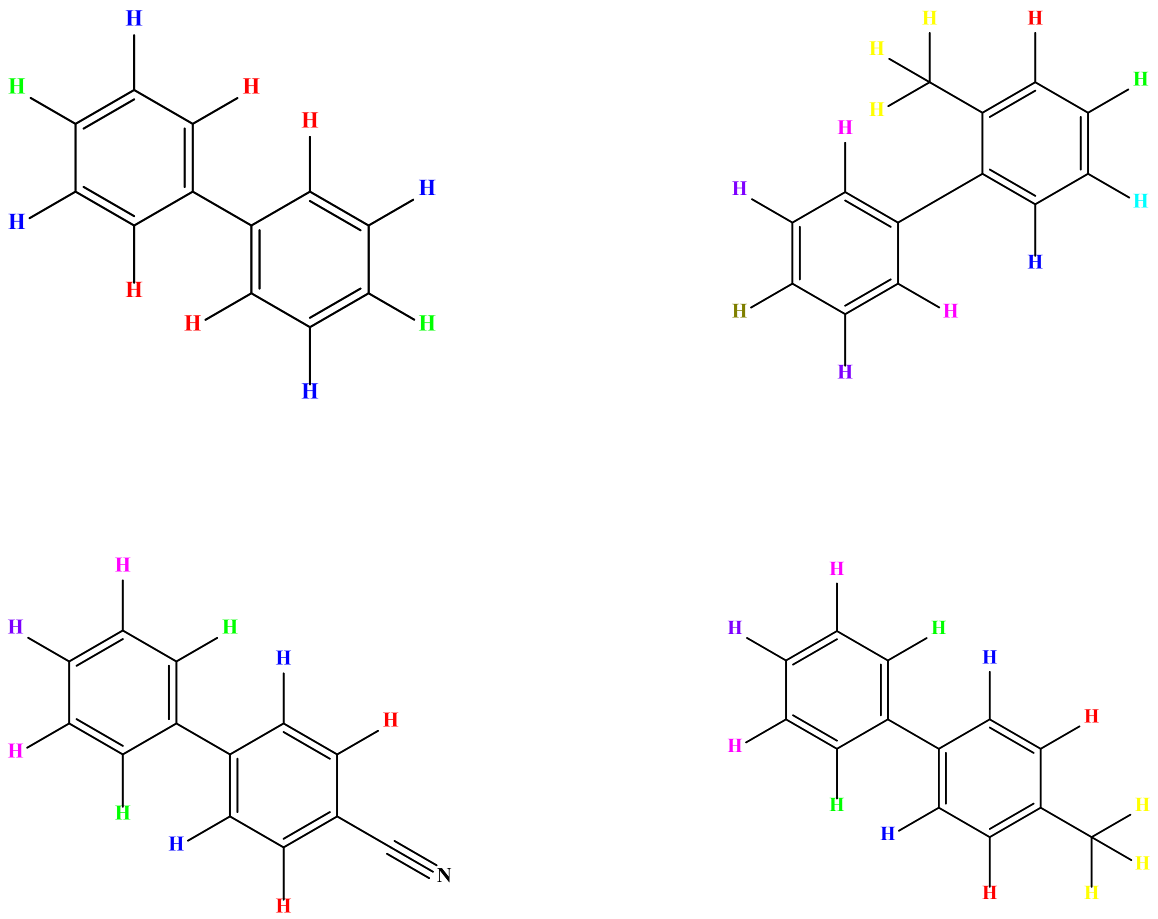

Figure 2.4. Chemically equivalent protons in different molecules with each chemically equivalent proton is depicted with the same color.

2.2.3 Spin-spin splitting (n+1) rule

NMR peaks of the protons are split by their neighboring protons attached to the adjacent carbon atoms by the n+1 rule, where n is the number of protons on the adjacent carbon. Spin–spin splitting arises because hydrogens on a particular carbon atom can sense the spin direction of the hydrogens on the adjacent carbon. The chemical shift of a particular proton is influenced by the direction of the spin in the protons attached to the adjacent carbon.[77]

2.3 X-ray photoelectron spectroscopy (XPS)

XPS is a surface analysis technique used to identify elemental composition and chemical states on a material's surface. XPS is based on the photoelectric effect, where electrons can be emitted from a metal by an incident light (Figure 2.5). X-rays (hν) are shot onto a sample, and if this energy of the x-ray source is enough to overcome the binding energy of the electron in the sample (BE), the electron is ejected from the sample with a certain kinetic energy (KE). Hence, KE = hν – BE.[78-79]

.

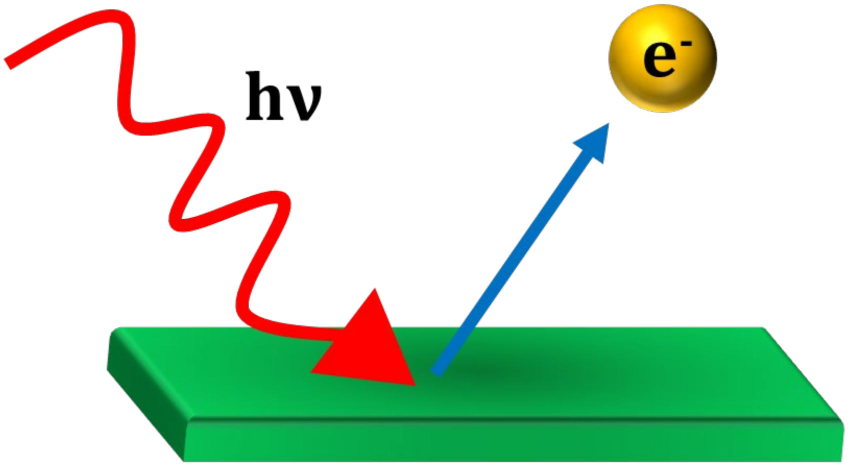

Figure 2.5. The photoelectric effect.

2.3.1 Spin-orbit splitting

The common nomenclature used to describe XPS principles are n, l, s, and j, and m_j, where n is the principal quantum number, l is the orbital quantum number, s is the spin quantum number ($s = ½$), j is the total angular momentum quantum number of the electron ($j = l + s,\ l+s-1,\ \ldots|l-s|$). and m_j is the magnetic quantum number (m_j varies from $+j$ to $-j$ in integer steps excluding zero). The orbital letters associated with l are s, p, d, and f, where s corresponds to $l = 0$, p to $l = 1$, d to $l = 2$, and f to $l = 3$. For the orbital levels p, d, and f with two states of the same energy, a magnetic interaction between the spin of the electron (up or down) and its orbital angular momentum may lead to a splitting of the degenerate state into two components. This is called spin–orbit coupling.[79] Let us consider some examples of spin-orbit coupling of the three elements reported in this dissertation as the choice of metal catalysts.

2.3.1.1 Spin–orbit coupling in the Pd 3d orbitals

If we consider the 3d orbitals of Pd, $n = 3$, $l = 2$ for the d orbitals, $s = + 1/2$, and $j = 5/2$ or $3/2$ (since $j = l + s, l+s-1, \ldots |l-s|$), $m_{5/2} = 5/2, 3/2, ½, -1/2, -3/2, -5/2$, and $m_{3/2} = 3/2, ½, -1/2, -3/2$. The ratio of their respective degeneracies, $2j + 1$, determines the intensities of the components. In other words, for $j = 5/2$, $2j + 1 = 6$; hence, there are six values for $m_{5/2}$. Similarly, for $j = 3/2$, $2j + 1 = 4$; hence, there are four values for $m_{3/2}$. Their ratio of 6:4 or 3:2 determines the relative intensity of the area under the curve of the two spin-orbit coupling peaks of $j = 5/2$ and $j = 3/2$, respectively. Further, if the orbitals are more than half-filled as in Pd $3d^{10}$ orbital, higher j value ($j = 5/2$ in this case) is at the lower energy than $j = 3/2$. On the other hand, if the orbitals are less than half-filled, higher j value is at the higher energy.

2.3.1.2 Spin–orbit coupling in the Cu 2p orbitals

If we consider the 2p orbitals of Cu, $n = 2$, $l = 1$ for the p orbital, $s = +1/2$, $j = 3/2$ or ½ (since $j = l + s, l+s-1, \ldots |l-s|$), $m_{3/2} = 3/2, ½, -1/2, -3/2$, and $m_{1/2} = ½, -1/2$. For $j = 3/2$, $2j + 1 = 4$; hence, there are four values for $m_{3/2}$. Similarly, for $j = 1/2$, $2j + 1 = 2$; hence, there are two values for $m_{1/2}$.Their ratio of 4:2 or 2:1 determines the relative intensity of the area under the curve of the two spin-orbit coupling peaks of $j = 3/2$ and $j = 1/2$, respectively. Further, since the 2p orbitals are more than half-filled as in Cu $2p^6$, higher j value ($j = 3/2$) is at the lower energy than $j = 1/2$.

2.3.1.3 Spin–orbit coupling in the Ni 2p orbitals

The spin-orbit coupling of the Ni 2p orbitals follow the similar rule as the Cu 2p orbitals. If we consider the 2p orbitals of Ni, $n = 2$, $l = 1$ for the p orbital, $s = +1/2$, $j = 3/2$ or ½ (since $j = l + s, l+s-1, \ldots|l-s|$), $m_{3/2} = 3/2, ½, -1/2, -3/2$, and $m_{1/2} = ½, -1/2$. For $j = 3/2$, $2j + 1 = 4$; hence, there are four values for $m_{3/2}$. Similarly, for $j = 1/2$, $2j + 1 = 2$; hence, there are two values for $m_{1/2}$.Their ratio of 4:2 or 2:1 determines the relative intensity of the area under the curve of the two spin-orbit coupling peaks of $j = 3/2$ and $j = 1/2$, respectively. Further, since the 2p orbitals are more than half-filled as in Ni $2p^6$, higher j value ($j = 3/2$) is at the lower energy than $j = 1/2$.

2.3.2 Satellite peaks

The outgoing electron interacts with a valence electron and excites it to a higher energy level. The kinetic energy of the emitted photoelectron is reduced, and a satellite structure appears at a higher binding energy point than the core level position.[79]

2.4 X-ray absorption spectroscopy (XAS)

XAS measurements and analysis were performed at the Argonne National Lab.

XAS is a technique that is used to find local coordination number in a sample. The absorption edge energy corresponds to the energy required to eject one of the core electrons to a higher energy state. The two main regions in the XAS spectrum are called X-ray Absorption Near Edge Structure (XANES) and Extended X-ray Absorption Fine Structure (EXAFS). When the energy of the incident photon reaches the binding energy of a core-electron, the probability of an excitation increases sharply. This is referred to as an edge. The XANES region is the structure that rises up to around 50 eV above the edge. Similarly, the fine structure that extends from about 50 eV above the edge for several hundred eV is the EXAFS region. XANES is used to determine the oxidation state and coordination chemistry of the absorbing atom, while the EXAFS is used to determine the distances, coordination number, and species of the neighbors of the absorbing atom.[80] A typical X-ray absorption spectrum with these regions is shown in Figure 2.6.

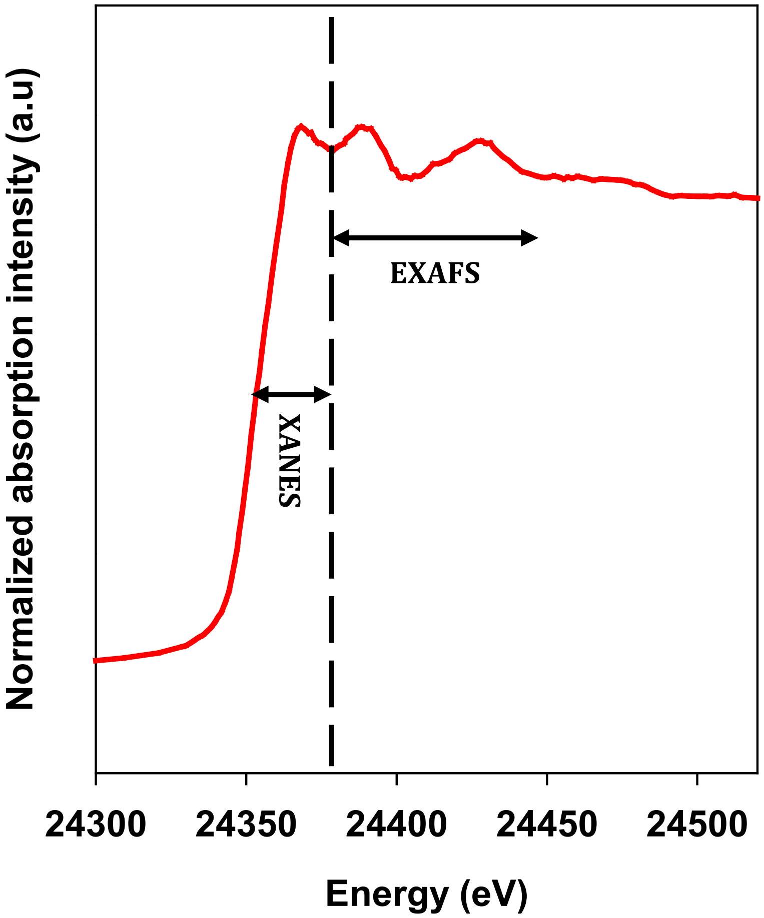

Figure 2.6. A typical X-ray absorption spectrum showing the XANES and EXAFS regions.

2.5 Ultraviolet – Visible Spectroscopy (UV-Vis)

UV-Vis spectroscopy is an analytical technique in which light of the ultraviolet and visible region (200-800 nm) is absorbed by the molecule, which results in the excitation of the electrons from the ground state to a higher energy state. Electrons in different bonding environments in a sample require different amounts of energy to promote them to a higher energy state. Shorter wavelengths of light carry more energy and longer wavelengths carry less energy. The more easily excited the electrons, the longer the wavelength of light it can absorb. The absorption of ultraviolet light by a molecule produces a distinct spectrum which aids in the identification of the compound.

2.6 Transmission Electron Microscopy (TEM)

TEM is an electron microscopy technique that studies the interactions between the electrons and the atoms to decipher the morphology and elemental analysis of a sample. TEM works by using a heated tungsten filament in the electron gun to produce an electron beam in a vacuum chamber. These electrons are focused on the sample by the condenser lenses. The vacuum chamber allows electrons to produce a clear image without colliding with any air molecules which may deflect them. When the electron beam strikes the sample, some of the electrons are transmitted depending upon the thickness. The transmitted electrons are focused by the objective lenses forming an image. The image is, then, passed down the column through the intermediate and projector lenses, and finally on the fluorescent screen creating a large clear image. The denser the sample, the darker the region of a TEM image because fewer electrons are transmitted and more electrons are scattered (absorbed), and fewer electrons reach the screen for visualization. On the other hand, thinner and more transparent samples appear brighter because more electrons are transmitted and fewer electrons are scattered (absorbed), and more electrons reach the screen for visualization.[81] A cartoon of the TEM instrumentation is shown in Figure 2.7.

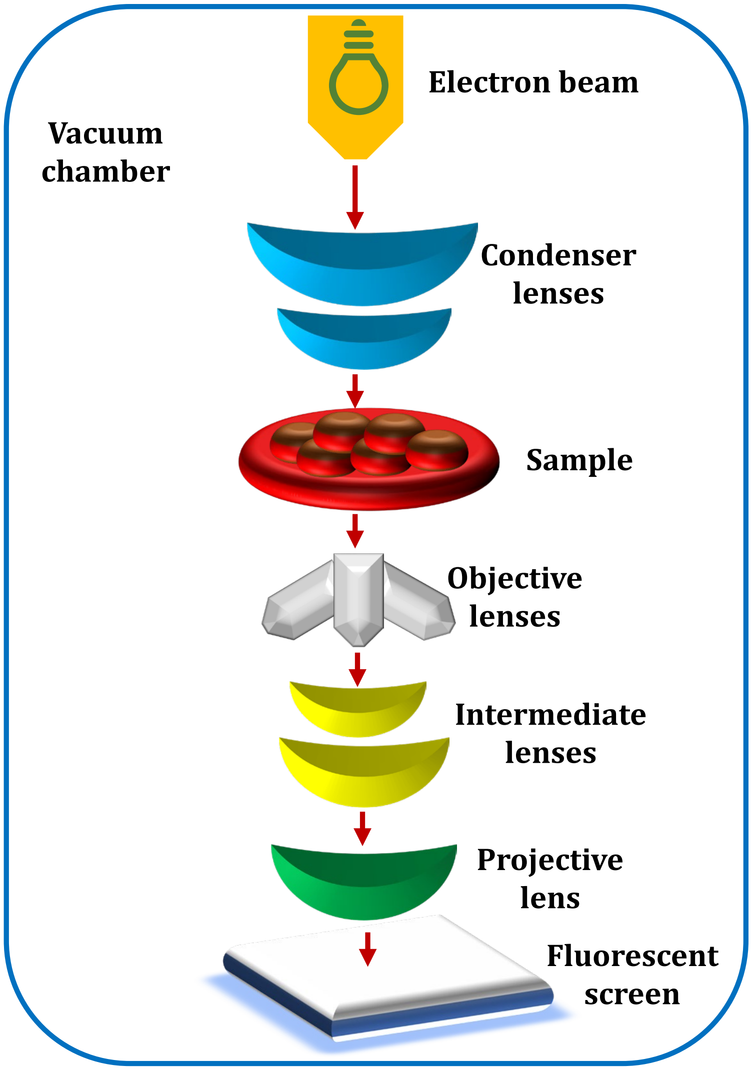

Figure 2.7. A cartoon depicting the TEM instrumentation basic working principle.

2.7 Computational Methods

Quantum computational methods provide information that is complementary to experimental data regarding the structures, properties, and reactions of substances. The calculations presented in this dissertation were performed using density functional theory (DFT). DFT works on the principle that the ground state electronic energy is determined by the electron density, and by not focusing on individual electrons. This theory defines a “function” as an algorithm for producing a number from a set of variables. Here, the electron density is a “function” of a set of variables. A “functional” is an algorithm for generating a number from a function, which in turn depends on variables. Here, the energy, which depends on the electron density, is a “functional.”[82] In this dissertation, the DFT method used is called B3LYP, which is named so due its developers, Becke, Lee, Yang, and Parr. It uses Becke 3 parameter functional (B3) methods with the correlation functional of Lee, Yang, and Parr.[83-84] Quantum chemical calculations use certain mathematical formula called basis sets. A basis set is a set of functions, which are formed by the linear combinations of atomic orbitals to create molecular orbitals. For the work presented in this dissertation, the basis set of aug-cc-pVTZ is used. The prefix “aug” stands for “augmented,” and it denotes diffuse functions. These are very shallow Gaussian basis functions, which more accurately represent the "tail" portion of the atomic orbitals, which are distant from the atomic nuclei. Diffuse functions are known to be critical in describing the electron distribution of anions, weak interactions, such as hydrogen bonds, and evaluating activation barriers. The term “cc” means “correlation consistent,” “p” indicates polarization functions, “V” indicates they are valence-only basis sets, and “TZ” stands for Triple-zeta. These basis sets have had redundant functions removed to increase computational efficiency.[85]

CHAPTER 3. WATER-SOLUBLE PALLADIUM NANOCLUSTERS AS CATALYSTS IN LIGAND-FREE SUZUKI-MIYAURA CROSS-COUPLING REACTIONS

This chapter is reproduced with permission from "Water-Soluble Palladium Nanoclusters as Catalysts in Ligand-Free Suzuki–Miyaura Cross-Coupling Reactions" *ACS Appl. Nano Mater.* 2022, 5, 3, 3188–3193. https://doi.org/10.1021/acsanm.2c00389

3.1 Introduction

Transition-metal catalyzed cross coupling is a powerful synthetic method for constructing carbon-carbon and carbon-heteroatom bonds in pharmaceuticals, agrichemicals, and precursors for materials.[1, 23, 86-89] Among various cross-coupling schemes, the Suzuki-Miyaura (SM) reaction uses an organoboron nucleophile and an organic halide electrophile as coupling partners and has the most important technical significance due to the relatively mild reaction conditions and the non-toxic, air/moisture tolerant nature, and wide availability of organoboron derivatives.[1, 57, 90] Although ligand-stabilized, unsaturated Pd(0) complexes are generally known as catalysts in solution-phase cross-coupling reactions, new catalytical species have recently been proposed for both homo- and hetero-geneous reactions.[44, 91-94]

For reactions employing Pd complexes that are stabilized with phosphine ligands, unusual Pd(I) and Pd_3(IV) catalysts were reported recently.[44, 91-92] The Pd(I) catalyst was a binuclear complex and formed by the reduction of a Pd(II) precursor in the presence of a phosphine ligand.[44] The formation of the Pd(I) species depended on the nature of the Pd (II) precursor, the choice of the phosphine ligand, the stoichiometry of the Pd to phosphine, and the order of the addition of the reagents. The Pd_3(IV) catalyst with each Pd atom in an oxidation state of +4/3 was formed by the reaction of a Pd(II) salt and a phosphine in the presence of $NaBH_4$.[91] In the SM coupling between various aryl bromides and phenylboronic acid, the Pd_3(IV) catalyst reacted first with phenylboronic acid to generate an intermediate, which is in contrast to the well-established SM coupling mechanism where an oxidative addition is the first step.[91] As to the transmetallation step, tri- and tetra-coordinate boron complexes were identified as containing Pd-O-B linkages.[95]

For ligand-free cross-coupling reactions with Pd-containing solids, the physical state and chemical identity of catalytical species remains under debate.[1,39-40, 42, 47, 93-94, 96-98] Several studies proposed that Pd catalysts were in solid states,[47, 93-94, 99] while others argued that they were molecular species produced by leaching of solid precatalysts in solutions.[39-40, 42, 96-98] In supporting the argument of heterogeneous catalysis, a stable single-atom Pd catalyst anchored on exfoliated graphitic carbon nitride was reported through scanning transmission electron spectroscopy;[93] a direct contact between aryl bromides with the metal surface of Au-Pd superstructures was proposed through surface-enhanced Raman spectroscopic measurements;[94] and the SM coupling reactivity was observed to correlate with surface changes on Pd nanoparticles supported on carbon nanotubes.[47] On the other hand, there is emerging evidence toward a scenario that Pd-containing solids only serve as a reservoir of soluble catalytically active Pd species.[96] However, the chemical identity of the soluble Pd species is being actively debated. Several studies proposed Pd oxides as active species leached out from Pd supported on metal oxides, nanotubes, wire, foil, or sponge,[40, 96-97] while others suggested small Pd clusters formed in N-methyl pyrrolidone as active species,[42] or the identity of the molecular species in solutions was unknown.[39, 98]

In this work, we have identified water-soluble neutral Pd_4 and Pd_3 nanoclusters as catalysts in the SM coupling reaction between bromobenzene and phenylboronic acid with Pd(II) nitrate as a precatalyst and in the presence of ethanol and potassium hydroxide (Figure 3.1). The $Pd_{4,3}$ nanoclusters are formed by leaching of spherical Pd(0) nanoparticles in the reaction medium. The Pd(0) nanoparticles are produced by the reduction of Pd(II) nitrate, and the reduction is induced by the alcohol and enhanced by the base.

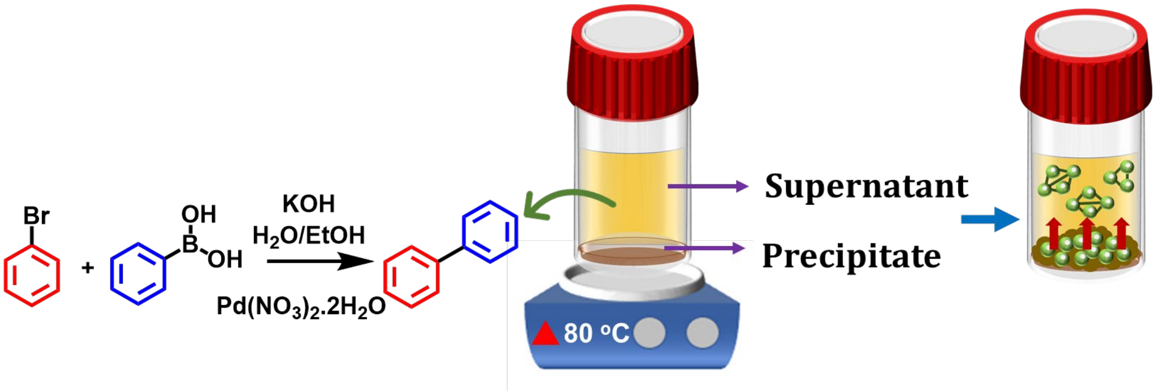

Figure 3.1. Schematic representation of the water-soluble $Pd_{3,4}$ nanoclusters formed by leaching of Pd (0) nanoparticles catalyze the SM coupling between C_6H_5Br and $C_6H_5B(OH)_2$ with $Pd(NO_3)_2.2H_2O$ as a precatalyst.

3.2 Experimental

3.2.1 Materials

Palladium dinitrate dihydrate was purchased from Strem Chemicals, bromobenzene (> 99% GC) from Fisher Scientific, biphenyl (99%) and 2-phenyltoluene (97%) from Aldrich, 2-bromotoluene (99%) from Thermo Scientific, and phenylboronic acid (99% HPLC) from Chem Impex International, while potassium hydroxide (85.0%) and anhydrous ethanol were purchased from VWR. All the chemicals were used without further purification. Millipore deionized water was used in all the experiments.

3.2.2 Suzuki – Miyaura coupling reactions

The procedure for the Suzuki-Miyaura coupling (S-M) reaction was adapted from the literature.[100]

3.2.2.1 Catalyst preparation without substrates and SM reactions

In a round bottom flask, the catalyst was prepared using 10 mg (0.0375 mmol) of $Pd(NO_3)_2.2H_2O$ and 53.8 mg (0.96 mmol) of KOH dispersed in a solution of 4 mL H_2O:EtOH (1:1). The flask was kept in an oil bath at 80 °C for 60 minutes under constant magnetic stirring. The reaction was done in air. After the reaction, the mixture was separated into a supernatant and a precipitate by centrifugation at 5000 rpm for 5 minutes, and the supernatant and precipitate were then placed in two separate vials for future reactions.

Reactions with the precipitate: The precipitate was cleaned with 3 mL of ethyl acetate by centrifuging at 5000 rpm for 5 minutes twice and then dried under nitrogen flow for half an hour. The nitrogen-dried precipitate was used as a catalyst for the first reaction at 80 °C for 1 hour and with 33.6 μL (0.32 mmol) of bromobenzene, 46.3 mg (0.38 mmol) of phenylboronic acid, and 53.8 mg (0.96 mmol) of KOH in a solution of 4 mL H_2O:EtOH (1:1). The reaction was done in air. After the reaction, the reaction mixture was again separated into a supernatant and a precipitate by centrifugation at 5000 rpm for 5 minutes. Because any coupling product would be in the solution phase, the solution was injected into the GC-MS for product. A flowchart of the reaction experiment is shown in Figure S3.6.

Reactions with the supernatant: The supernatant was extracted with ethyl acetate and water three times resulting in clearly-separated organic and inorganic phases. The organic phase was discarded, whereas the inorganic phase was used for further reactions and characterizations. The inorganic layer was then added with 2 mL of ethanol, 33.6 μL (0.32 mmol) of bromobenzene, 46.3 mg (0.38 mmol) of phenylboronic acid, and 53.8 mg (0.96 mmol) of KOH to perform the reaction at 80 °C for 2 hours. After the reaction, the reaction product, biphenyl, was measured with the GC-MS analysis. The reaction mixture was also extracted three times with ethyl acetate and water to collect the organic and inorganic layers. The resultant organic layer was treated with anhydrous sodium sulfate (Na_2SO_4) to remove any remining water, and the Na_2SO_4 was then removed from the organic layer through filtration. Biphenyl crystals were obtained through rotary vaporization of the filtrate and dried with nitrogen. The inorganic layer was again added with fresh ethanol, bromobenzene, phenylboronic acid, and KOH to perform the reaction at 80 °C for 1 hour. The procedure was repeated for additional runs until no product was detected.

3.2.2.2 Catalyst preparation with substrates and SM reactions

In a round bottom flask, 10 mg (0.0375 mmol) of palladium dinitrate dihydrate, 33.6 μL (0.32 mmol) of bromobenzene, 46.3 mg (0.38 mmol) of phenylboronic acid, and 53.8 mg (0.96 mmol) of KOH were dispersed in a solution of 4 mL H_2O:EtOH (1:1). The flask was kept in an oil bath at 80 °C for 30 minutes under constant magnetic stirring. The reaction was done in air. After the reaction, the reaction mixture was separated into a supernatant and a precipitate by centrifugation at 5000 rpm for 5 minutes, and the supernatant and precipitate were then placed in two vials for future reactions. The coupling product, biphenyl, in the supernatant was measured through GC-MS analysis. To purify the product, the supernatant was extracted with ethyl acetate and water three times. The resultant organic layer was treated with anhydrous Na_2SO_4 to remove any remining water, and the sodium sulfate was then removed from the organic layer through filtration. Biphenyl crystals were obtained through rotary vaporization of the filtrate and dried with nitrogen.

Reactions with the precipitate: The precipitate was cleaned with 3 mL of ethyl acetate by centrifuging at 5000 rpm for 5 minutes twice and then dried under nitrogen flow for half an hour. The nitrogen-dried precipitate was used as a catalyst for the next run also at 80 ^{o}C for 30 min and with the same amount of fresh bromobenzene, phenylboronic acid, KOH, and ethanol. The procedure was repeated for additional runs until no product was detected. A flowchart of the reaction experiment is shown in Figure S3.7.

Reactions with the supernatant: After the extraction of the organic layer in the supernatant, the inorganic layer was collected and extracted three times with ethyl acetate and water to remove any remaining organic compounds. The inorganic layer was then added with fresh ethanol, bromobenzene, phenylboronic acid, and KOH to perform the reaction at 80 ^{o}C for 30 minutes. The procedure was repeated for additional runs until no product was detected.

3.2.3 Control experiments

Control experiments were also conducted in two methods: preparing the catalyst first without substrates and preparing the catalyst with substrates.

3.2.3.1 Catalyst preparation without substrates and SM reactions

Reaction with bromobenzene: The catalytic mixture was prepared, and the inorganic phase of the supernatant layer was isolated as described above in Section 3.2.2.1. The inorganic layer was then added with 2 mL of ethanol, 33.6 μL (0.32 mmol) of bromobenzene, and 53.8 mg (0.96 mmol) of KOH to perform the reaction at 80 °C for 1 hour. After the reaction, the reaction product, biphenyl, was measured with the GC-MS analysis.

Reaction with phenylboronic acid: The catalytic mixture was prepared, and the inorganic phase of the supernatant layer was isolated as described above in Section 3.2.2.1. The inorganic layer was then added with 2 mL of ethanol, 46.3 mg (0.38 mmol) of phenylboronic acid, and 53.8 mg (0.96 mmol) of KOH to perform the reaction at 80 °C for 1 hour. After the reaction, the reaction product, biphenyl, was measured with the GC-MS analysis.

Reaction with 2-bromotoluene: The catalytic mixture was prepared, and the inorganic phase of the supernatant layer was isolated as described above in Section 3.2.2.1. The inorganic layer was then added with 2 mL of ethanol, 34.9 μL (0.32 mmol) of 2-bromotoluene, 46.3 mg (0.38 mmol) of phenylboronic acid, and 53.8 mg (0.96 mmol) of KOH to perform the reaction at 80 °C for 1 hour. After the reaction, the reaction product, 2-phenyltoluene, was measured with the GC-MS analysis.

3.2.3.2 Catalyst preparation with substrates and SM reactions

Reaction with bromobenzene: In a round bottom flask, 10 mg (0.0375 mmol) of palladium dinitrate dihydrate, 33.6 μL (0.32 mmol) of bromobenzene, and 53.8 mg (0.96 mmol) of KOH were dispersed in a solution of 4 mL H_2O:EtOH (1:1). The flask was kept in an oil bath at 80 °C for 30 minutes under constant magnetic stirring. The reaction was done in air. After the reaction, the reaction mixture was separated into a supernatant and a precipitate by centrifugation at 5000 rpm for 5 minutes. The coupling product, biphenyl, in the supernatant was measured through GC-MS analysis.

Reaction with phenylboronic acid: In a round bottom flask, 10 mg (0.0375 mmol) of palladium dinitrate dihydrate, 46.3 mg (0.38 mmol) of phenylboronic acid, and 53.8 mg (0.96 mmol) of KOH were dispersed in a solution of 4 mL H_2O:EtOH (1:1). The flask was kept in an oil bath at 80 ºC for 30 minutes under constant magnetic stirring. The reaction was done in air. After the reaction, the reaction mixture was separated into a supernatant and a precipitate by centrifugation at 5000 rpm for 5 minutes. The coupling product, biphenyl, in the supernatant was measured through GC-MS analysis.

Reaction with 2-bromotoluene: In a round bottom flask, 10 mg (0.0375 mmol) of palladium dinitrate dihydrate, 34.9 µL (0.32 mmol) of 2-bromotoluene, 46.3 mg (0.38 mmol) of phenylboronic acid, and 53.8 mg (0.96 mmol) of KOH were dispersed in a solution of 4 mL H_2O:EtOH (1:1). The flask was kept in an oil bath at 80 ºC for 30 minutes under constant magnetic stirring. The reaction was done in air. After the reaction, the reaction mixture was separated into a supernatant and a precipitate by centrifugation at 5000 rpm for 5 minutes. The coupling product, biphenyl, in the supernatant was measured through GC-MS analysis.

3.2.4 Catalyst preparation for XPS analysis

Precipitate: 0.0375 mmol of $Pd(NO_3)_2.2H_2O$ and 53.8 mg (0.96 mmol) of KOH dispersed in a solution of 4 mL H_2O:EtOH (1:1) at 80 ºC for 30 minutes under constant magnetic stirring. The reaction was done in air. After the reaction, the mixture was separated into a supernatant and a precipitate by centrifugation at 5000 rpm for 5 minutes, and the precipitate was used for XPS analysis for the precipitate.

Supernatant: In a round bottom flask, the catalyst was prepared using 50 mg (0.1875 mmol) of $Pd(NO_3)_2.2H_2O$ and 2 mg (0.0357 mmol) of KOH dispersed in a solution of 1 μL ethanol and 2 mL H_2O. The flask was kept in an oil bath at 80 °C for 30 minutes under constant magnetic stirring. The reaction was done in air. After the reaction, the mixture was separated into a supernatant and a precipitate by centrifugation at 5000 rpm for 5 minutes, and the extracted inorganic layer of the supernatant was used for XPS analysis for the supernatant.

3.2.5 Reduction of $Pd(NO_3)_2.2H_2O$ and oxidation of ethanol

10 mg (0.0375 mmol) of palladium dinitrate dihydrate, 53.8 mg (0.96 mmol) of KOH, and 2 mL of ethanol were added to a reaction vessel and stirred at RT for a half hour under air. The reaction mixture was separated by centrifugation. The organic layer of the solution was collected to identify the ethanol-oxidation product by ^{13}C NMR, and the precipitate was used to identify the Pd oxidation state after the reduction of the Pd salt by XPS.

3.2.6 Characterization

3.2.6.1 GC-MS

GC-MS analysis of the reaction product was performed using an Agilent Technologies 6890N GC with split injection and with 5973 Mass Selective Detector (MSD). Ultra-high purity He gas (99.999%) was used as the carrier gas at 0.5 mL/min after passing through an oxygen and moisture trap. Samples for the GC-MS analysis were prepared at a concentration of 1 mg/mL in an ethyl acetate solvent. Following automated injection of 0.1 mL, the oven was held at 70 °C for 3 minutes, then ramped at 10 °C/min to 280 °C, where it was held for 22 minutes to complete the run.

3.2.6.2 ^{13}C NMR

NMR experiments were performed on a 400 MHz Bruker AVANCE NEO (Billerica, MA, USA) instrument equipped with a 5 mm Smart Probe. The solvent used was deuterated chloroform ($CDCl_3$). Samples were prepared using 100 μL of the sample and 400 μL of $CDCl_3$.

3.2.6.3 XPS

XPS data was collected using a Thermo VG Scientific Sigma Probe system with an Al K_α X-ray source (1486.3 eV) at an energy resolution of 0.47 eV full width at half maximum (FWHM) under ultrahigh vacuum (10^{-8} Torr). The samples for XPS measurements were prepared using the drop-casting method. First, 3μL of the Pd-containing suspension in water was drop casted on a silicon (Si) wafer. Then, it was dried in air for 30 minutes. This drop-casting method was repeated ten times to ensure uniform spreading of the sample on the Si wafer. Pd 3d XPS spectra were obtained with 10 scans in the range 330 to 350 eV with a spot size of 400 μm. Deconvolution of the XPS spectra was performed using Thermo Avantage software with a full width at half max (FWHM) of 1.50 eV for each peak and a 30% Lorentzian/Gaussian (L/G) mixed convolution.

3.2.6.4 XAS

XAS spectra were collected at 20-BM beamline of the Argonne National Laboratory. A Si (111) double-crystal monochromator beam was focused by toroidal mirror. Harmonic rejection was facilitated by using a Rh-coated mirror (2 mrad) as well as a 15% detuning of the beam intensity at 24800 eV. 20% Ar and 80% N_2 were used for all ionization chambers. Details on the beamline optics and instruments can be found elsewhere.[101] The liquid samples were measured inside the Eppendorf vials in transmission mode at room temperature. Several spectra were collected for each sample to ensure the reproducibility of the spectra and good signal-to-noise ratios. Samples were scanned at energies near the Pd K absorption edge (24,350 eV). The standard Pd foil was scanned simultaneously, between the transmission and reference ionization chambers and used for calibration. Extended X-ray absorption fine structure (EXAFS) at the Pd K-edge was recorded at room temperature and the Pd local coordination environment was determined using the EXAFS data. EXAFS oscillations were extracted using Athena code and analyzed using Arthemis software.[102] The local environment of Pd atoms was determined using the phase shift and amplitude functions of Pd−O and Pd-Pd contributions from $Pd(NO_3)_2$ and metallic Pd, respectively. The Pd foil was analyzed first and used to determine the amplitude reduction factor (S_0^2) for the samples Pd-Pd contribution. The samples and $Pd(NO_3)_2$ were analyzed simultaneously. Due to the nature difference between the Pd foil and the samples, the photoelectron energy origin correction (ΔE_0) determined for the foil could not be used for the samples and had to be fitted again being the same for all Pd-Pd contributions. S_0^2, ΔE_0 and Debye-Waller factor (σ_i^2) were fitted for the Pd-O path to reduce the number of variables. The coordination numbers (N_i) and distances (R_i) were adjusted freely and independently for each sample and each path. The range used to transform the EXAFS oscillations was ($k^2\ \chi(k)$) 3-10 and the interval where the fit was performed was $|\chi(R)|$= 1-3 Å.

3.2.6.5 UV-Vis

UV-Vis absorption spectra were collected using an Evolution™ 201 UV-Vis spectrophotometer. The instrument was equipped with a double beam scanning technology with sample and reference cuvette positions and Czerny-Turner Monochromator. The detector used was dual silicon photodiodes, while the lamp was a Xenon Flash Lamp. Data were obtained using a baseline flatness of 200 to 700 nm, a data interval of 1 nm, a spectral bandwidth of 1.0 nm, and an integration time of 2.5 seconds. The blanks were performed using water. UV-Vis samples were prepared using 10 μL of the sample and 2 mL of water as the solvent. UV-Vis was measured for the inorganic layer of the supernatant phase for each run so as to avoid any interference from the organics (reactants, solvent, or products).

3.2.6.6 TEM

TEM was operated on FEI Talos F200X. The energy of the field emission gun was maintained at 200 keV. The resolution was kept at 0.16 nm. A high-speed Ceta camera of 16 megapixel with 40 frames per second was operated at 4K resolution. TEM tomography was also used. TEM samples were prepared by dispersing a small amount of the isolated Pd-containing precipitate in ethyl acetate and by sonicating the mixture for 30 minutes. Then, 10 μL of the diluted solution mixture was drop-cast onto a 300 mesh Cu grid with a holey carbon film.

3.2.7 Computational methods

The DFT method with the B3LYP hybrid function was employed to calculate geometries and vibrational frequencies of water-solvated Pd_n (n =1-4) and PdO.[83] The Stuttgart/Dresden (SDD) basis set was used for Pd and 6-311G+(d,p) for O.[103] The solvent effect was treated by the polarization continuum model.[104] At the ground-state geometry, the time-dependent (TD) DFT calculations were then performed to determine their excited states. The result was plotted as the UV-Vis spectrum for each species. All calculations were performed with the Gaussian 09 software package.[105]

3.3 Results and Discussion

3.3.1 SM Coupling is Catalyzed by Homogeneous Catalytic Mechanism

To investigate if the SM coupling is catalyzed homogeneously or heterogeneously, we performed the reactions separately with water-soluble Pd species and solid Pd particles. The soluble and solid Pd were isolated from catalytical mixtures that were prepared at 80 ºC in two batches: one with the bromobenzene and phenylboronic acid substrates (batch A) and the other without them (batch B), both in the presence of Pd(II) nitrate, potassium hydroxide, water, and ethanol. Upon isolation, the soluble Pd species reside in the inorganic layer of the supernatant while the solid Pd particles are in precipitate. The SM reactions were then carried out at 80 ºC, separately with the inorganic supernatants and precipitates isolated from the two batch mixtures in fresh base and alcohol aqueous solutions. The details of the mixture preparation, isolation, and SM reactions are presented in Figures S3.6 and S3.7, and results are summarized in Table 3.1. The yields of the coupling product, biphenyl, were measured by GC-MS (Figures S3.8-S3.10). As shown in the table, both the soluble and solid Pd prepared from batch A exhibit a high catalytical activity, while with batch B, only the soluble Pd species catalyzes the SM reaction.

Table 3.1. SM coupling of bromobenzene and phenylboronic acid substrates catalyzed by soluble Pd species and solid Pd particles isolated from catalytical mixtures.

Mixture[a]	Yield (%) with soluble Pd species[b]	Yield (%) with solid Pd particles[b]
With substrates (batch A)	91	89
Without substrates (batch B)	61	0

[a] In both cases, the mixtures consisted of $Pd(NO_3)_2.H_2O$ (0.0375 mmol), KOH (0.96 mmol) and 4 mL 1:1 H_2O: CH_3CH_2OH and were stirred in air at 80°C for 0.5 h (batch A) and 1 h (batch B).

[b] Yields of biphenyl were measured with GC-MS. SM coupling reactions of bromobenzene and phenylboronic acid were carried out with stir in air at 80°C for 0.5 h (with batch A) or 1 h (with batch B) in the solution of KOH (0.96 mmol) and 4 mL 1:1 H_2O: CH_3CH_2OH.

3.3.2 Pd(0) particles serve as a reservoir from which catalytical species are discharged into the solutions

To help understand the activity difference between the solid Pd from the two mixtures, we measured the Pd 3d x-ray photoelectron spectra (XPS) and observed the Pd particles prepared from the two batches are both in the zero-oxidation state even though their reaction yields are 0 and 89%, respectively. We also measured UV-Vis spectra of the inorganic layers isolated from the reaction mixtures and found that the spectra are the same with the soluble and solid Pd prepared with the substrates. These spectroscopic measurements suggest that the Pd(0) particles themselves are not an active catalyst but serves as a reservoir from which catalytical species are discharged into the solutions, which is consistent with numerous previous studies.[39-40, 42, 96-98] The leaching and activity are enhanced for the solid Pd (0) particles that were isolated from the mixture with the organic substrates, as previously reported for Pd supported on alumina or carbon in SM and Heck reactions.[106-107] Activity enhancement is also observed for the soluble Pd species from the mixture with the substrates. In addition, we tested the activity of the soluble and solid Pd from the two batch mixtures prepared at the room temperature and found that the reaction yields (e.g., 83 and 66% for the soluble and solid Pd, respectively, with the substrates and no product for both Pd without the substrates) are lower than those prepared at 80 ºC (Table 3.1) This observation suggests that an increased temperature enhances the Pd leaching and activity as well.

3.3.3 Reusability and stability of the water-soluble Pd catalyst

We then investigated the reusability and stability of the water-soluble Pd catalyst. Figure 3.2 presents the yields of biphenyl obtained from several runs by using the soluble and solid Pd isolated from the mixture with the substrates, each run was carried out in triplicate. The yields of biphenyl from the first three consecutive runs were similar in two cases. After the third run, the reaction with the Pd(0) particles delivered no product, while the reaction with the soluble Pd species still showed fair activity in two additional runs under the same conditions. The fewer catalytical cycles with the Pd (0) particles are likely due to the redeposition of the discharged soluble Pd species on the surface of the solid. To test the stability of the soluble Pd species in the solution, we performed the SM coupling after the fresh inorganic supernatant was stored at room temperature for 12 weeks and found the reaction generated biphenyl with 40% yield. This observation shows the water-soluble Pd species is very stable under ambient conditions, a clearly desirable property for any catalysts.

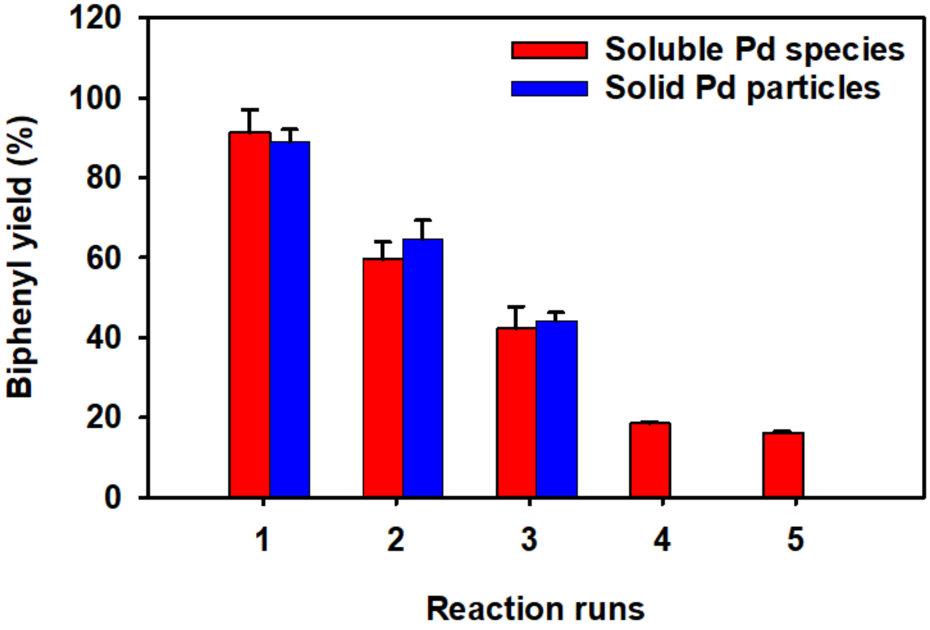

Figure 3.2. Comparison of biphenyl yields of the SM reaction catalyzed with soluble Pd species (red) and Pd(0) particles (blue). The yields were measured with GC-MS.

3.3.4 Control experiments

To confirm that biphenyl was formed by the SM cross-coupling between C_6H_5Br and $C_6H_5B(OH)_2$, rather than through the homocoupling of C_6H_5Br or $C_6H_5B(OH)_2$, we carried out three control experiments with a) C_6H_5Br, b) $C_6H_5B(OH)_2$, and c) 2-bromotoulene (C_7H_7Br) and $C_6H_5B(OH)_2$. These reactions were conducted separately with the soluble Pd species from the mixtures with and without substrates. The reactions with only C_6H_5Br or $C_6H_5B(OH)_2$ yielded no product in both cases, whereas the cross coupling of C_7H_7Br and $C_6H_5B(OH)_2$ produced the product of 2-phenyltoleuene in 90% yield with the substates and 53 % without them (Figure S3.11-S3.13).

3.3.5 The soluble Pd species consist of Pd_4 as the major species and Pd_3 as the minor species

After the identification of the SM coupling being catalyzed by water-soluble Pd species, we proceeded with the experiment to determine their chemical identities. It is observed that the soluble Pd species consist of Pd_4 as the major species and Pd_3 as the minor one, as shown by comparing the experimental and computational UV-Vis spectra in Figure 3.3. The experimental spectrum was obtained by subtracting the spectrum of the spent inorganic supernatant after the final run from the spectrum of a fresh solution prior to the SM reaction to minimize the interference from organic chemicals. The supernatant after the final run contains no Pd clusters, while the clusters are not consumed in the fresh solution. The experimental spectrum was recorded in the range of 200-700 nm, but no signal was observed beyond 400 nm. The theoretical spectra were computed using Time-dependent density functional theory (TD-DFT), and the solvent (i.e., water) effect was treated by the polarizable continuum model.[108] We considered several small Pd_n species (n=1-4) and PdO in our calculations because these two classes of molecules were previously proposed as possible catalytical species in ligand-free Pd-catalyzed SM reactions.[40, 42, 96-97] Because they are stable in aqueous solutions under ambient atmosphere, these species are expected to be in singlet electronic states where all electrons are paired, rather than other spin states with one or more unpaired electrons. The singlet spin states are the electronic states of the neutral molecules. The calculated spectrum of a nearly-planar Pd_4 cluster ($^1A'$, C_s) shows well-matched maximum absorption wavelength (~ 275 nm) and profile with the measured spectrum. The spectrum of a planar Pd_3 cluster ($^1A_1$, C_{2v}) displays a much broader absorption profile and a lower intensity with the maximum at ~ 270 nm. Its contribution may not be excluded but must be considerably smaller than that of the Pd_4 cluster. For other species, the spectral maxima are predicted at 309 nm for Pd (^1S), 316 nm for Pd_2 ($^1\Sigma^+_g$, $D_{\infty h}$) and 250 nm for PdO ($^1\Sigma^+$, $C_{\infty v}$); all have much lower intensities. Thus, these molecules are not significant in the supernatant. The Pd tetramer and trimer (Figure S3.14) serve as a catalyst because they are the major soluble Pd species, their existence leads to the formation of the coupling product, and they are the reactants and products in multiple runs until their activity is diminished. The current work is consistent with the previous study where $Pd_{3,4}$ clusters formed in N-methylpyrrolidone and estimated with the jellium model were proposed to be active species,[42] but inconsistent with other studies where palladium oxides were reported to be catalytically active.[40, 96-97] However, the electronic states and relative contributions of the Pd clusters were not identified with the jellium model that was used for size estimation in the previous study.[42] Nevertheless, it is interesting that the jellium model that is based on the uniform electron gas and often used in solid physics is capable for estimating the size of such small metal clusters in aqueous solutions. We have also located a singlet Pd_4 cluster in a three-dimensional structure. However, the calculated UV-Vis spectrum of the three-dimensional Pd_4 singlet state has a much lower intensity and broader absorption than that of the experimental spectrum (Figure S3.15). Thus, the three-dimensional Pd_4 is not a significant species of the catalyst.

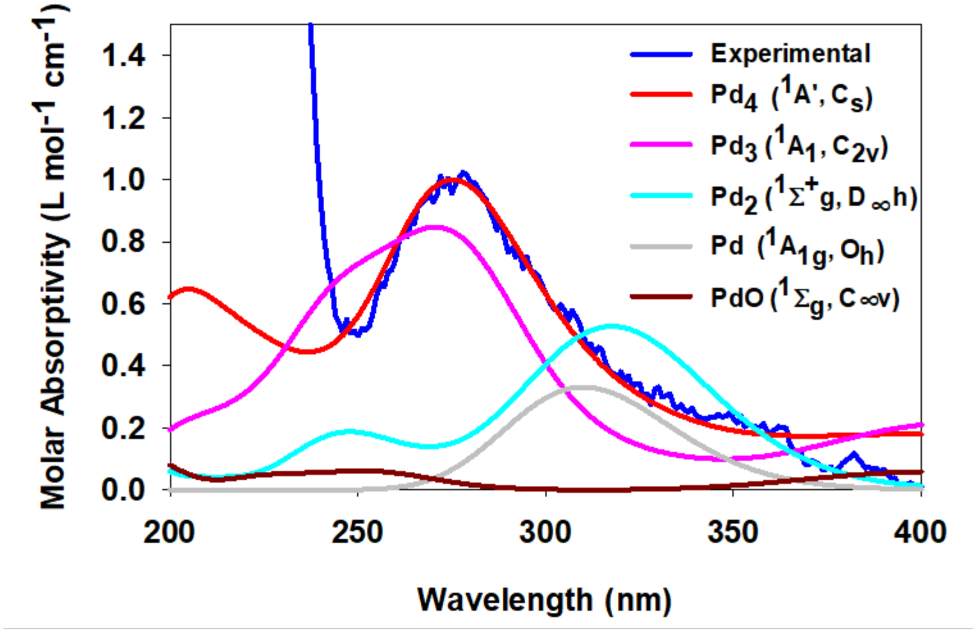

Figure 3.3. Measured UV-Vis spectrum of soluble Pd species and calculated spectra of Pd_{1-4} and PdO by TD-DFT calculations with the continuum solvation model.

3.3.6 Characterization of the solid Pd particles that serve as the reservoir of the Pd clusters

3.3.6.1 Morphology

The next issue that was addressed is the size and shape of the solid Pd particles that serves as the reservoir of the Pd clusters. Figure 3.4 shows the transmission electron microscopy (TEM) images of the Pd nanoparticles prior to the SM reaction (a) and after the final run (b), taken with the electron beam perpendicular to the sample surface, while those in Figure S3.16 are images taken at other angles. Before the SM reaction, most of the Pd nanoparticles have a spherical shape, and the average diameter of fifty-five nanoparticles is estimated to be 2.99 ± 1.32 nm. After the final run of the SM reaction, the shape of most Pd nanoparticles becomes roughly cylindrical with the average dimension of 2.71 ± 1.18 nm in diameter and 7.42 ± 0.97 nm in length. The spherical shape of the Pd nanoparticles before the reaction suggests that the constituent molecular species have negligible total electric dipole moments. Indeed, the electric dipole moments of the Pd_4 and Pd_3 clusters are predicted to be zero and 0.027 D, respectively. On the other hand, the cylindrical shape of the Pd nanoparticles after the final run of the reaction suggests that the constituent inactive molecular species should have a larger electric dipole in one direction than those in other two directions. One of the inactive species is presumably PdO, which is predicted to have the electric dipole of 8.352 D along the molecular axis and zero along the axes perpendicular to the molecular axis.

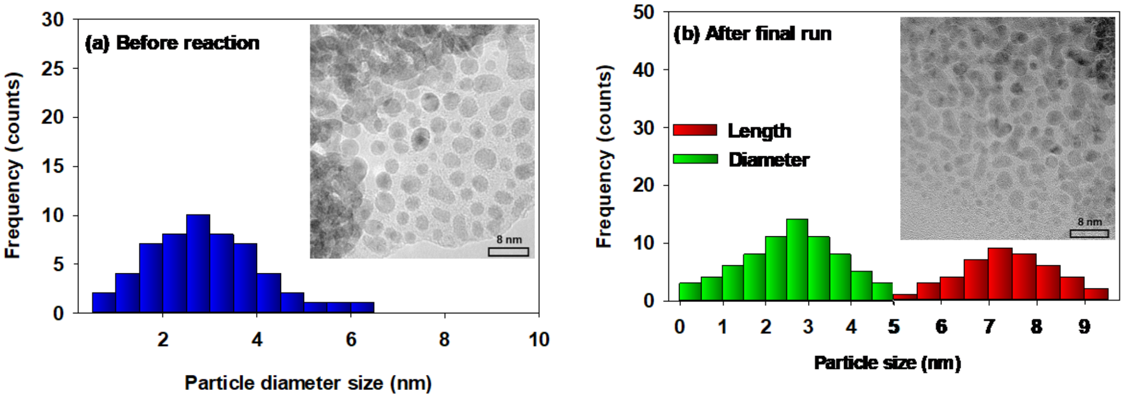

Figure 3.4. TEM images and size histograms of the spherical Pd nanoparticles before the SM reaction (a) and the cylindrical Pd particles after the final run (b). The dimension of the cylindrical particle size is represented by the diameter of the cross section and the length.

3.3.6.2 Local coordination of the Pd nanoparticles

The existence of PdO on the surface of the Pd nanoparticles after the final run of the reaction is also consistent with the XPS measurements, where Pd(II) was observed as a major oxidation state (Figure S3.17). In contrast, only Pd(0) was detected on the surface of the Pd nanoparticles before the reaction (Figure S3.17). To investigate the local coordination of the Pd nanoparticles, we performed Pd-K-edge x-ray absorption spectroscopic measurements. The extended x-ray absorption fine structure (EXAFS) single-shell fits in the R-space indicate that the local coordination number of Pd-Pd is 4.3 ± 0.9 for the sample before the reaction and reduces slightly to 3.4 ± 0.6 for the sample after the final run of the reaction (Table 3.2 and Figure S3.18). The EXAFS measurements are consistent with the UV-Vis spectra that show the $Pd_{4,3}$ clusters are leached to the supernatant from the surface. The EXAFS measurements also show an increase of Pd-O from the before-reaction to the after final-run sample. Such an increase correlates with the degradation of activity of the Pd catalyst.

Table 3.2. EXAFS parameters from the best single-shell fits.[a]

	N_{Pd-O}	R_{Pd-O} (Å)	N_{Pd-Pd}	R_{Pd-Pd} (Å)	σ_i^2 (Å^2)
Pd foil			12	2.740 (2)	0.0054(4)
$Pd(NO_3)_2$	2	2.02 (2)			0.009 (1)
Sample 1	1.1(4)	1.97 (4)	4.3 (9)	2.75 (1)	
Sample 2	1.7(3)	1.99 (2)	3.4 (6)	2.78 (1)	

[a] For $Pd(NO_3)_2$, only the first Pd-O contribution is listed in the table.
Sample 1: the sample before the reaction.
Sample 2: the sample after the final run of the reactions.
$\Delta E_{0(Pd-Pd)} = 0.8 \pm 1$; $S_0{}^2{}_{(Pd-Pd)} = 0.78 \pm 0.04$; $S_0{}^2{}_{(O-O)} = 1.1 \pm 0.2$; $\Delta E_{0(Pd-O)} = 8 \pm 2$; $\Delta E_{0(Pd\ foil)} = 4.6 \pm 0.3$

3.3.7 Pd(0) nanoparticles are formed by the reduction of Pd(II) nitrate induced by ethanol and enhanced by KOH

The Pd(0) nanoparticles are formed by the reduction of Pd(II) nitrate induced by ethanol and enhanced by potassium hydroxide at the room and reaction (80 ºC) temperatures. The reduction was monitored by the XPS measurements of Pd 3d electron binding energies (Figure 3.5). For $Pd(NO_3)_2.2H_2O$ dissolved in water (Figure 3.5a), the Pd (II) 3d electron binding energies are measured to be 337.2 and 342.5 eV, which correspond to the $3d_{5/2}$ and $3d_{3/2}$ spin-orbit terms, respectively. The energy ordering of the two spin-orbit terms arising from the $3d^9$ configuration upon ionization is consistent with Hund's rules, where for a more than half-filled subshell, the state with a larger total angular momentum J has a lower binding energy. The relative intensity of the $3d_{5/2}$ to $3d_{3/2}$ bands is governed by the (2J+1) degeneracy of each term, where J = 5/2 and 3/2. There is a weak satellite band at the higher energy side of each main band, and these weak bands arise from a shake-up process where the outgoing 3d electron interacts with a valence electron and excite it to a higher energy level. The addition of KOH to the Pd(II) nitrate solution has no effect on the Pd 3d binding energies (Figure 3.5b), implying that the Pd oxidation state remains to be +2. However, the addition of ethanol to the Pd(II) nitrate solution produces two extra bands in the XPS spectrum (Figure 3.5c), and these two bands are easily assigned to Pd(0) $3d_{5/2}$ at 335.2 eV and $3d_{3/2}$ at 340.5 eV. Surprisingly, adding KOH to the solution of Pd(II) nitrate and ethanol vanishes the Pd(II) 3d bands (Figure 3.5d), indicating that the reduction of Pd(II) to Pd(0) is now complete. We also measured the Pd 3d photoelectron spectra for the soluble Pd species by using an increased amount of Pd(II) nitrate to obtain a reasonable XPS signal. We observed that Pd in the supernatant is in zero-oxidation state

(Figure 3.5e), which is consistent with the comparison of the experimental and computed UV-Vis spectra that shows $Pd_{4,3}$ are neutral clusters. The slightly blue shift of the Pd 3d electron binding energy (0.4 eV) from the nanoparticles in the precipitate to the soluble species in the supernatant reflects the well-known size-dependent electron property of metal clusters and particles.[109]

The comparison of the Pd 3d photoelectron spectra in Figure 3.5(a-d) shows that ethanol acts as the reducing agent for the reduction of $Pd(NO_3)_2.2H_2O$ and KOH enhances the alcohol-induced reduction even though the base alone is not capable to reduce the palladium salt. These observations can be understood by the following two reactions:

$$CH_3CH_2OH + Pd(NO_3)_2 = Pd(0) + CH_3CHO + 2HNO_3 \quad (1)$$

$$KOH + HNO_3 = KNO_3 + H_2O \quad (2)$$

The observed ethanol-induced Pd(II) reduction (1) is consistent with well-known Pd-catalyzed oxidation of alcohols.[110] The formation of CH_3CHO is confirmed by the ^{13}C NMR spectrum in Figure S3.19, where the 30.7 and 200.83 ppm bands are indicative of the production of acetaldehyde.[111] The Pd(II) reduction is enhanced by the simple acid-base reaction (2), which consumes nitric acid and thus shifts the reduction equilibrium to the Pd(0) side. The role of the base observed in this work is complementary to the previously reported base effect on the transmetallation and reductive elimination in Pd-catalyzed SM reactions.[112-113]

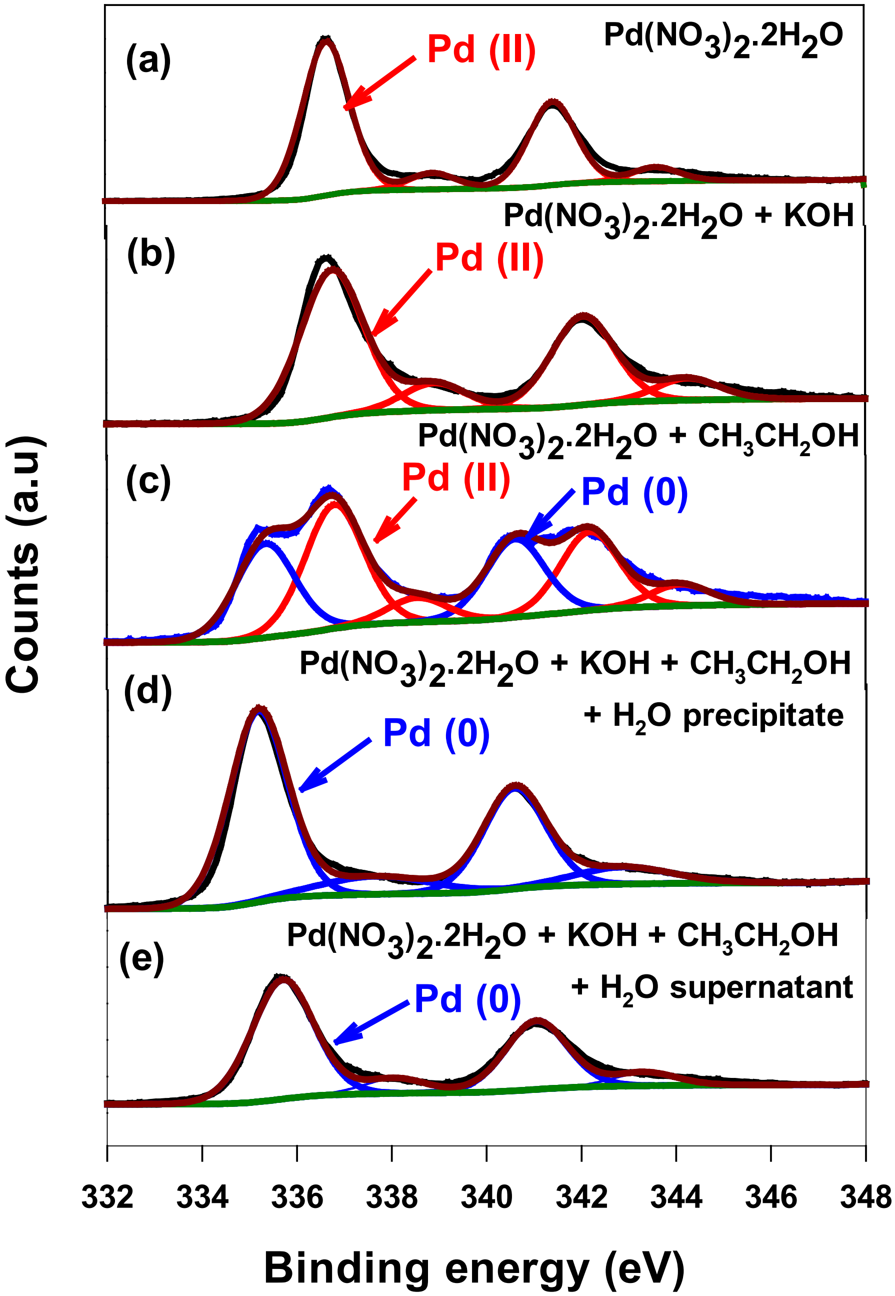

Figure 3.5. XPS spectra of Pd 3d for the aqueous solutions of $Pd(NO_3)_2.2H_2O$ (a), $Pd(NO_3)_2.2H_2O$ + KOH (b), $Pd(NO_3)_2.2H_2O$ + CH_3CH_2OH (c), and $Pd(NO_3)_2.2H_2O$ + CH_3CH_2OH + KOH [(d) for the precipitate and (e) for the supernatant].

3.4 Conclusions

In summary, we report Pd-nanocluster catalysts and their formation in the SM coupling reaction between benzene bromide and phenylboronic acid with palladium nitrate as a precatalyst. The SM coupling is homogenous in nature without any stabilizing organic ligands. The Pd catalyst consists of mainly neutral Pd tetramers with secondary Pd trimers in their singlet electronic states. The Pd nanoclusters are generated by leaching of the Pd(0) nanoparticles and stable in aqueous solutions for at least three months at the room temperature. The Pd(0) nanoparticles are formed by reducing Pd(II) nitrate, and the reduction is induced by ethanol and enhanced by potassium hydroxide. Without the base, the extent of the Pd(II) nitrate reduction is not sufficient for the SM coupling. Although this study is carried out with Pd(II) nitrate as a precatalyst and ethanol and potassium hydroxide as reducing agents, we envision that conclusions reached in this work about the Pd catalyst will likely be valid for SM reactions with other inorganic Pd(II) salts as precatalysts and other alcohols and bases as Pd(II) reducing agents.

3.5 Supporting Information

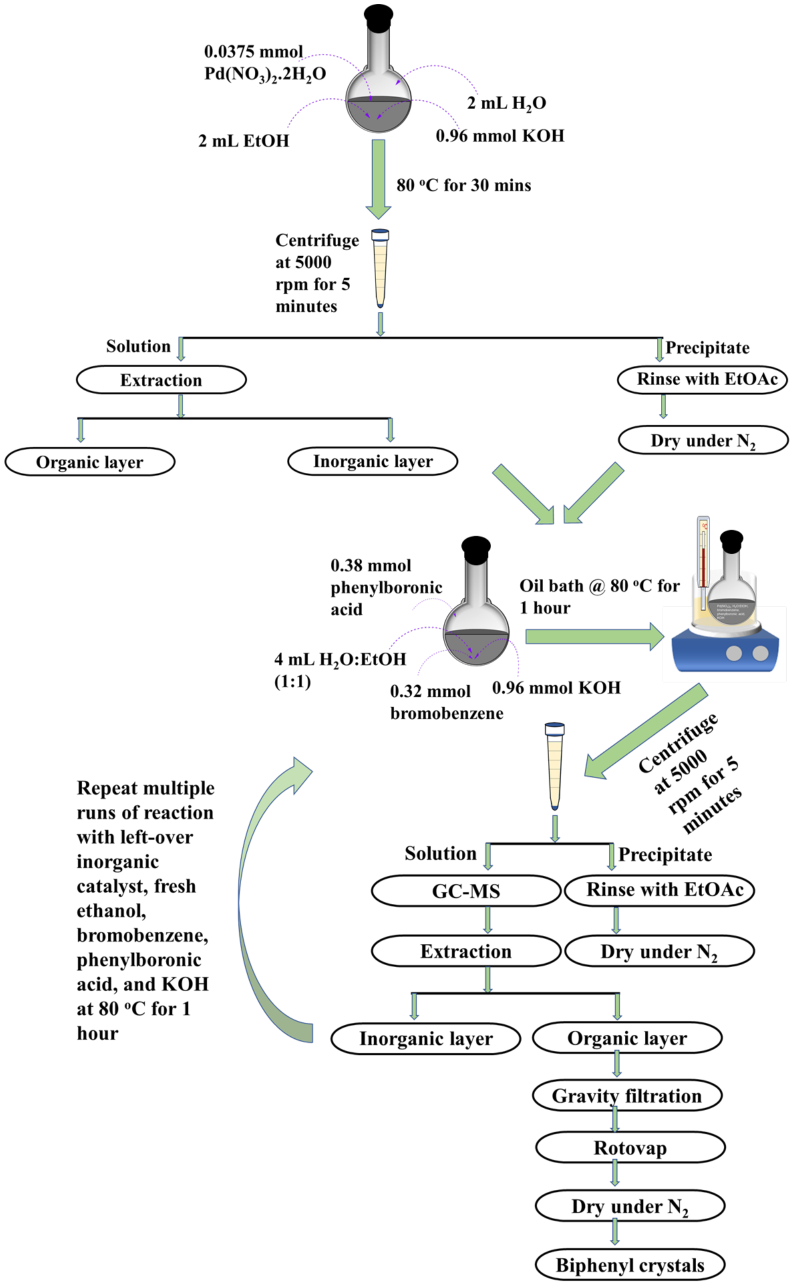

Figure S3.6. Experimental flowchart depicting catalyst preparation, reaction conditions, steps for the purification of the crude product, and recyclability of the precipitate and soluble catalysts. The catalyst was prepared without the bromobenzene and phenylboronic acid substrates.

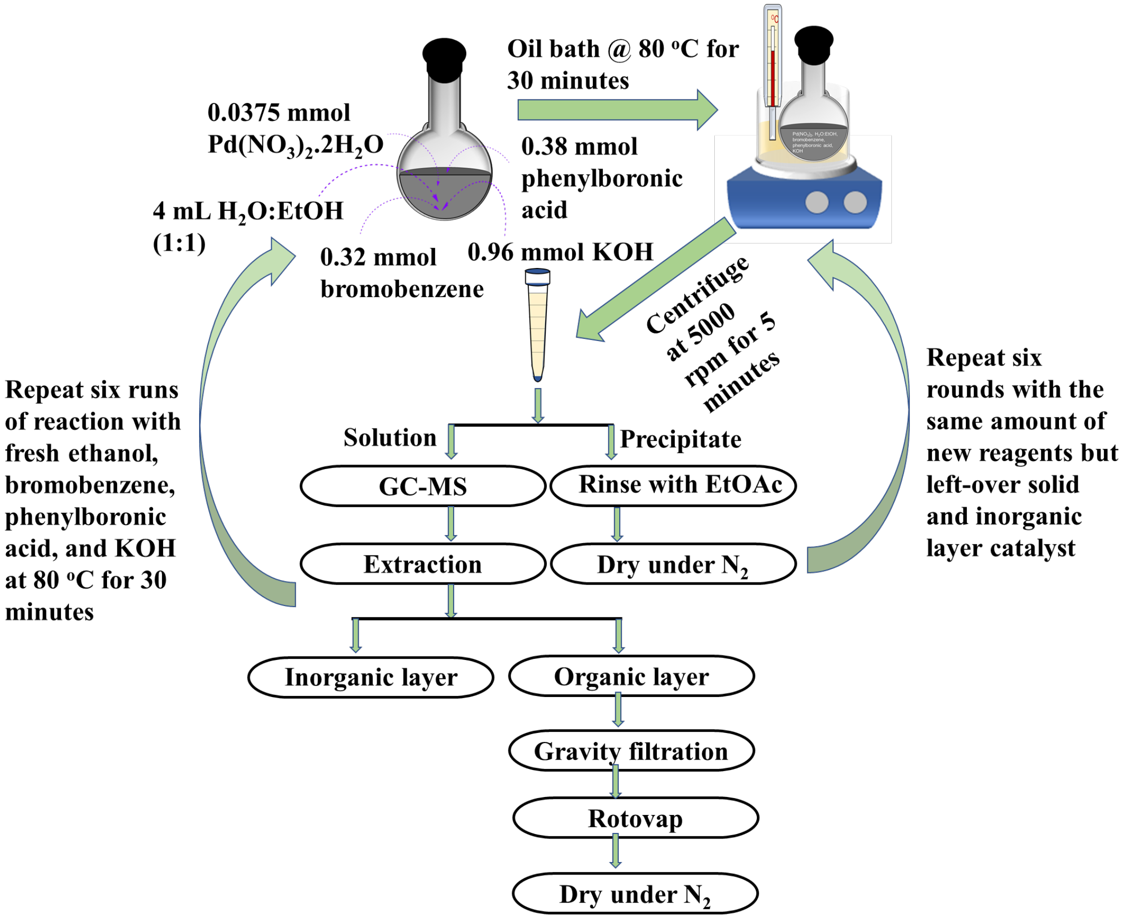

Figure S3.7. Experimental flowchart depicting reaction conditions, steps for the purification of the crude product, and recyclability of the precipitate and soluble catalysts. The catalyst was prepared with the bromobenzene and phenylboronic acid substrates.

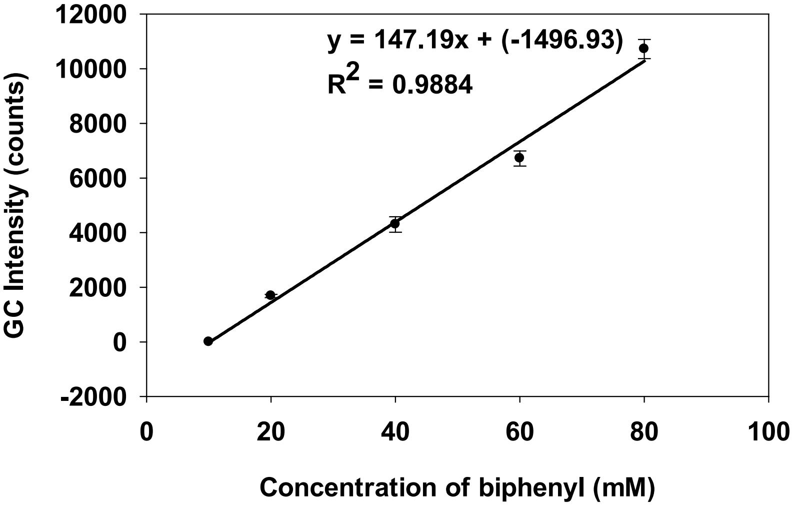

Figure S3.8. Calibration curve of pure biphenyl for determining the yields of biphenyl produced in SM reactions. Triplicates of 80-, 60-, 40-, 20-, and 10-mM solutions were prepared from a stock solution of 100 mM. Each sample was injected into the GC-MS instrument to yield a certain GC intensity. The error bars correspond to the GC intensities of three samples at each concentration.

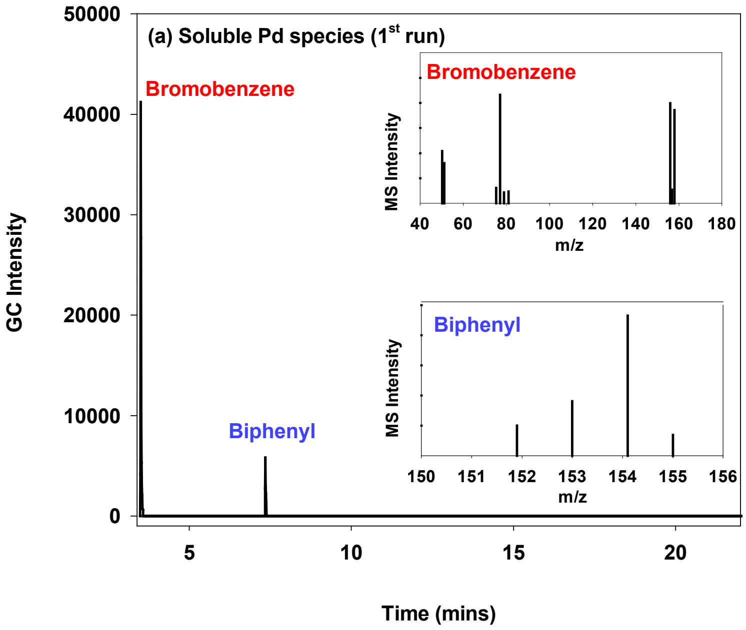

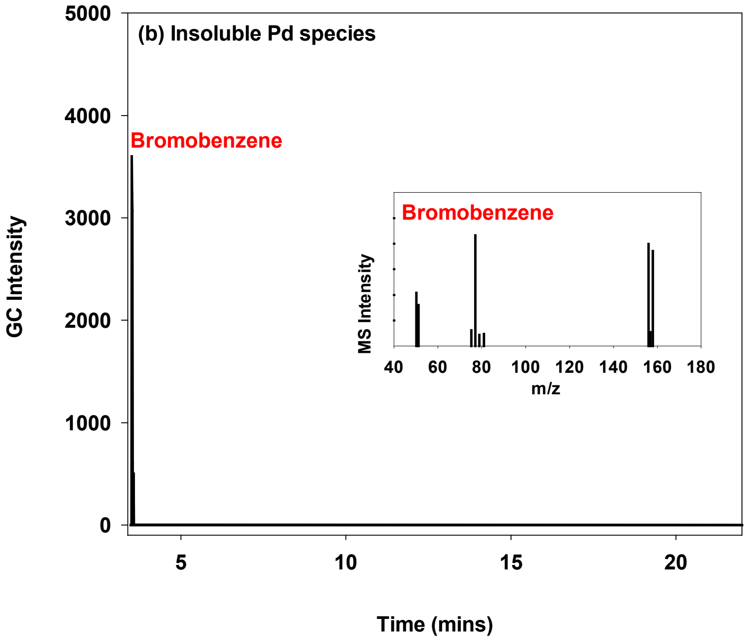

Figure S3.9. GC-MS spectra of the organic layer from the first run of the SM reactions catalyzed with the inorganic layer of the supernatant (a) and the precipitate (b). The catalyst was prepared without the organic substrates. The insets show the MS spectra of the limiting reactant (bromobenzene) and the product (biphenyl). The reaction was carried out at 80 °C for 1 hour.

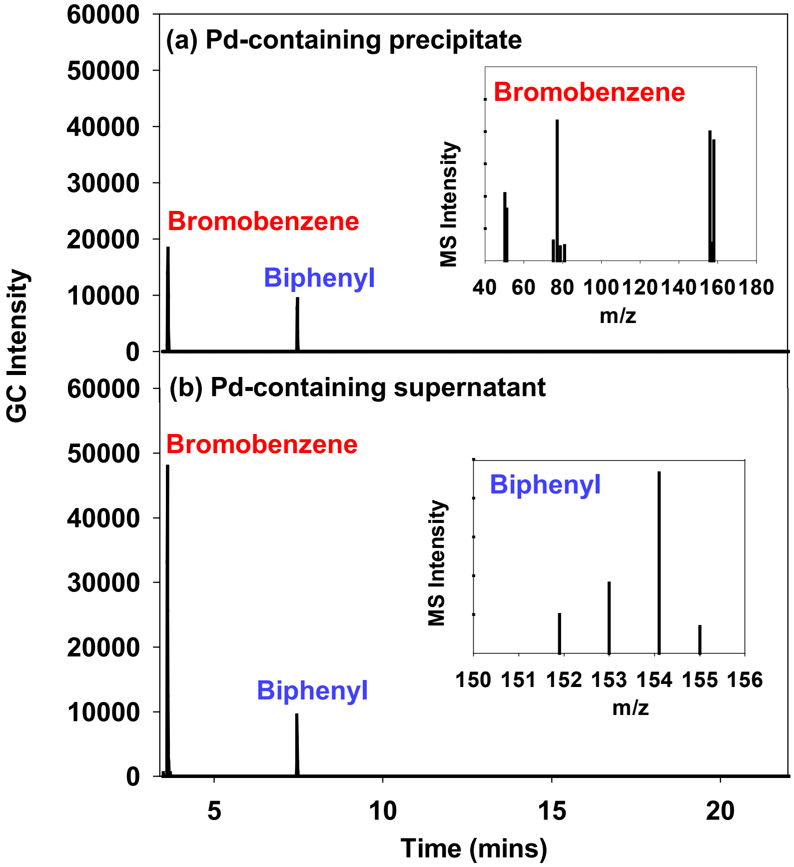

Figure S3.10. GC-MS spectra of the organic layer from the first run of the SM reactions catalyzed with the inorganic layer of the supernatant (a) and the precipitate (b). The catalyst was prepared with the substrates. The insets show the MS spectra of the limiting reactant (bromobenzene) and the product (biphenyl). The insets are applicable for both samples. The reaction was carried out at 80 °C for 30 minutes.

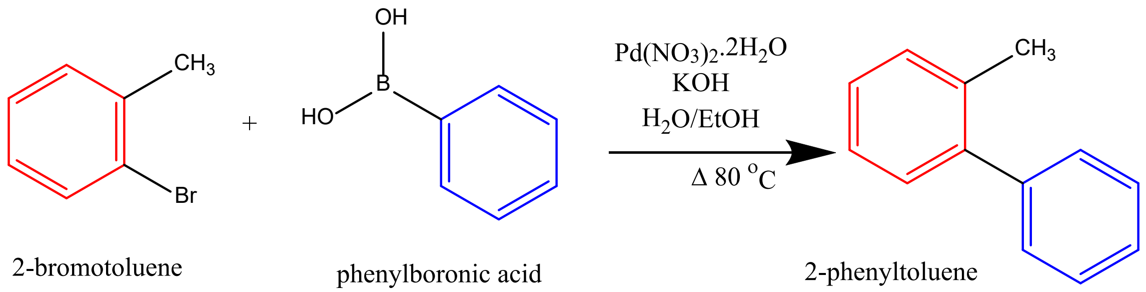

Figure S3.11. Schematic representation of the reaction conditions of the control experiment between C_7H_7Br and $C_6H_5B(OH)_2$.

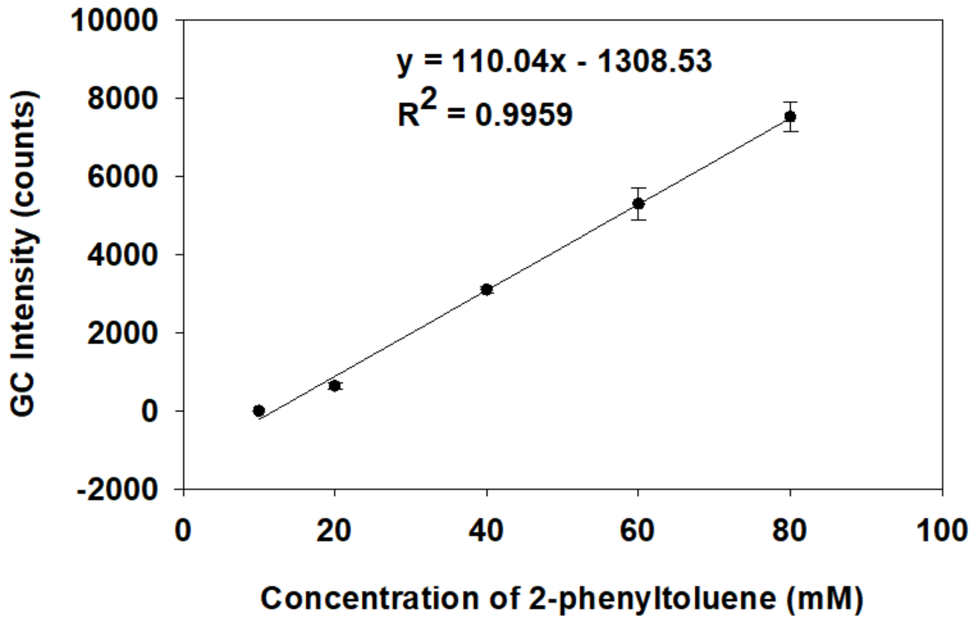

Figure S3.12. Calibration curve of pure 2-phenyltoluene for determining the yields of -2-phenyltoluene produced in the control SM reaction between C_7H_7Br and $C_6H_5B(OH)_2$. Triplicates of 80-, 60-, 40-, 20-, and 10-mM solutions were prepared from a stock solution of 100 mM. Each sample was injected into the GC-MS instrument to yield a certain GC intensity. The error bars correspond to the GC intensities of three samples at each concentration.

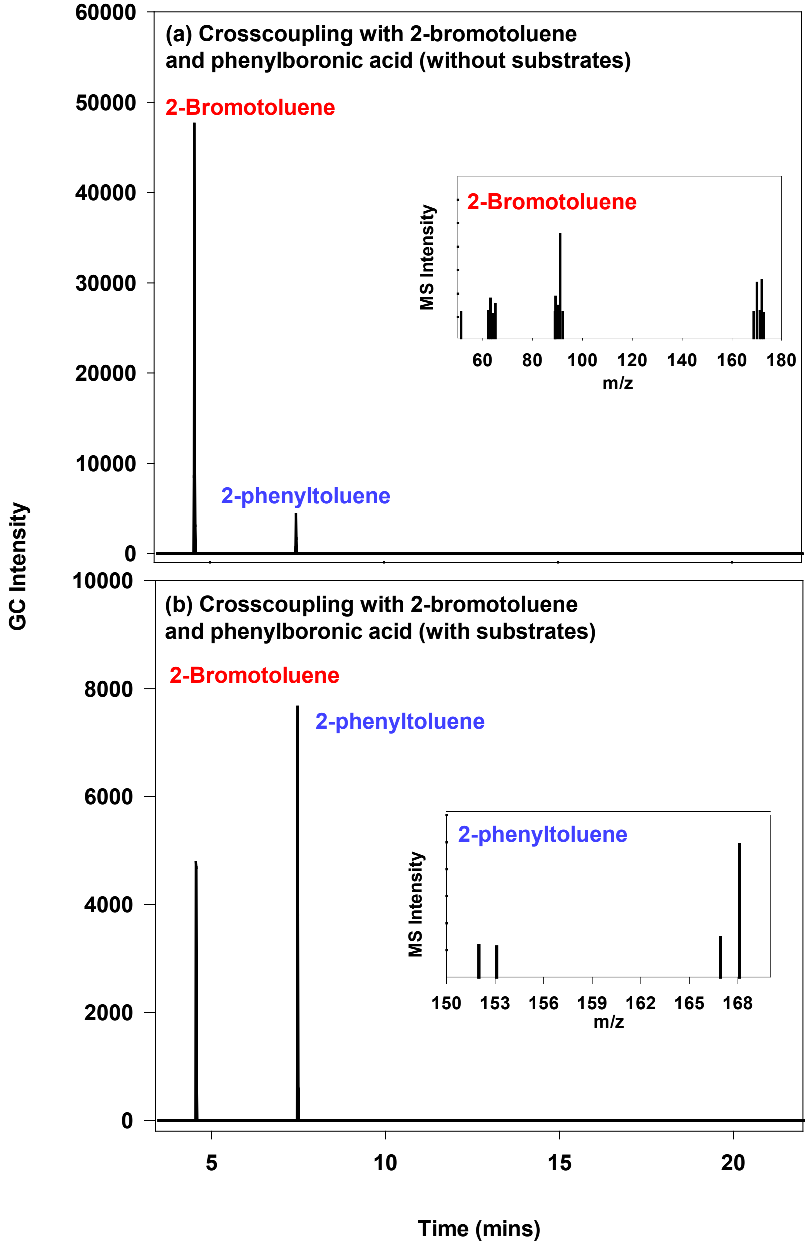

Figure S3.13. GC-MS spectra of the C_7H_7Br and $C_6H_5B(OH)_2$ coupling reaction with the catalyst prepared without the substrates (a) and with the substrates (b). The insets show the MS spectra of the limiting reactant (2-bromotoluene) and the product (2-phenyltoluene). The reaction was carried out at 80 °C for 60 min without the substrates and for 30 min with them to keep consistent with the main reactions.

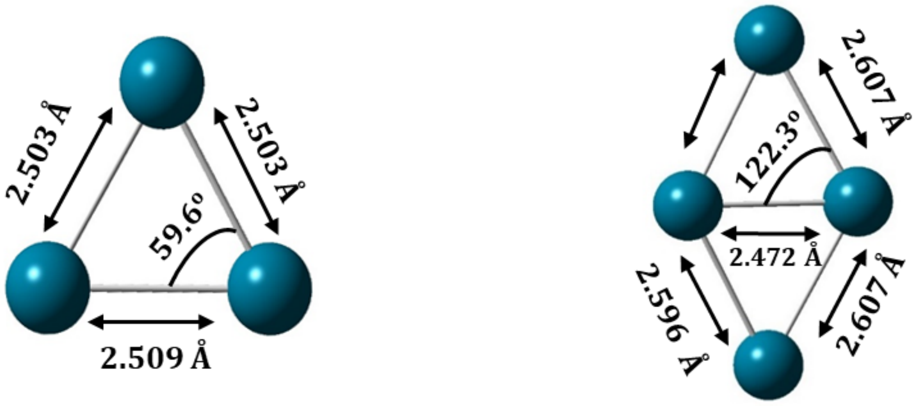

(a) (b)

Figure S3.14. Structures of neutral Pd_3 ($^1A_1$, C_{2v}) (a) and Pd_4 ($^1A'$, C_s) (b) nanoclusters in their singlet electronic states.

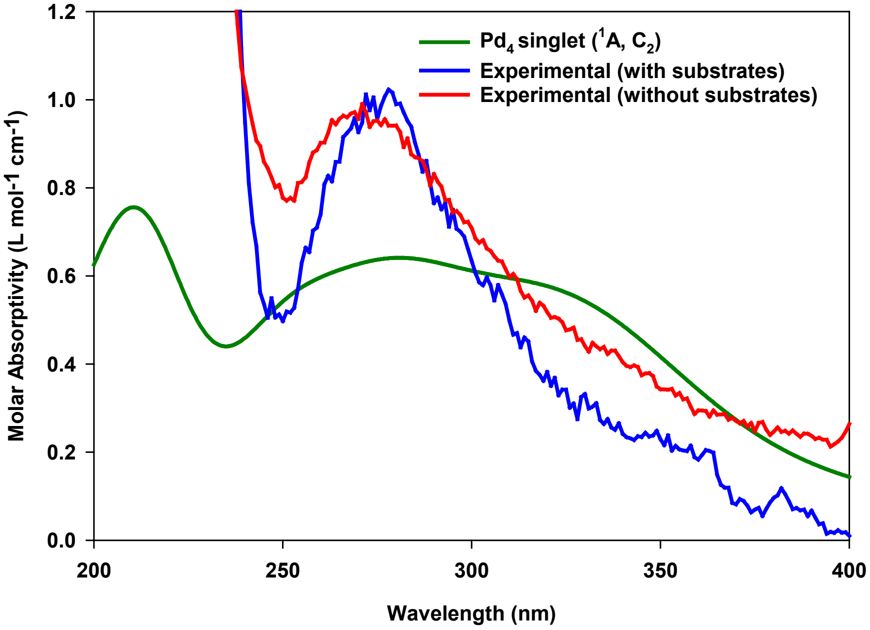

Figure S3.15. Experimental UV-Vis spectrum of soluble Pd species in the inorganic layer of the supernatant from the catalyst prepared with the substrates (blue) and without the substrates (red), and TD-DFT calculated spectrum of a three-dimensional Pd_4 nanocluster in the singlet electronic state. The predicted spectrum shows a much broader transition and a much lower intensity at the experimental maximum than the observed spectrum.

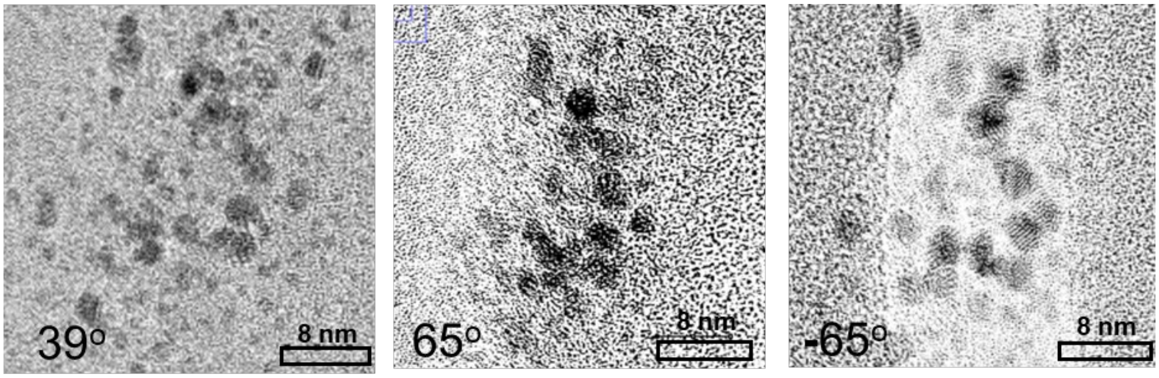

Figure S3.16. TEM images taken at different tilt angles for the before-reaction sample.

.

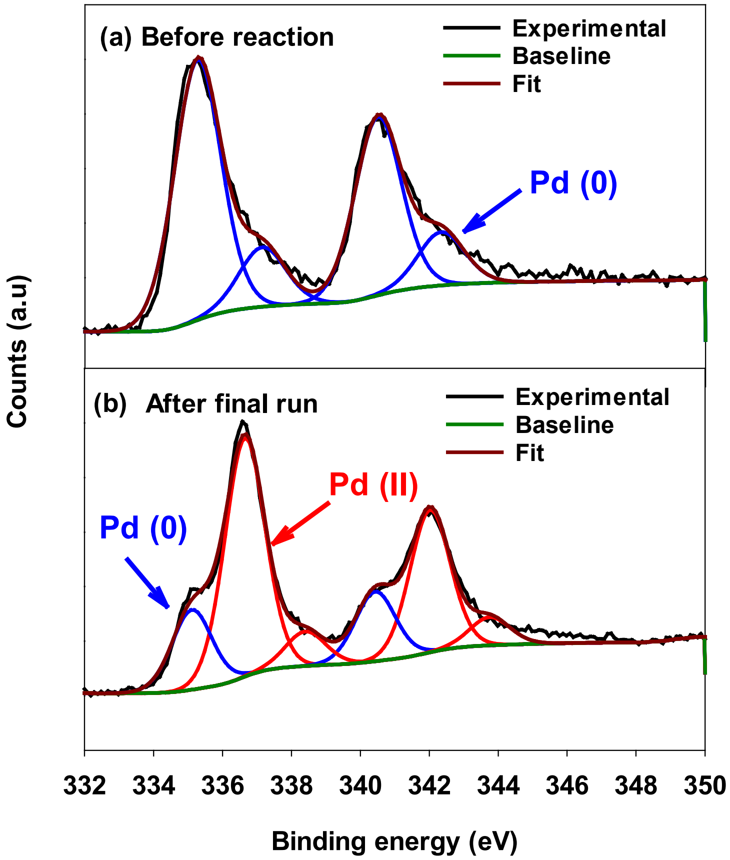

Figure S3.17. Pd 3d XPS spectra of Pd nanoparticles before the SM reaction (a) and after the final run of the reaction (b). The catalyst was prepared with the substrates. The spectrum of the before-reaction sample shows only Pd(0) bands, while the spectrum after the final run displays predominantly Pd(II) bands.

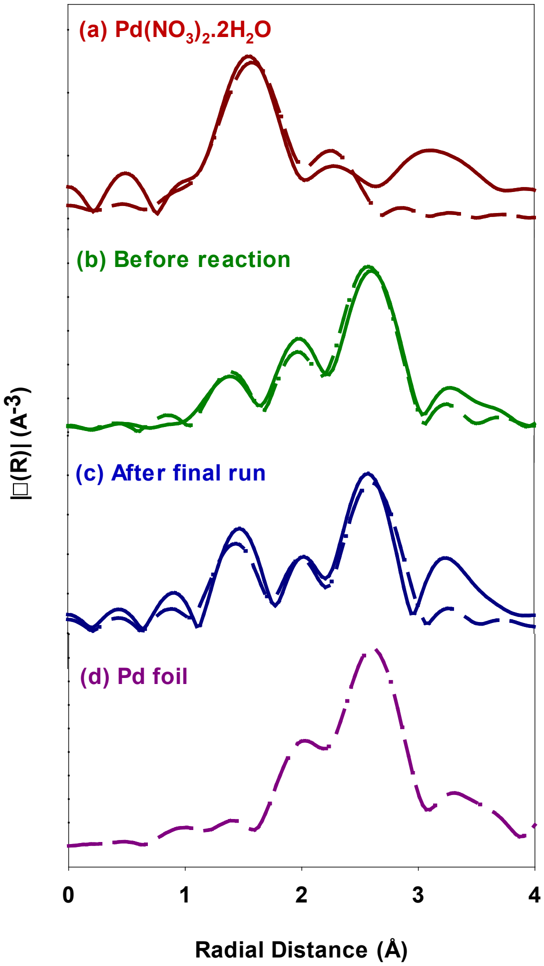

Figure S3.18. Pd K-edge EXAFS single-shell fits in R-space for $Pd(NO_3)_2.2H_2O$ (a), Pd nanoparticles before the SM reaction (b), Pd nanoparticles after the final run of the reaction (c), and Pd foil (d). The catalyst was prepared with the substrates.

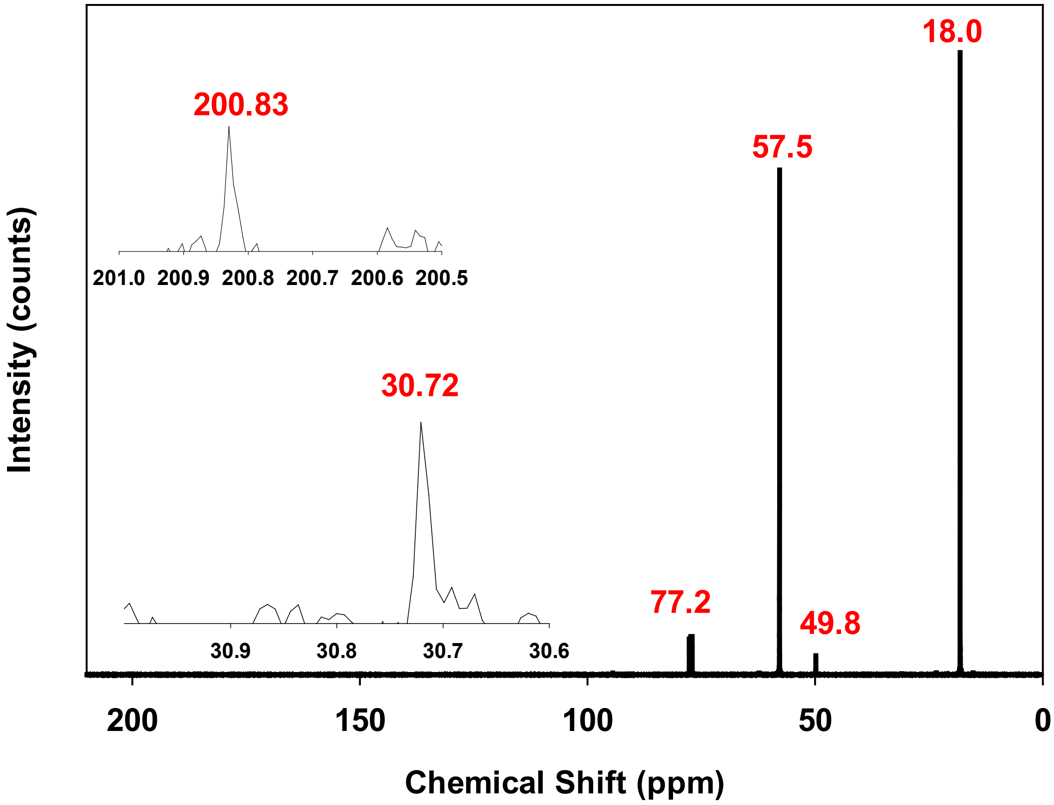

Figure S3.19. ^{13}C NMR spectrum of the organic-layer reaction mixture formed by the $Pd(NO_3)_2.2H_2O$ reduction with ethanol and KOH at room temperature for a half hour recorded in a CD_3Cl solvent. The bands at 30.72 and 200.83 ppm in the magnified inserts indicate the formation of acetaldehyde. The bands at 18.0 and 57.5 ppm are attributed to ethanol, while the triplet at 77.2 ppm is due to the deuterated chloroform solvent. The small band at 49.8 ppm could be a residue peak of C-Cl from the deuterated chloroform solvent.

CHAPTER 4. WATER-SOLUBLE COPPER (I) HYDROXIDE CATALYST AND ITS FORMATION IN LIGAND-FREE SUZUKI-MIYAURA CROSS-COUPLING REACTIONS

This chapter is reproduced with permission from “Water-Soluble Copper(I) Hydroxide Catalyst and Its Formation in Ligand-Free Suzuki−Miyaura Cross-Coupling Reactions” *J. Phys. Chem. C* 2023, 127, 12, 5791–5799. https://doi.org/10.1021/acs.jpcc.3c00268 Copyright © (2023) American Chemical Society.

4.1 Introduction

The record of cross-coupling reactions has been present in the literature since the 1940s when several transition metals were used to catalyze such reactions, including Fe, Ni, and Cu, among others.[23] The first study of Pd-catalyzed SM reactions was reported in 1979,[114] and since then Pd increasingly became the metal of choice for transition metal - catalyzed SM cross coupling reactions due to its high stability, C-H activation ability, and the capability to catalyze reactions at trace amounts.[1, 22-23, 44, 115-116] However, there are growing concerns about its long-term sustainability due to the low nature abundance, prohibitive costs, and high toxicity of Pd metal.[51-54]

Recently, Cu has reemerged as an alternative metal for metal-catalyzed cross-coupling reactions because of its cost-effectiveness, readily availability, and less toxicity.[51-53, 117] Many studies have been reported for non-SM types of homogeneous ligand-stabilized Cu-catalyzed cross-coupling reactions. A survey of the literature shows that Cu(I) complexes stabilized with β-diketones, phosphines, or 1,10-phenanthrolines were generally reported as the catalytical species in the Cu-catalyzed cross-coupling reactions.[118-123] The chemical identity of the active Cu(I) species depended on the oxidation states of the Cu precursors (i.e., Cu (0),[120] Cu (I),[119, 121-122, 124] or Cu (II)[120-121]) and types of stabilizing ligands. Examples of active Cu (I) species included Cu(I) −dative complexes formed from Cu (0) precursors and 1,3-diketonates,[120] copper(I) acetylides from Cu (I) salts and phosphines,[119] and [Cu(I)(1,10-phenanthroline)(thioacetate)] compounds from Cu (II) salts and 1,10-phenanthrolines.[121] On the other hand, fewer studies have been reported for homogeneous ligand-stabilized Cu-catalyzed SM cross-coupling reactions. These SM reactions included the coupling of aryl/vinyl halides and arylboronic acids catalyzed by (1,4-diazabicyclo[2.2.2]octane)$_3$Cu(I) with CuI as the precatalyst,[125] the coupling of aryl/heteroaryl iodides and aryl/heteroarylboronate esters by {[o-(di-tert-butylphosphino)-N,N-dimethylaniline]Cu(I)F}$_2$ Cu(I) also with CuI as the precatalyst,[126] and the coupling of aryl halides and arylboronic acids possibly by (PEG-400)$_2$Cu(0) with Cu(0) powder as the precatalyst.[127] In the case of (PEG-400)$_2$Cu(0) catalyst, the polymeric ligand served as both the solvent and stabilizing ligand.[127]

Although Cu-catalyzed coupling reactions with stabilizing ligands have been reported consistently to be homogeneous, the nature of catalysis and the identity of catalytically active species for ligand-free Cu catalysis are under active debate. Both homo- and hetero-generous reactions have been reported for non-SM cross-coupling. In support of the homogeneous catalysis, a catalytically active Cu(I) species called $Cu(CH_3NH_2)_2^+$ has been proposed to form in-situ from a Cu(0) powder pre-catalyst in the Ullman cross-coupling reaction between aryl halide and methylamine,[128] deoxygenated Cu(I) clusters with up to seven Cu atoms within a polymer generated in situ from various Cu salts or oxides (e.g., $Cu(OAc)_2$, CuO, CuCl, $CuSO_4$, CuCN, CuBr, $CuBr_2$, and CuI) in the Goldberg cross-coupling between iodobenzene and amide,[129] and copper (I) thiolates leached into the solution from the surface of the CuO and Cu_2O nanoparticles in the coupling of thiophenol with 4-iodotoluene.[53] In supporting the heterogenous catalysis, functionalized CuO hollow nanospheres have been reported as active catalysts dispersed on a CuO-acetylene black or a CuO-charcoal in the Ullman coupling reactions between aryl iodides and thiophenols,[130] CuO nanoparticles for C-X (X= C, N, S) coupling,[131] and Cu(0) particles for C-X (X = C, N, O, S, and Se) coupling.[132] For the SM coupling, even fewer studies have been reported for ligand-free Cu catalysts. An early study reported on

Cu nanocluster catalyzed coupling of aryl halide and phenylboronic acid with a CuCl precatalyst,[133] but there was no discussion about the nature of catalysis. A more recent study reported the ligand-free Cu-catalyzed SM coupling of alkynyl bromides with boronic acids with CuI as a precatalyst under microwave irradiation.[134] The coupling was assumed to be homogeneous with CuI being the active catalyst, though no experimental evidence was presented.[134] Possible reaction mechanisms involving transmetalation, oxidative addition, and reductive elimination were also reported but without experimental evidence of either active catalysts or reaction intermediates.[54, 126]

Without using stabilizing ligands, ligand-free metal-catalyzed cross-coupling offers several benefits. They include that precatalysts are readily available and easy to be recovered, reactions can be conducted in air, and products are easily isolated with less contaminations. In this study, we have identified that (a) the ligand-free SM coupling between iodobenzene and phenylboronic acid is homogeneous in nature with CuI as a precatalyst, (b) the active catalyst is water-soluble cuprous hydroxide, Cu(OH), in its singlet electronic state, (c) Cu(OH) is generated from the leaching of oval shaped Cu(I) nanoparticles, and (d) the leaching and reactivity are enhanced from ambient temperature to 80 ºC. The SM coupling reaction is presented in Figure 4.1.

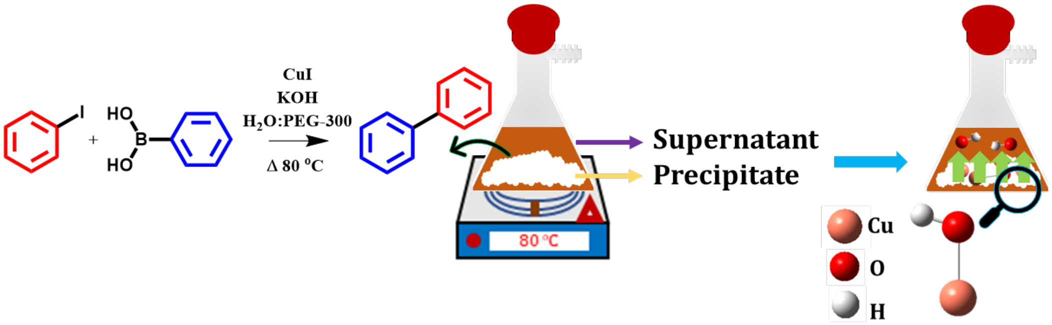

Figure 4.1. Schematic representation of the water-soluble Cu(OH) leached from Cu-containing precipitates catalyzes the SM coupling between C_6H_5I and $C_6H_5B(OH)_2$ with CuI as a precatalyst.

4.2 Experimental

4.2.1 Materials

Copper (I) nitrate and biphenyl (99%) were purchased from Sigma-Aldrich, polyethylene glycol 300 (99%) was purchased from TCI America, 4-iodobenzonitrile (98%) and 4-cyanobiphenyl from Matrix Scientific, potassium hydroxide (85.0%) from VWR, while iodobenzene (98%) was from Alfa Aesar and phenylboronic acid (99% HPLC) from Chem Impex International. All the chemicals were used without further purification. Millipore deionized water was used in all the experiments.

4.2.2 Suzuki – Miyaura coupling reactions

The SM reaction conditions, including solvents, base, and temperatures, were adapted from literature.[100, 135-136]

4.2.2.1 Catalyst preparation without substrates and SM reactions

In a reaction vial, the catalyst was prepared using 8.28 mg (0.0435 mmol) of CuI and 53.8 mg (0.96 mmol) of KOH dispersed in a solution of 4 mL H_2O:PEG-300 (1:1). The flask was kept in an oil bath at 80 °C for 2 hours under constant magnetic stirring. The vial was capped, and the reaction was done in air. After the reaction, the mixture was separated into a supernatant and a precipitate by centrifugation at 5000 rpm for 5 minutes, and the supernatant and precipitate were then placed in two separate vials for future reactions.

Reactions with the precipitate: The precipitate was cleaned with 2 mL of ethyl acetate and then with 2 mL of water by centrifuging at 5000 rpm for 5 minutes twice and later dried under nitrogen flow for half an hour. The nitrogen-dried precipitate was used as a catalyst for the first reaction at 80 °C for 2 hours and with 35.81 µL (0.32 mmol) of iodobenzene, 46.3 mg (0.38 mmol) of phenylboronic acid, and 53.8 mg (0.96 mmol) of

KOH in a solution of 4 mL H_2O:PEG-300 (1:1). The reaction vial was capped, and the reaction was done in air. After the reaction, the reaction mixture was again separated into a supernatant and a precipitate by centrifugation at 5000 rpm for 5 minutes. Because any coupling product would be in the solution phase, the solution was injected into the GC-MS for product identification. A flowchart of the reaction experiment is shown in Figure S4.6.

Reactions with the supernatant: The supernatant was extracted with ethyl acetate and water three times resulting in clearly separated organic and inorganic phases. The organic phase was discarded, whereas the inorganic phase was used for further reactions and characterizations. The inorganic layer was then added with 2 mL of PEG-300, 35.81 μL (0.32 mmol) of iodobenzene, 46.3 mg (0.38 mmol) of phenylboronic acid, and 53.8 mg (0.96 mmol) of KOH to perform the reaction at 80 °C for 2 hours. After the reaction, the reaction product, biphenyl, was measured with the GC-MS analysis. The reaction mixture was also extracted three times with ethyl acetate and water to collect the organic and inorganic layers. The organic layer was discarded, and the inorganic layer was again added with fresh PEG-300, iodobenzene, phenylboronic acid, and KOH to perform the reaction at 80 °C for 2 hours. The procedure was repeated for additional runs until no product was detected.

4.2.2.2 Catalyst preparation with substrates and SM reactions

In a reaction vial, 8.28 mg (0.0435 mmol) of CuI, 35.81 μL (0.32 mmol) of iodobenzene, 46.3 mg (0.38 mmol) of phenylboronic acid, and 53.8 mg (0.96 mmol) of KOH were dispersed in a solution of 4 mL H_2O:PEG-300 (1:1). The flask was kept in an oil bath at 80 °C for 2 hours under constant magnetic stirring. The vial was capped, and the reaction was done in air. After the reaction, the mixture was separated into a supernatant and a precipitate by centrifugation at 5000 rpm for 5 minutes, and the supernatant and precipitate were then placed in two separate vials for future reactions. The coupling product, biphenyl, in the supernatant was measured through GC-MS analysis.

Reactions with the precipitate: The precipitate was cleaned with 2 mL of ethyl acetate and then with 2 mL of water by centrifuging at 5000 rpm for 5 minutes twice and then dried under nitrogen flow for half an hour. The nitrogen-dried precipitate was used as a catalyst for the next run also at 80 °C for 2 hours and with the same amount of fresh iodobenzene, phenylboronic acid, KOH, water, and PEG-300. The procedure was repeated for additional runs until no product was detected. A flowchart of the reaction experiment is shown in Figure S4.7.

Reactions with the supernatant: After the extraction of the organic layer in the supernatant, the inorganic layer was collected and extracted three times with ethyl acetate and water to remove any remaining organic compounds. The inorganic layer was then added with fresh PEG-300, iodobenzene, phenylboronic acid, and KOH to perform the reaction at 80 °C for 2 hours. The procedure was repeated for additional runs until no product was detected.

4.2.3 Control experiments

Control experiments were also conducted in two methods by preparing the catalyst without and with substrates.

4.2.3.1 Catalyst preparation without substrates and SM reactions

The catalytic mixture was prepared, and the inorganic phase of the supernatant layer was isolated as described above in Section 4.2.2.1.

Reaction with iodobenzene: The inorganic layer was then added with 2 mL of PEG-300, 35.81 µL (0.32 mmol) of iodobenzene, and 53.8 mg (0.96 mmol) of KOH to perform the reaction at 80 °C for 2 hours. After the reaction, the reaction product, biphenyl, was measured with the GC-MS analysis.

Reaction with phenylboronic acid: The inorganic layer was then added with 2 mL of PEG-300, 46.3 mg (0.38 mmol) of phenylboronic acid, and 53.8 mg (0.96 mmol) of KOH to perform the reaction at 80 °C for 2 hours. After the reaction, the reaction product, biphenyl, was measured with the GC-MS analysis.

Reaction with 4-iodobenzonitrile: The inorganic layer was then added with 2 mL of PEG-300, 73.28 mg (0.32 mmol) of 4-iodobenzonitrile, 46.3 mg (0.38 mmol) of phenylboronic acid, and 53.8 mg (0.96 mmol) of KOH to perform the reaction at 80 °C for 1 hour. After the reaction, the reaction product, 4-cyanobiphenyl, was measured with the GC-MS analysis.

4.2.3.2 Catalyst preparation with substrates and SM reactions

The catalytic mixture was prepared, and the inorganic phase of the supernatant layer was isolated as described above in Section 4.2.2.2.

Reaction with iodobenzene: The inorganic layer was then added with 2 mL of PEG-300, 35.81 µL (0.32 mmol) of iodobenzene, and 53.8 mg (0.96 mmol) of KOH to perform the reaction at 80 °C for 2 hours. After the reaction, the reaction product, biphenyl, was measured with the GC-MS analysis.

Reaction with phenylboronic acid: The inorganic layer was then added with 2 mL of PEG-300, 46.3 mg (0.38 mmol) of phenylboronic acid, and 53.8 mg (0.96 mmol) of

KOH to perform the reaction at 80 °C for 2 hours. After the reaction, the reaction product, biphenyl, was measured with the GC-MS analysis.

Reaction with 4-iodobenzonitrile: The inorganic layer was then added with 2 mL of PEG-300, 73.28 mg (0.32 mmol) of 4-iodobenzonitrile, 46.3 mg (0.38 mmol) of phenylboronic acid, and 53.8 mg (0.96 mmol) of KOH to perform the reaction at 80 °C for 1 hour. After the reaction, the reaction product, 4-cyanobiphenyl, was measured with the GC-MS analysis.

4.2.4 Catalyst preparation for XPS analysis

Precipitate: 8.28 mg (0.0435 mmol) of CuI and 53.8 mg (0.96 mmol) of KOH were dispersed in a solution of 4 mL H_2O:PEG-300 (1:1) at 80 °C for 2 hours under constant magnetic stirring. The vial was capped, and the reaction was done in air. After the reaction, the mixture was separated into a supernatant and a precipitate by centrifugation at 5000 rpm for 5 minutes, and the precipitate was used for XPS analysis for the precipitate.

Supernatant: In a reaction vial, the catalyst was prepared using 35.71 mg (0.1875 mmol) of CuI and 2 mg (0.0357 mmol) of KOH dispersed in a solution of 1 μL PEG-300 and 2 mL H_2O. The flask was kept in an oil bath at 80 °C for 2 hours under constant magnetic stirring. The vial was capped, and the reaction was done in air. After the reaction, the mixture was separated into a supernatant and a precipitate by centrifugation at 5000 rpm for 5 minutes, and the extracted inorganic layer of the supernatant was used for XPS analysis for the supernatant.

4.2.5 Characterization

4.2.5.1 GC-MS

GC-MS analysis of the reaction product was performed using an Agilent Technologies 6890N GC with split injection and 5973 Mass Selective Detector (MSD). Ultra-high purity He gas (99.999%) was used as the carrier gas at 0.5 mL/min after passing through an oxygen and moisture trap. Samples for the GC-MS analysis were prepared at a concentration of 1 mg/mL in an ethyl acetate solvent. Following automated injection of 0.1 mL, the oven was held at 70 °C for 3 minutes, then ramped at 10 °C/min to 280 °C, where it was held for 22 minutes to complete the run.

4.2.5.2 ^{1}H NMR

^{1}H NMR experiments were collected on a 400 MHz Bruker AVANCE NEO (Billerica, MA, USA) equipped with a 5 mm smart probe. The solvents used were deuterium oxide (D_2O) and deuterated chloroform ($CDCl_3$).

4.2.5.3 UV-Vis

UV-Vis absorption spectra were collected using an Evolution™ 201 UV-Vis spectrophotometer. Data were obtained using a baseline flatness of 200 to 700 nm, a data interval of 1 nm, a spectral bandwidth of 1.0 nm, and an integration time of 2.5 seconds. The blanks were performed using water. UV-Vis samples were prepared using 10 µL of the sample and 2 mL of water as the solvent. UV-Vis was measured for the inorganic layer of the supernatant phase for each run so as to avoid any interference from the organics (reactants, solvent, or products).

4.2.5.4 XPS

XPS data was collected X was collected using a Thermo VG Scientific Sigma Probe system with an Al K_α X-ray source (1486.3 eV) at an energy resolution of 0.47 eV full width at half maximum (FWHM) under ultrahigh vacuum (10^{-8} Torr). The samples for XPS measurements were prepared using the drop-casting method. First, 1μL of the Cu-containing suspension in water was drop casted on a silicon (Si) wafer. Then, it was dried in the oven for 10 minutes. This drop-casting method was repeated several times to ensure uniform spreading of the sample on the Si wafer. Cu 2p XPS and Cu LMM Auger spectra were obtained with 10 scans in the range 925 to 965 eV and 560 to 580 eV, respectively, with a spot size of 400 μm. Deconvolution of the XPS spectra was performed using Thermo Avantage software with a FWHM of 1.50 eV for each peak and a 30% Lorentzian/Gaussian mixed convolution.

4.2.5.5 XAS

XAS spectra were collected at 20-BM beamline of the Argonne National Laboratory. A Si (111) double-crystal monochromator beam was focused by toroidal mirror. Harmonic rejection was facilitated by using a Rh-coated mirror (4 mrad) as well as a 15% detuning of the beam intensity at 9300 eV. 100% N_2 gas were used for all ionization chambers. Details on the beamline optics and instruments can be found elsewhere.[101] The solid samples were measured on the Kapton tape in transmission mode at room temperature. Several spectra were collected for each sample to ensure the reproducibility of the spectra and good signal-to-noise ratios. Samples were scanned at energies near the Cu K absorption edge (8,978.9 eV). The standard Cu foil was scanned simultaneously, between the transmission and reference ionization chambers and used for calibration. Extended X-ray absorption fine structure (EXAFS) at the Cu K-edge was recorded at room temperature and the Cu local coordination environment was determined using the EXAFS data. EXAFS oscillations were extracted using Athena code and analyzed using Artemis software.[102] The local environment of Cu atoms was determined using the phase shift and amplitude functions of Cu−O and Cu-Cu contributions from CuO, Cu_2O, and metallic Cu. The Cu foil was analyzed first and used to determine the amplitude reduction factor (S_0^2), which was fixed as 0.82. The photoelectron energy origin correction (ΔE_0), coordination numbers (N), distances (R), and Debye-Waller factor (σ^2) were treated as adjustable parameters during the fitting process. The EXAFS fitting were done within the R range of 1.0-3.4 and 1.0 -3.1 Å, and the k range of 3.0-11.4 and 3.0-11.8 $Å^{-1}$ was used for the fresh precipitate sample and spent precipitate sample, respectively, under the k^2-weighted $\chi(k)$ functions with Hanning windows (dk=1.0$Å^{-1}$).

4.2.5.6 TEM

TEM images were obtained using FEI Talos F200X. The energy of the field emission gun was maintained at 200 keV. The resolution was kept at 0.16 nm. A high-speed Ceta camera of 16 megapixel with 40 frames per second was operated at 4K resolution. TEM samples were prepared by dispersing a small amount of the isolated Cu-containing precipitate in ethanol and by sonicating the mixture for 30 minutes. Then, 10 µL of the diluted solution mixture was drop-cast onto a 300 mesh Au grid with a lacey carbon film.

4.2.6 Computational methods

The density functional theory (DFT) method with the B3LYP hybrid function was employed to calculate geometries and vibrational frequencies of water-solvated Cu(OH), $Cu(OH)_2$, $Cu(H_2O)_n$ (n = 1-2), Cu_2O, CuO, and CuI_n (n = 1-2).[83] The Aug-cc-pVTZ basis set was used for H, O, Cu, and I. At the ground-state geometry, the time-dependent (TD) DFT calculations were then performed to determine their excited states. The solvent effect was treated by the polarization continuum model.[105, 137-138] The result was plotted as the

UV-Vis spectrum for each species. All calculations were performed with the Gaussian 09 software package.[105]

4.3 Results and Discussion

4.3.1 SM coupling is catalyzed by homogeneous catalytic mechanism

Two sets of experiments were performed independently to investigate if the reaction proceeded with a homogeneous or heterogenous catalytic mechanism, one with water-soluble Cu species and the other with the Cu-containing precipitates. The soluble Cu species and Cu precipitates were isolated from catalytical mixtures that were prepared at 80 °C in two batches: one with the iodobenzene and phenylboronic acid substrates (batch A) and the other without them (batch B), both in the presence of CuI, potassium hydroxide, water, and polyethylene glycol (PEG-300). After the separation of the two layers, the soluble Cu species were present in the yellow-orange inorganic layer of the supernatant after aqueous extraction, while the solid Cu particles resided in the reddish-brown precipitate. These supernatant and precipitate layers were then used to perform the reactions at 80 °C for two hours with fresh reactants, base, and solvent. The details of the chemicals used, the SM reactions, the separation of the two layers are presented in Figures S4.1 and S4.2, and the results are summarized in Table 4.1. The yields of the coupling product, biphenyl, were measured by GC-MS.[136]. Biphenyl was also characterized with ^{1}H NMR spectroscopy (Figure S4.8). As shown in the table, both the soluble and solid Cu prepared from batch A exhibit a higher biphenyl yield than that with batch B where only the soluble Cu species catalyzes the SM reaction. Because no product was observed with the solid Cu particles isolated from batch B, the SM coupling must be catalyzed by a molecular Cu catalyst in the water-soluble supernatant. These observations are similar to the SM coupling between bromobenzene and phenylboronic acid with $Pd(NO_3)_2$ as a precatalyst.[106, 136]

Table 4.1. SM coupling of iodobenzene and phenylboronic acid catalyzed by soluble Cu species and solid Cu particles isolated from catalytical mixtures.

Mixture[a]	Yield (%) with soluble Cu species[b]	Yield (%) with solid Cu particles[b]
With substrates (batch A)	44	28
Without substrates (batch B)	37	0

[a] In both cases, the mixtures consisting of CuI (0.0435 mmol), KOH (0.96 mmol) and 4 mL 1:1 H_2O:PEG-300 were stirred in air at 80°C for 2 h. The amounts of iodobenzene and phenylboronic acid were 0.32 and 0.38 mmol, respectively.
[b] Yields of biphenyl were measured with GC-MS. SM coupling reactions of iodobenzene and phenylboronic acid were carried out with stir in air at 80°C for 2 h in the solution of KOH (0.96 mmol) and 4 mL 1:1 H_2O: PEG-300.

To confirm that biphenyl was formed by the SM cross-coupling between C_6H_5I and $C_6H_5B(OH)_2$ rather than by the homocoupling of C_6H_5I or $C_6H_5B(OH)_2$, we conducted three separated control experiments with (a) C_6H_5I, (b) $C_6H_5B(OH)_2$, and (c) 4-iodobenzonitrile (IC_6H_4CN) and $C_6H_5B(OH)_2$, each with the soluble Cu species prepared with and without substrates. The reactions with only C_6H_5I or $C_6H_5B(OH)_2$ yielded no product in both cases, whereas the cross coupling between IC_6H_4CN and $C_6H_5B(OH)_2$ produced the cross-coupling product of 4-cyanobiphenyl in 39% yield with the substates and 0% without them (Figure S4.9 and 4.10). The higher yield observed in the reactions with the substrates than without has also been reported previously in Pd-catalyzed SM reactions.[106, 136] The formation of 4-cyanobiphenyl was also confirmed by the ^1H NMR spectrum shown in Figure S4.11.

4.3.2 The homogeneous catalyst is identified as cuprous hydroxide [Cu(OH)] in the singlet electronic state

To identify the chemical identity and electronic state of the molecular Cu catalyst, we measured UV-Vis spectra of the inorganic supernantnat extracted from the Cu soluble mixture and the Cu solid particles prepared with the substrates (i.e., batch A) and compare them with the theoretical spectra of numerous molecular Cu species. The experimental spectra in both cases were obtained by subtracting the spectrum of the spent inorganic supernatant after the final run from the spectrum of a fresh solution prior to the SM reaction to minimize the interference from organic chemicals. Both spectra show an absorption maximum at 222(2) nm and similar spectral profiles (Figure S4.12), suggesting that both inorganic supernatants contain the same soluble Cu species. The theoretical spectra were calculated for copper hydroxides, hydrates, iodides, and oxides in various charge states and are shown in Figures 4.2 and S4.13-S4.15 in comparison with the experimental spectrum. The computed spectra in Figure 4.2 are for Cu(I) species and Figure S4.13 for Cu(II) molecules, while Figures S4.14 and S4.15 are for Cu(I)/Cu(II) iodides and Cu(I)/Cu(II) oxides, respectively. We considered these Cu(I)/Cu(II) species in our computational search because water, a base (KOH), and CuI were used in the SM coupling reactions, and the reactions were conducted in air. It is clear from Figures 4.2 and S4.13-S4.15 that only the spectrum of the neutral Cu(OH) (C_s) in its singlet electronic state ($^1A'$) (red) is consistent with the experimental measurement (blue), suggesting that among all Cu species considered only cuprous hydroxide in the singlet electronic state is the active catalyst. The structure of the singlet Cu(OH) molecule is shown in Figure S4.16, and the calculated bond lengths and angle are in agreement with a previous study.[139] Cu(OH) could also be in a triplet electronic state ($^3A'$), but the triplet state has a much higher energy (2.21 eV) than that of the singlet state, and the spectrum of the triplet state showing the absorption maximum at 341 nm is not consistent with the experimental spectrum having the absorption maximum at 222 nm.

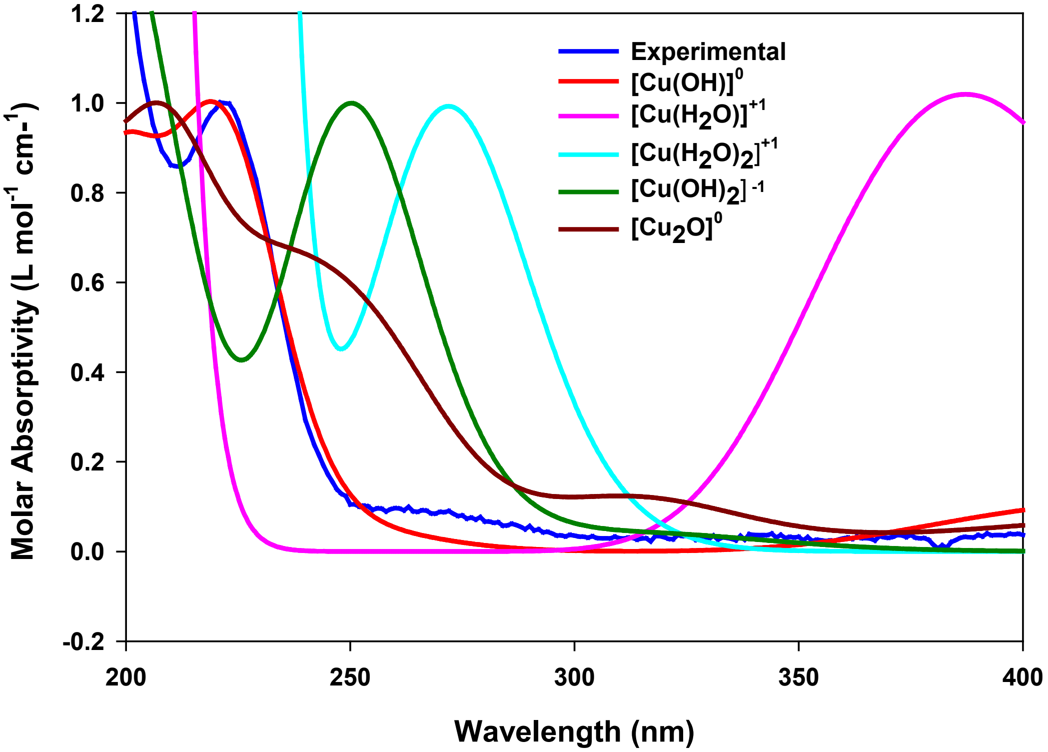

Figure 4.2. Measured UV-Vis spectrum of the inorganic supernatant and TD-DFT/B3LYP calculated spectra of various Cu (I) species with the continuum solvation model.

We then investigated the stability of the water-soluble Cu(OH) catalyst by storing the fresh inorganic supernatant at room temperature for four weeks and found that the SM coupling with the four-week-old supernatant generated biphenyl with 31% yield. This observation demonstrates that the Cu(OH) species is stable for at least four weeks under ambient conditions, a desirable feature for any catalyst. The stability of Cu(OH) in the solution also confirms that the molecule is in the singlet electronic state where all electrons are paired, rather than a triplet state with an unpaired electron. However, a test for the reusability of the Cu(OH) catalyst showed that it could only be recycled for two runs with the third run yielding no product. The exact reason for the low recyclability of Cu(OH) is not clear under the experimental conditions, but it could be due to the formation of catalytically inactive Cu_2O via the decomposition reaction $2Cu(OH) = Cu_2O + H_2O$,[139] the formation of $Cu(OH)_2$ via the oxidation reaction $4Cu(OH) + H_2O + O_2 = 4\ Cu(OH)_2$,[140] or the redeposition of the soluble Cu catalytic species onto the precipitate.[141]

4.3.3 Cu(OH) is generated through leaching of the Cu-containing precipitate

With the identification of the water-soluble Cu(OH) catalyst, we proceeded to investigate its formation. Presumably Cu(OH) could be formed directly in the solution or through leaching of Cu-containing precipitates. In the solution, Cu(OH) could be formed by a dissociation reaction $Cu(OH)_2^- = Cu(OH) + OH^-$ (if $Cu(OH)_2^-$ exists in the solution), or by a double-ligand exchange reaction CuI + KOH = CuOH + KI. However, the dissociation of $Cu(OH)_2^-$ requires an energy of 63(3) kcal mol^{-1}, and the existence of KOH in the reaction mixture makes the dissociation unfavorable.[142] Moreover, because we observed the significant SM product by using the Cu particles prepared with the substrates (Table 4.1), Cu(OH) is unlikely produced directly from reactions in the solution. Instead, Cu(OH) is most likely generated through the leaching of the Cu particles under our experimental conditions, and the leaching is enhanced by the presence of the substrates and increasing temperatures. The effect of the substrates on leaching is evident by the observations presented in Table 4.1, where the SM reaction with the Cu particles produced biphenyl (28 % yield) if they were prepared with the substrates but no products if they were prepared without the substrates. To investigate which substrate enhanced the leaching process, we performed the SM reaction using the soluble Cu species prepared with only iodobenzene or phenylboronic acid and obtained a yield of 35% with iodobenzene and 31% with phenylboronic acid. These observations indicate the presence of both substrates has a larger effect on the leaching (with 44% yield) than a single substrate, which are in contrast to a previous study that reported phenylboronic acid contributed more to the Pd leaching than the aryl halide.[106] Our temperature-dependent experiments showed that the biphenyl yield increased from 0% at room temperature to 34% at 60 ^{0}C to 44% at 80 ^{o}C with the presence of both substrates but 0% at the ambient temperature and 60 ^{o}C and 28% at 80 ^{o}C without substrates. This temperature effect on the leaching of Cu species is consistent with previous reports on leaching of other Cu particles[53] or Pd nanoparticles.[97-98]

4.3.4 Cu_2O Nanoparticles in the Precipitates Serve as the Reservoir for the Cu(OH) Catalyst

4.3.4.1 XPS/Auger Spectroscopy

Because the precipitates serve as a reservoir for the molecular catalyst, we conducted experiments to characterize the Cu particles using X-ray Auger electron and absorption spectroscopies and transmission electron microscopy (TEM). The X-ray spectroscopies were used to determine the oxidation state and local coordination of Cu, while TEM was employed to characterize the size and morphology of the Cu particles. We also measured the Cu 2p photoelectron spectra in the binding energy region of 920-970 eV and observed the main bands at 932.5 eV and at 952.5 eV. But, the Cu 2p electron ionization band is not sensitive to distinguish among various Cu oxidation states (i.e., 0, +1, +2), consistent with previous reports.[143-145] Figure 4.3 presents the LMM Auger electron spectra of the fresh precipitates prepared with and without the presence of the substrates [Figure 4.3(a,b)] and the spent precipitate with the substrate (Figure 4.3c). The fresh precipitates are those with catalytical activity (i.e., 44% and 37% biphenyl yields with and without the substrates, respectively), while the spent precipitate shows no catalytical reactivity. The main bands (red trace) of the spectra in Figure 4.3(a, b) are measured to be at about the same energy (916.5 and 916.4 eV, respectively). They can easily be assigned to Cu (I) $L_3M_{4,5}M_{4,5}$ Auger electron created when a hole in the $2p_{3/2}$ level (L_3) is filled by a $3d_{3/2}$ electron (M_4) with a simultaneous ejection of another $3d_{5/2}$ electron (M_5), [78, 146,143, 147] and the specific Cu(I) species can be assigned as Cu_2O.[148] The weak satellite bands (blue) on both sides of the main band are measured as 920.4 and 912.3 eV, respectively, which correspond to the so-called Coster-Kronig transitions.[146, 148-150] The Coster-Kronig transition of the 912.3 eV peak involves the $L_2L_3M_{4,5}$ Auger electron created when a hole in the $2p_{1/2}$ level (L_2) is filled by a $2p_{3/2}$ electron (L_3) with a simultaneous ejection of a 3d electron ($M_{4,5}$).[146, 149-151]

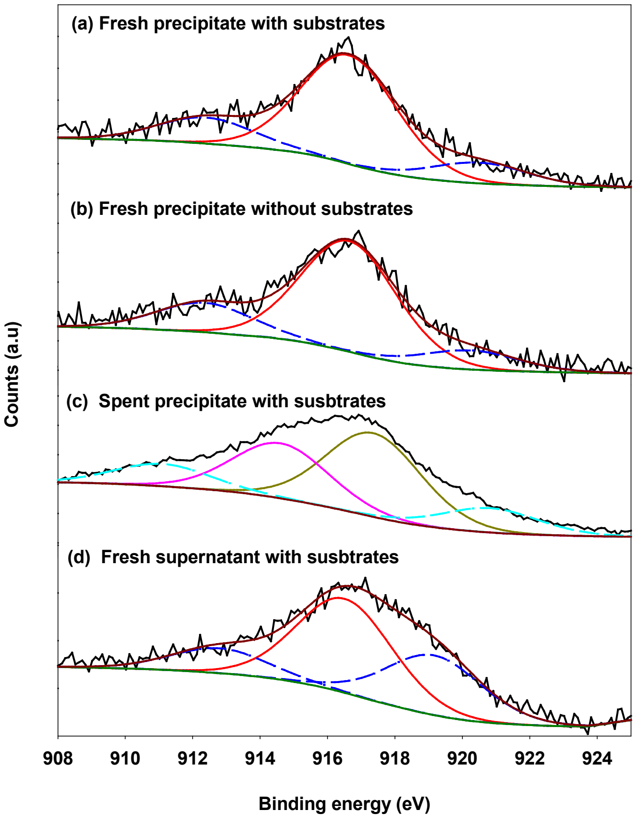

Figure 4.3. Cu Auger LMM spectra of the fresh precipitates with (a) and without (b) the substrates, the spent precipitate (c), and the fresh inorganic supernatant (d).

Compared to the fresh precipitates, the Auger electron spectrum (Figure 4.3c) of the spent precipitate is considerably broader and can be deconvoluted to two bands at 917.3 eV (yellow) and 914.5 eV (pink). Obviously, the main Cu species on the surface of the spent precipitate is not in the Cu(I) oxidation state. For the two fresh precipitates, their Auger spectra are essentially the same, but the precipitate prepared with the substrates generated a high biphenyl yield (44%) than the one without the substates (37 %). This again confirms the presence of the substrates enhances the leaching of the active Cu(OH), rather than generates different Cu particles on the surface of the precipitates. We also measured Auger electron spectrum of fresh inorganic supernatant prepared with the substates by using a higher CuI concentration (0.1875 mmol) in order to obtain a reasonable Auger signal. Its spectrum (Figure 4.3d) displays essentially the same main band position (916.4 eV) as that of the fresh precipitates, which is attributed to Cu(I). The Auger spectrum of the inorganic supernatant is consistent with the UV-VIS spectrum that shows the Cu active species in the Cu(I) oxidation state.

4.3.4.2 Local Coordination of the Pd nanoparticles

Figure 4.4 presents the Cu-K-edge EXAFS fits in the R-space for the fresh (top) and spent (bottom) precipitates prepared with the substrates. The solid traces are the fits for the experimental measurements, while the dashed traces are for the references of Cu-O paths of Cu_2O (top) and CuO (bottom). The overall agreement between the experimental and the Cu-O paths of Cu_2O/CuO fits indicates that the fresh precipitate consists of largely Cu_2O, while the spent sample contains largely CuO.

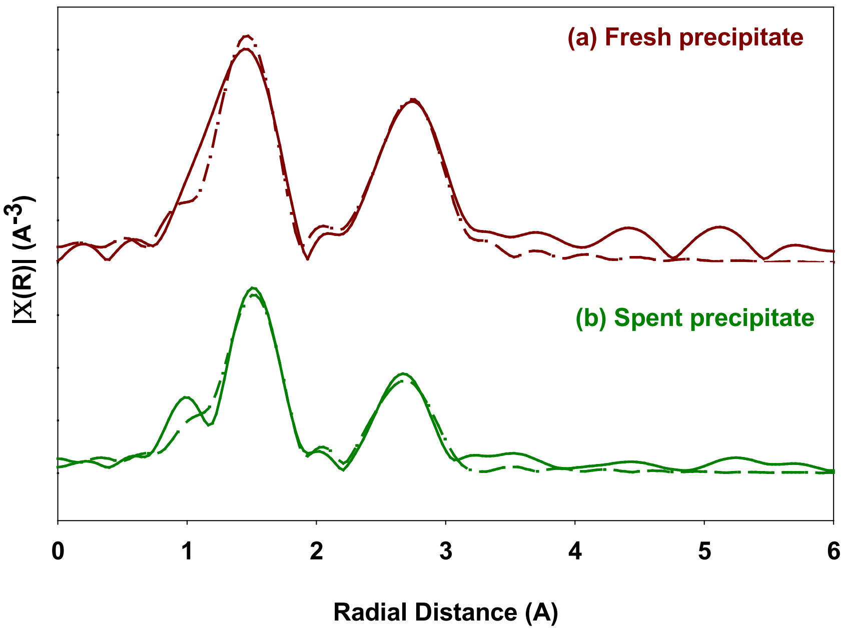

Figure 4.4. Cu K-edge EXAFS single-shell fits in the R-space for the Cu nanoparticles in the fresh (top) and spent precipitates (bottom).

The EXAFS measurement is consistent with the X-ray absorption near edge spectra (XANES) (Figure S4.17), which show that the absorption near edge of the fresh sample is close to that of Cu_2O, while the main rising edge of the spent sample shifts to a higher energy and largely overlaps with that of CuO. The EXAFS parameters of the fits are summarized in Table 4.2. The single-shell fits in Table 4.2 show that the Cu-O coordination number in the first-shell increases from Cu_2O to CuO, while the Cu-Cu coordination number decreases from Cu_2O to CuO, which are in line with the expectation from the viewpoint of the molecular stoichiometries. The Cu-O distance (1.86 ±0.01 Å) of Cu_2O in the first shell is about one-half of that (3.53±0.02 Å) in the second shell and about the same as that in CuO (1.91±0.04 Å). The similar EXAFES fitted Cu-O distances of Cu_2O and CuO in the first shell are comparable with the DFT/B3LYP computed distances of the two oxides (i.e., 1.80 and 1.76 Å, respectively).

Table 4.2. EXAFS parameters from the best single-shell fits depicting coordination numbers, radius, and Debye Waller factor.[a]

Sample	Path	CN	R (Å)	σ^2 (Å^2)	R factor
Fresh precipitate	Cu-O1	2.3 ± 0.4	1.86 ± 0.01	0.005 ± 0.002	0.015
	Cu-Cu	10.4 ± 7.4	3.01 ± 0.02	0.020 ± 0.007	
	Cu-O2	4.9 ± 2.9	3.53 ± 0.02	0.020 ± 0.007	
Spent precipitate	Cu-O	3.3 ± 0.2	1.91 ± 0.04	0.006 ± 0.001	0.009

[a] For the fresh precipitate, Cu_2O was used as the reference for fitting and $\Delta E_0 = 6.70 \pm 0.97$ eV; for the spent precipitate, CuO was used as the reference and $\Delta E_0 = 7.03 \pm 0.64$ eV.

Although Cu(OH) is stable in aqueous solutions, it has not been identified experimentally in the solid phase. However, bulk cuprous hydroxide may be obtained by assembling Cu(OH) molecules into structures that are intermediates between Cu_2O and H_2O as proposed by previous first-principle calculations.[139] Therefore, it should not be surprising for the leaching of Cu(OH) molecules from Cu_2O particles in aqueous solutions observed in this work.

4.3.4.3 Morphology

Figure 4.5 shows the TEM image of the fresh precipitate prepared with the substrates. Most of the Cu(I) particles are observed to have an oval shape, where the average semi-major axis diameter of thirty-three nanoparticles is estimated to be 15 ± 3 nm, while that of the semi-minor axis is 9 ± 4 nm. Interestingly, the TEM observation is consistent with the oval-shaped solvation cavity calculated with polarization continuum model. Because the Cu_2O molecule has non-zero electric dipole (6.08 D) with the positive change on Cu and negative charge on O, intermolecular interactions are expected to orient the molecules in such a way where the positive-charge is pointed to the negative one. We also recorded the TEM images of the spent precipitate (Figure S4.18) and found that the particles are highly agglomerated so that their sizes and shape are not measurable.

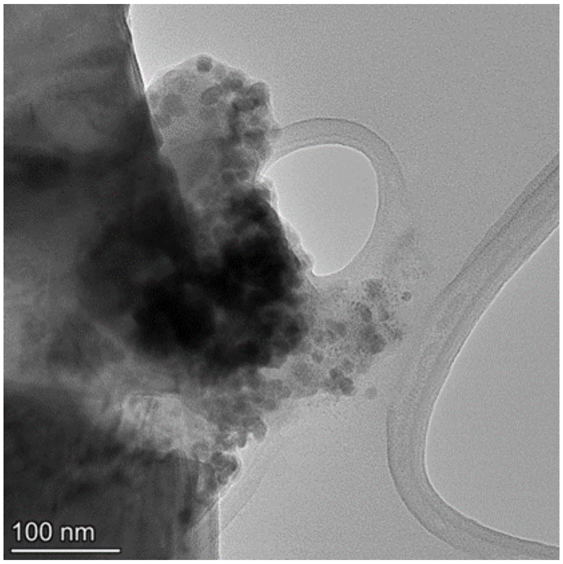

Figure 4.5. TEM image of the fresh precipitate prepared with the substrates.

4.4 Conclusions

In conclusion, we have identified the active Cu catalyst and its form in the SM coupling between benzene iodide and phenylboronic acid with copper iodide as a precatalyst. The SM coupling is homogenous in nature without any stabilizing organic ligands. The active catalyst is Cu(OH) in its singlet electronic state, which is stable in aqueous solutions for at least four weeks at the room temperature. The molecular catalyst is generated through the leaching of the oval-shaped Cu_2O nanoparticles on the solid surface at elevated temperatures, and the leaching is enhanced by the presence of the reaction substrates. Although this work is conducted with copper iodide as the precatalyst, we envision that the conclusions arrived in this study about the active catalyst will likely be valid for SM reactions with other inorganic Cu salts in aqueous solutions.

4.5 Supporting Information

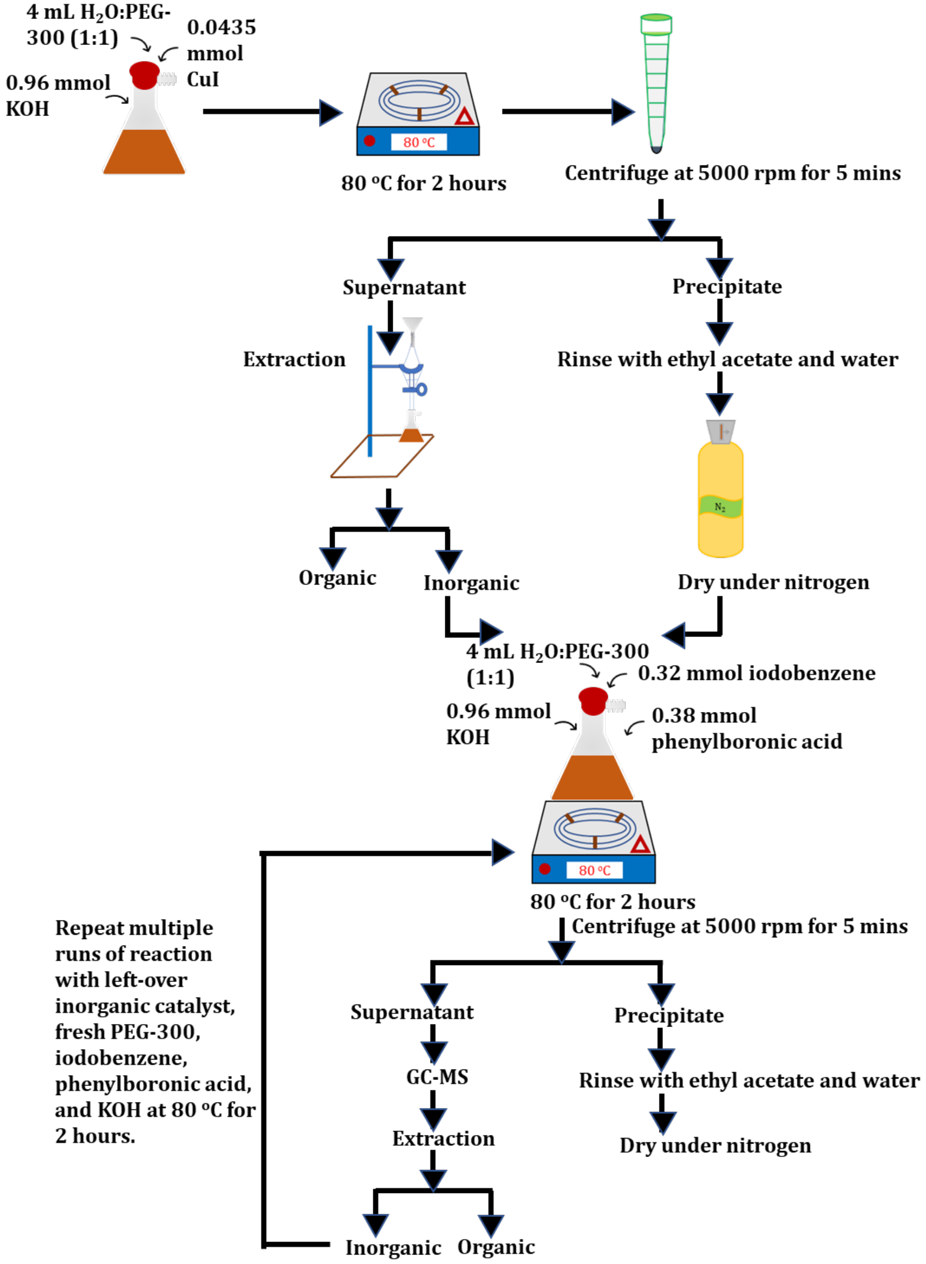

Figure S4.6. Experimental flowchart depicting catalyst preparation, reaction conditions, steps for the purification of the crude product, and recyclability of the precipitate and soluble catalysts. The catalyst was prepared without the iodobenzene and phenylboronic acid substrates.

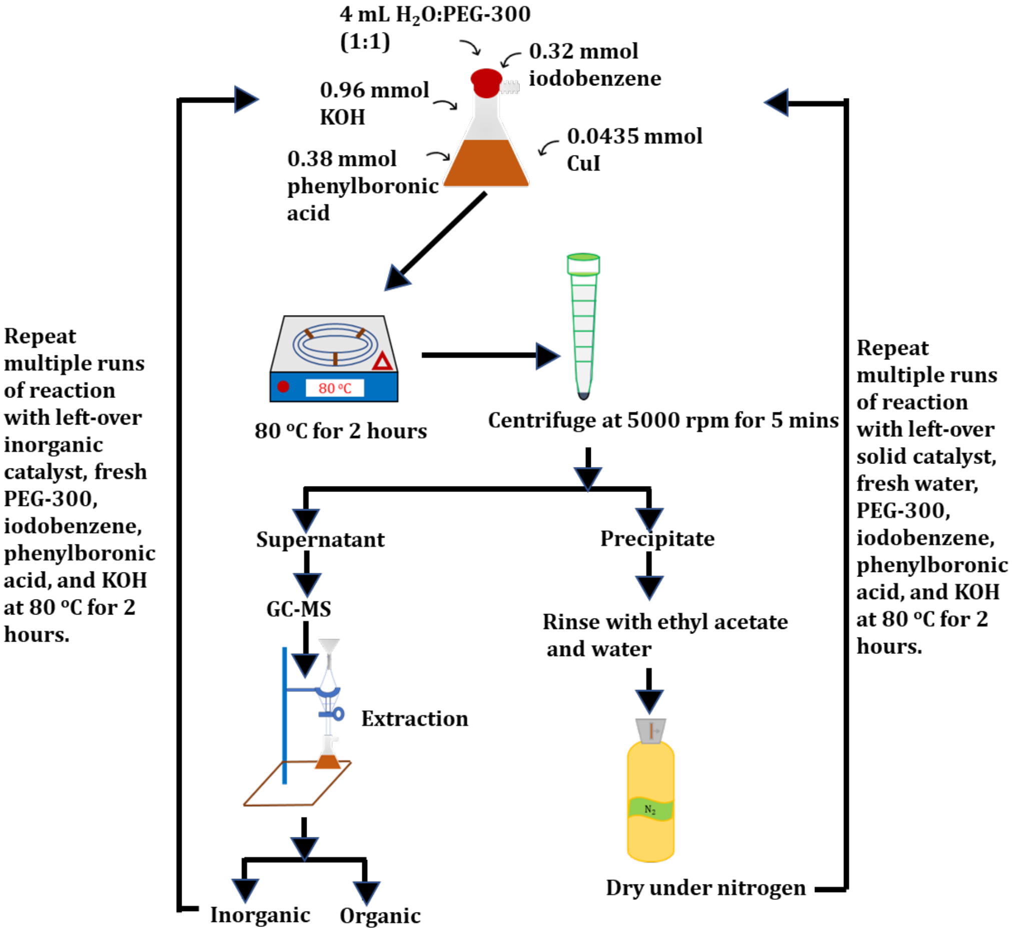

Figure S4.7. Experimental flowchart depicting reaction conditions, steps for the purification of the crude product, and recyclability of the precipitate and soluble catalysts. The catalyst was prepared with the iodobenzene and phenylboronic acid substrates.

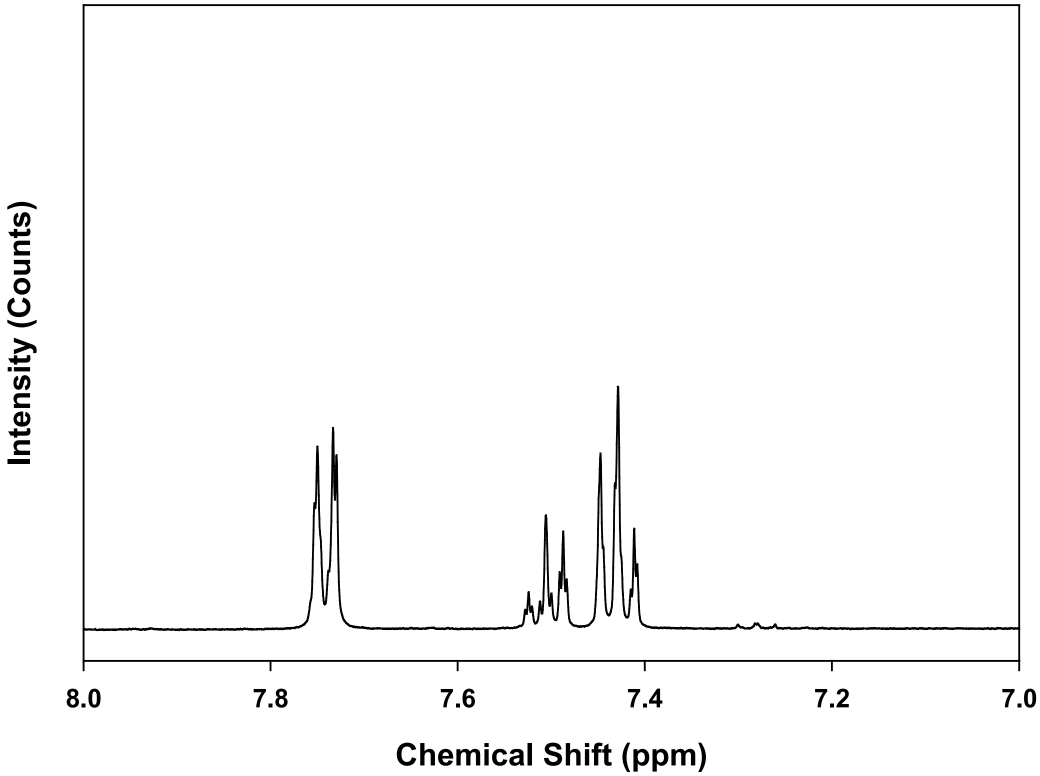

Figure S4.8. ^{1}H NMR (400 MHz, D_2O) of biphenyl: δ (ppm) 7.74(dd, J = 8.3, 1.5 Hz, 4H), 7.51(t, J = 8.0 Hz, 4H), 7.43(t, J = 8.0 Hz, 2H).[152-154]

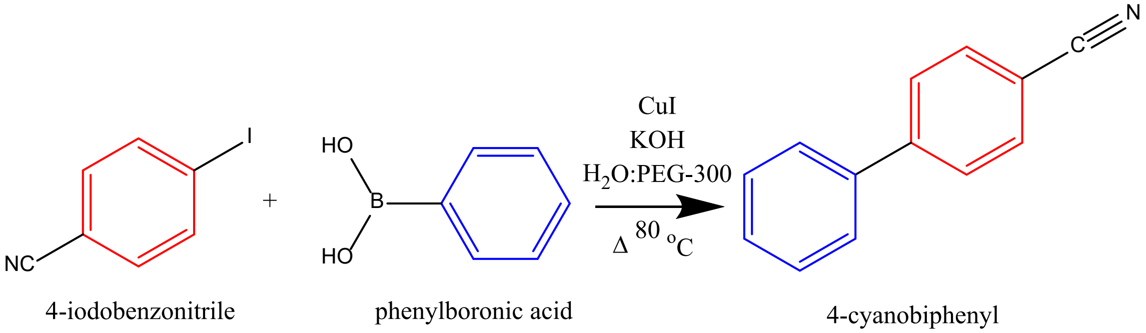

Figure S4.9. Schematic representation of the reaction conditions of the control experiment between C_7H_4IN and $C_6H_5B(OH)_2$.

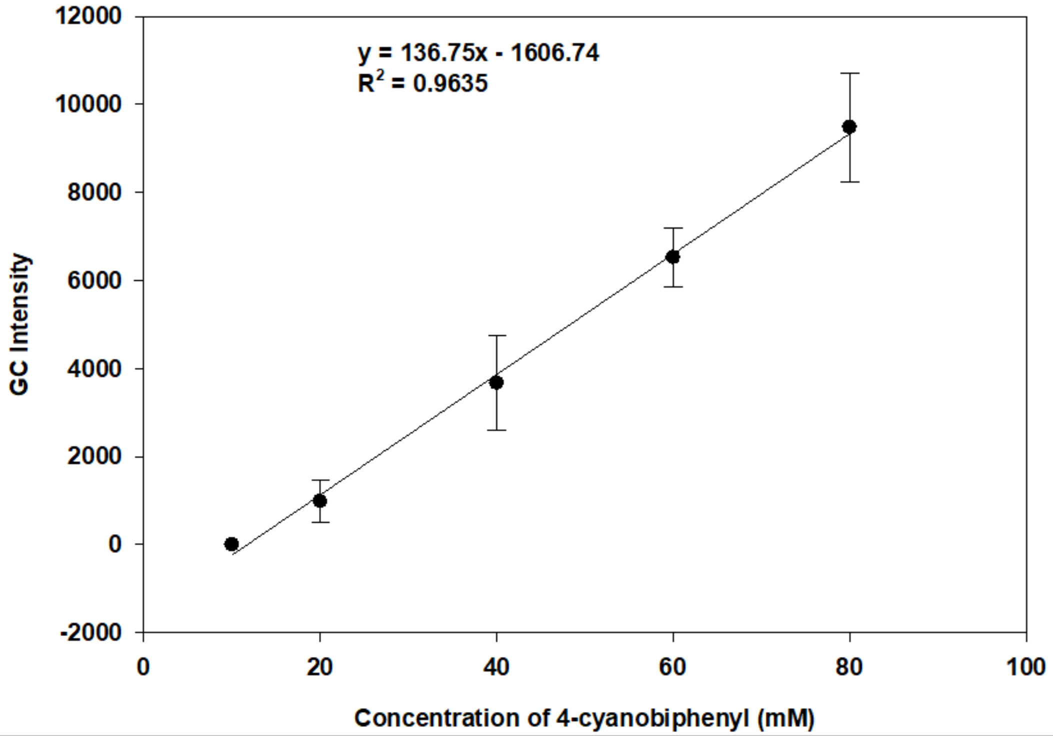

Figure S4.10. Calibration curve of pure 4-cyanobiphenyl for determining the yields of 4-cyanobiphenyl produced in the control SM reaction between C_7H_4IN and $C_6H_5B(OH)_2$. Triplicates of 80-, 60-, 40-, 20-, and 10-mM solutions were prepared from a stock solution of 100 mM. Each sample was injected into the GC-MS instrument to yield a certain GC intensity. The error bars correspond to the GC intensities of three samples at each concentration.

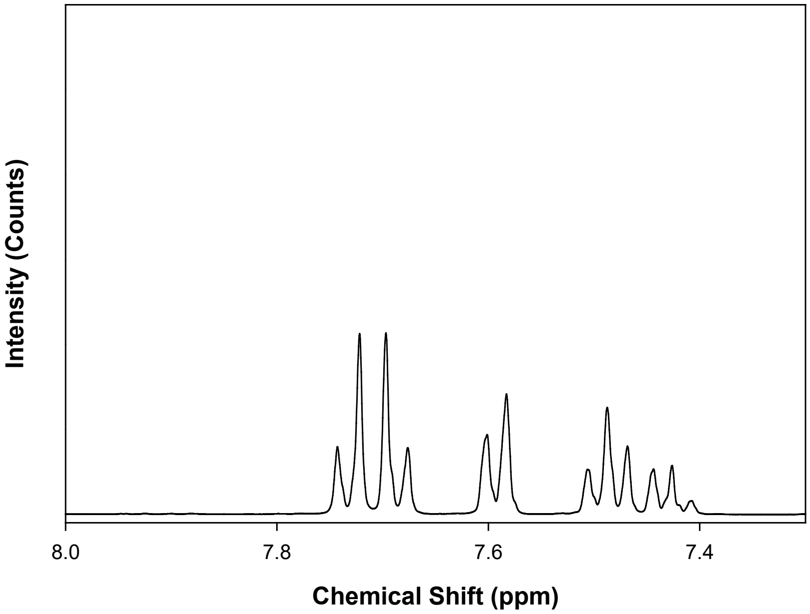

Figure S4.11. ^{1}H NMR (400 MHz, $CDCl_3$) of 4-cyanobiphenyl : δ (ppm) d: 7.71 (q, J = 8.3, 9.9, 8.4 Hz, 4H), 7.59 (d, J = 7.2 Hz, 2H), 7.49 (t, J = 7.6Hz, 2H), 7.43 (t, J = 7.2 Hz, 1H).[153, 155]

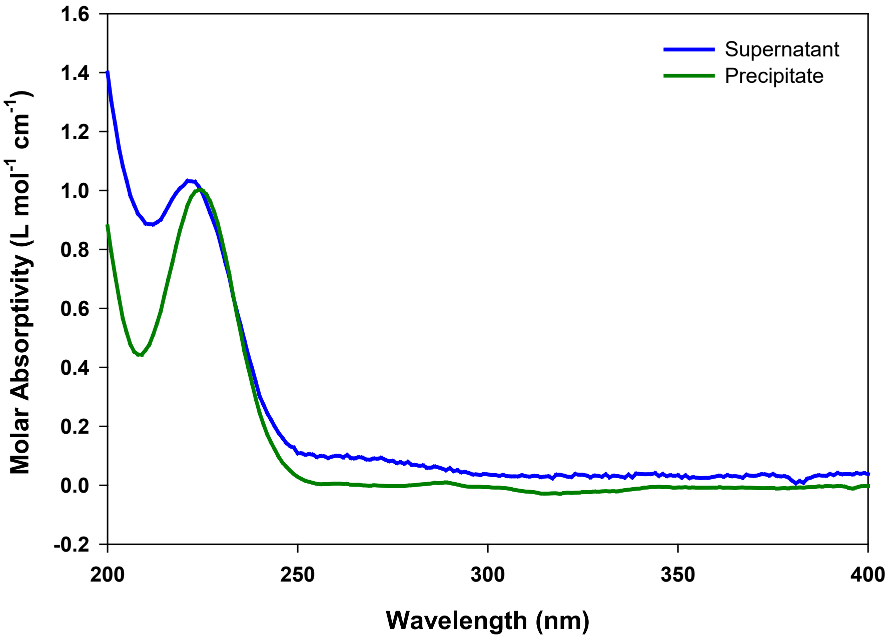

Figure S4.12. Measured UV-Vis spectra of the inorganic supernatants extracted from the soluble mixture and precipitate prepared with the substrates.

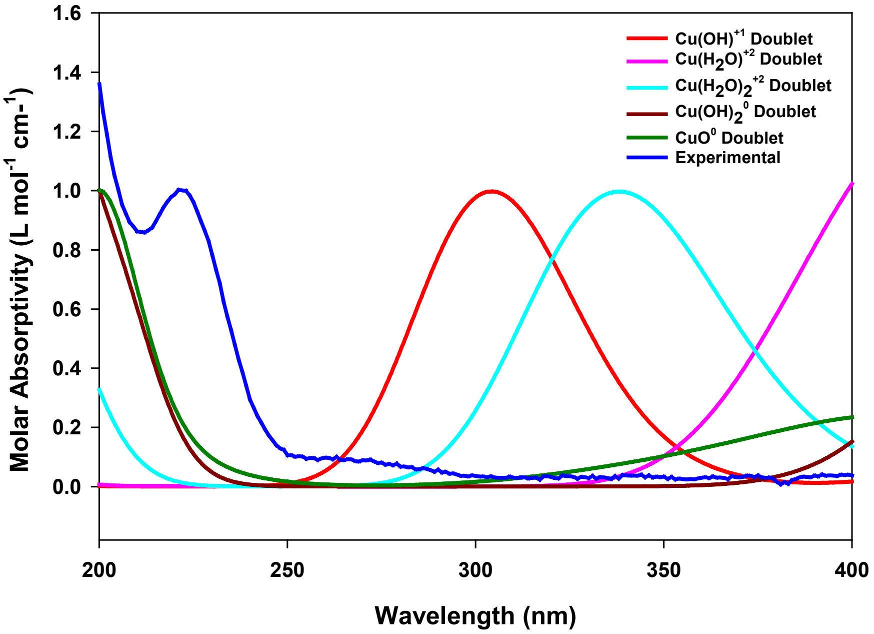

Figure S4.13. Measured UV-Vis spectrum of soluble Cu species and calculated spectra of Cu (II) species by TD-DFT calculations with water as the solvent and the continuum solvation model. The basis set used for Cu, O, and H is Aug-cc-pVTZ.

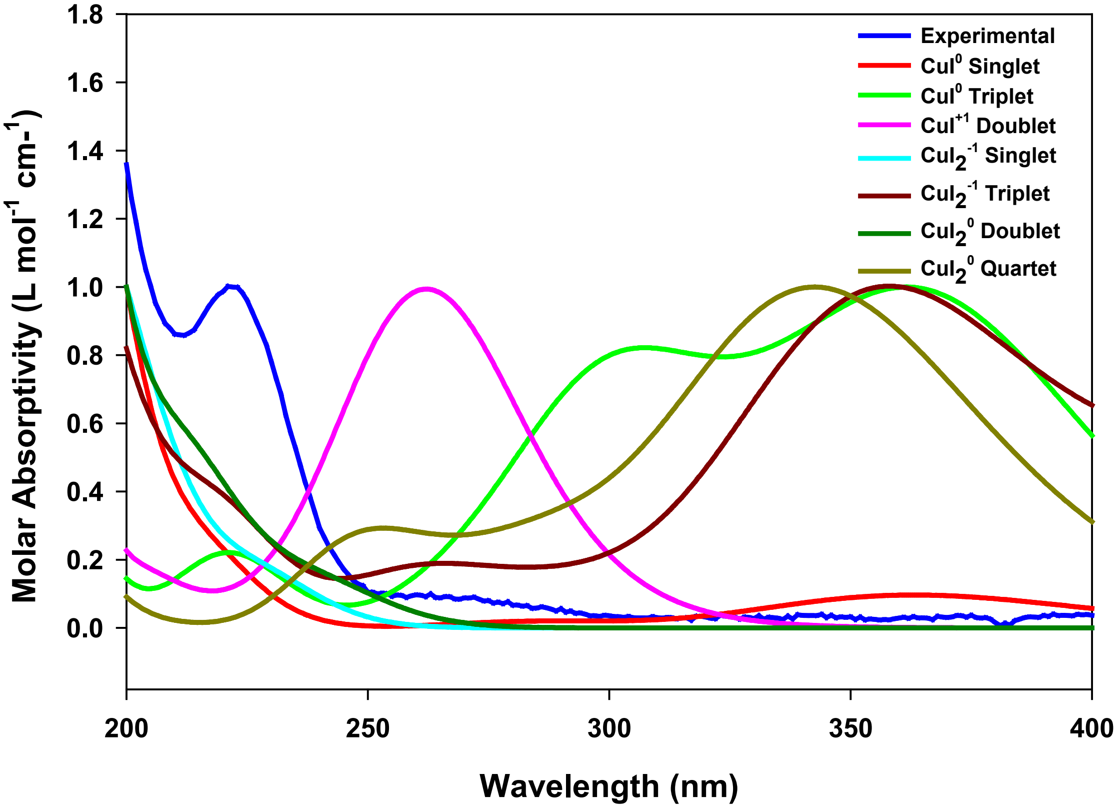

Figure S4.14. Measured UV-Vis spectrum of soluble Cu species and calculated spectra of various Cu(I) species by TD-DFT calculations with water as the solvent and the continuum solvation model. The charge stated after the name of the species in the legend corresponds to the charge of the whole molecule. The basis set used is LanL2DZ.

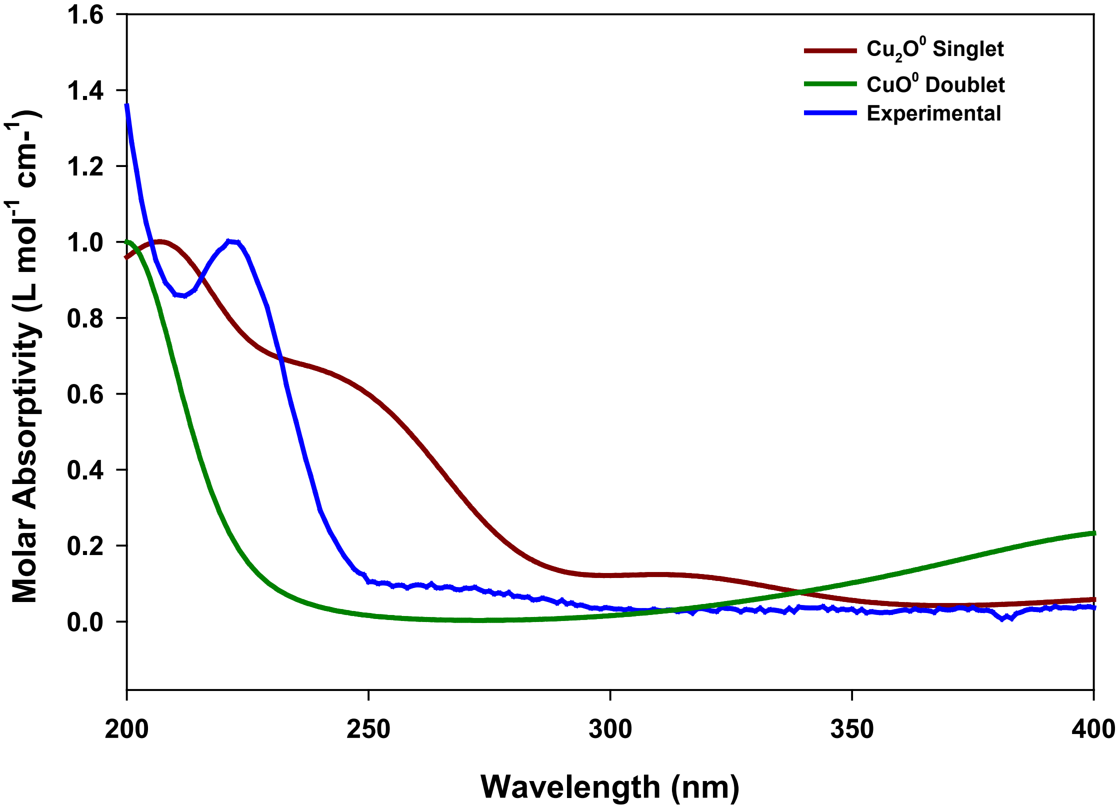

Figure S4.15. Measured UV-Vis spectrum of soluble Cu species and calculated spectra of Cu_2O and CuO by TD-DFT calculations with water as the solvent and the continuum solvation model. The basis set used for both Cu and O is Aug-cc-pVTZ.

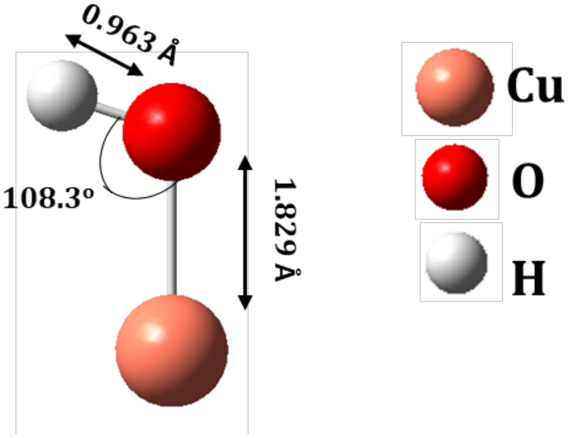

Figure S4.16. Structure of the neutral Cu(OH) in its $^1A'$ (C_s) singlet electronic state.

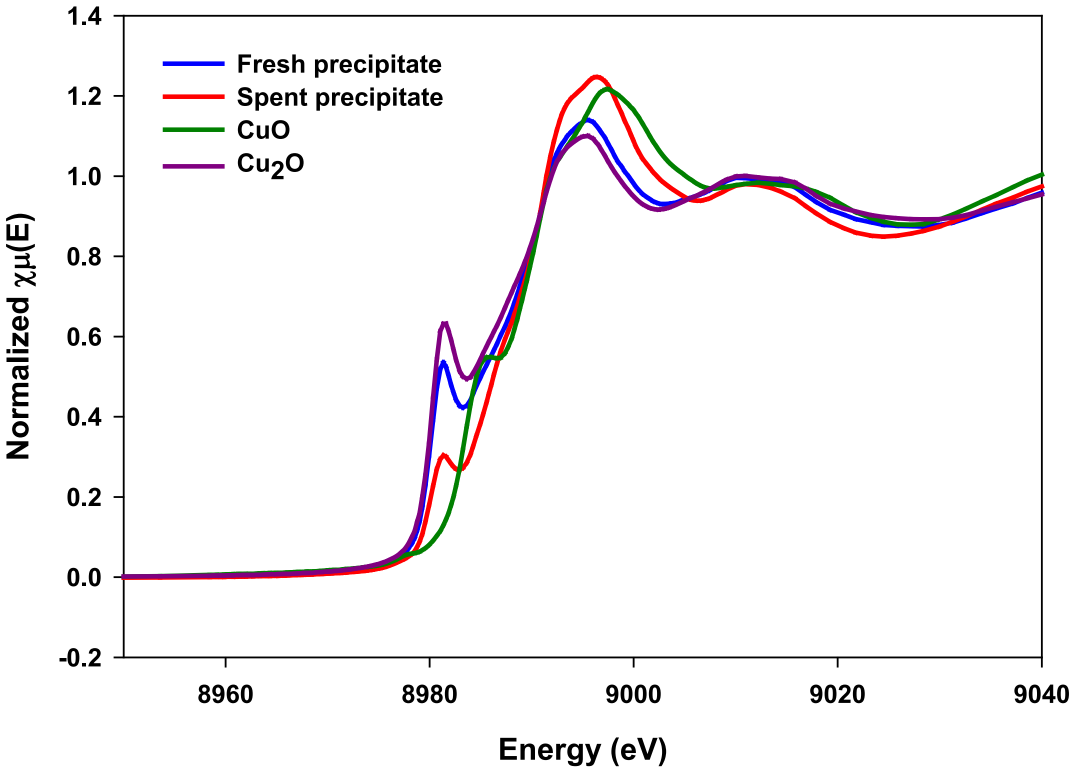

Figure S4.17. Cu XANES spectra after normalization. The absorption near edge of the fresh precipitate sample (blue) closely resembles that of Cu_2O (purple), while the main rising edge of the spent precipitate sample (red) shifts to higher energy and largely overlaps with that of CuO (green), indicating the oxidation of the nanoparticles after the final run.

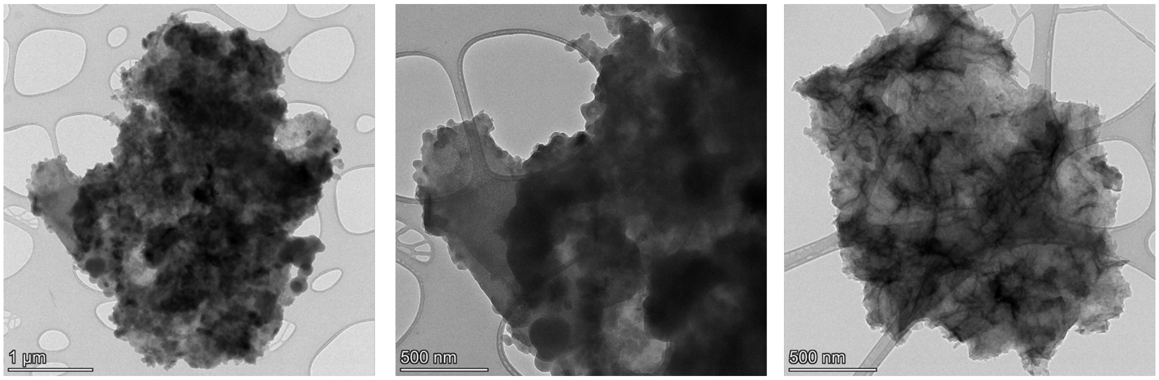

Figure S4.18. TEM images of the spent Cu nanoparticles after the SM reaction showing a high agglomeration of the particles.

CHAPTER 5. WATER-SOLUBLE NICKEL CATALYST AND ITS FORMATION IN LIGAND-FREE SUZUKI-MIYAURA CROSS-COUPLING REACTIONS

5.1 Introduction

SM cross-coupling that uses an organoboron nucleophile and an organic halide electrophile as coupling partners has important applications in pharmacy, agriculture, and precursors for materials.[1, 23, 57, 86-90] Pd has dominated as a catalyst for such reactions since the late 1970s because it offers a high stability, C-H activation ability, and can catalyze chemical reactions even when present in trace amounts.[1, 22-23, 44, 114-116] However, the development of the Ni catalysts due to lower cost, more reactivity to some electrophiles, and higher abundance than Pd has made Ni an increasing choice of catalyst in SM reactions.[55, 156-161] A survey of the literature suggests that more studies on the Ni catalyzed SM cross-coupling reactions have been performed in ligand-stabilized systems than the ligand-free ones.[156-157, 162-170] However, there is a scarcity of studies investigating the nature of catalysis, or the chemical identity of the Ni active catalyst is under debate.[157, 162, 164-165, 171-172]

For homogeneous ligand-stabilized Ni-catalyzed cross-coupling reactions, various active catalysts of Ni have been reported.[162, 165, 173-175] These reactions included the coupling of aryl sulfamates and boronic acids catalyzed by the ligand-stabilized Ni(0) species with (1,1′-bis(diphenylphosphino) ferrocene) $\mathrm{Ni^{II}}$(*o*-tolyl)(Cl) as the precatalyst,[162] the coupling of 2- aryl chlorides/bromides and phenylboronic acids catalyzed by the proposed Ni(0) species with phosphine ligand-supported Ni(0) or $\mathrm{Ni^{II}}$ complexes as precatalysts,[174-175] aryl bromides and phenylboronic acids catalyzed by the Ni (I) complex with the precatalyst made up of Ni(0) - 1,3-bis(2,4,6-trimethylphenyl)imidazol-2-ylidene ligand complexes,[165] and the coupling of 2-chloronaphthalene and 4-methoxyphenylboronic acid catalyzed by the Ni(I) species with phosphine ligand-supported Ni(0) or $\mathrm{Ni^{II}}$ complexes as precatalysts.[173] In an example of heterogeneous catalysis, molecular nickel catalyst [(2,2′:6′,2″-terpyridine-4′-benzoic acid)Ni(II)]Cl_2 (COOH-Ni) attached to a SiO_2 support is stated to be the active catalyst in the coupling between iodotoluene and phenylboronic acid, while the leaching of COOH-Ni from the surface of SiO_2 causes catalyst deactivation.[176] The findings were characterized by Inductively coupled plasma mass spectrometry (ICP-MS) and X-ray diffraction (XRD).[176]

Although Ni-catalyzed SM cross-coupling reactions with stabilizing ligands have been reported consistently to be homogeneous, not a rigorous study has been performed on the nature of catalysis and the identity of catalytically active species for ligand-free Ni catalysis.[177-179] These reactions included the coupling of 4-bromoanisole and phenylboronic acid with $NiCl_2 \cdot 6H_2O$ as the precatalyst,[177] the coupling of 4-iodotoluene and phenylboronic acid with Ni powder as the precatalyst,[179] where the active catalyst was not investigated in either of these literatures, and the coupling of 4-bromotoluene and phenylboronic acid with $NiBr_2$ as the precatalyst where the active species of Ni(0) was assumed without experimental evidence.[178] Similarly, for Ni-catalyzed SM cross-coupling reaction undergoing heterogeneous catalysis, the coupling of iodobenzene and phenylboronic acid with the synthesized Ni(II)-α-diimine- porous organic polymers as the precatalyst was performed where the catalytically active species of Ni(0) was also assumed without experimental evidence.[164] Another example of heterogeneous Ni-catalyzed SM coupling reaction was reported for the homocoupling of arylboronic acid with the synthesized nickel nanoparticles supported on reduced graphene oxide (RGO-Ni) as the precatalyst.[180] Here, the catalytically active species of Ni(0) was further only speculated and was stated to be present on the graphene surface. No leaching of the Ni nanoparticles from the RGO–Ni precatalyst was detected using inductively coupled plasma optical emission spectroscopy (ICP-OES).[180]

The reaction mechanism for the Ni-catalyzed SM cross-coupling includes three steps: oxidative addition, transmetalation, and reductive elimination. The two possible mechanisms include the Ni(0)/Ni(II) cycle in the order of oxidative addition, transmetalation, and reductive elimination, or the Ni(I)/Ni(III) cycle in the order of transmetalation, oxidative addition, and reductive elimination.[157]

Without the use of stabilizing ligands, ligand-free Ni-catalyzed SM cross-coupling offers several benefits, including the readily available and easily recoverable precatalysts, less air-sensitive chemical reactions, and less-painstaking purification methods to isolate the products. Although the work in the chemical identity of Ni catalyst presented in this dissertation is still ongoing, preliminary results suggest that the ligand-free SM coupling between 4-iodotoluene and phenylboronic acid is homogeneous in nature with Ni(0) powder as a precatalyst. The water-soluble active Ni(0) catalyst is generated from the leaching of Ni(0) nanoparticles, and the leaching and reactivity are enhanced from ambient temperature to 110 °C. The SM coupling reaction is presented in Figure 5.1.

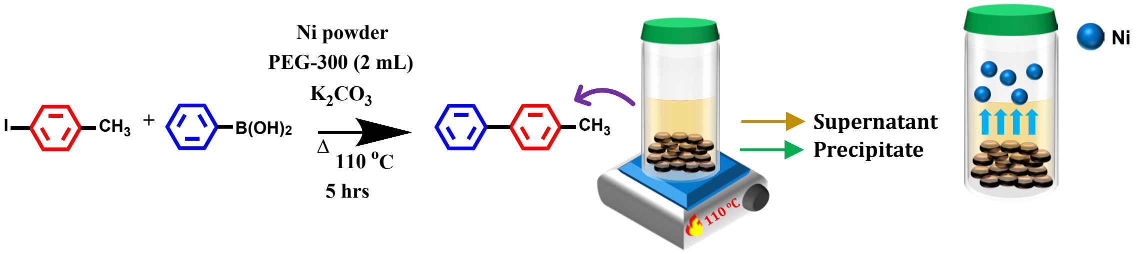

Figure 5.1. Schematic representation of the water-soluble Ni catalyst leached from Ni-containing precipitates catalyzes the SM coupling between C_7H_7I and $C_6H_5B(OH)_2$ with Ni(0) powder as a precatalyst.

5.2 Experimental

5.2.1 Materials

Nickel (0) powder (99%) was purchased from Sigma-Aldrich, 4-iodotoluene (98%) from Thermo Scientific Chemicals, phenylboronic acid (99% HPLC) from Chem Impex International, potassium carbonate (99%) from VWR, polyethylene glycol 300 (99%) was purchased from TCI America, and 4-phenyltoluene (98%) from Ambeed. All the chemicals were used without further purification. Millipore deionized water was used in all the experiments.

5.2.2 Catalyst Preparation and SM Reactions

The SM reaction conditions, including solvents, base, and temperatures, were adapted from the literature.[136, 179]

5.2.2.1 Catalyst preparation without substrates and SM reactions

In a reaction vial, the catalyst was prepared using 2.93 mg (0.05 mmol) of Ni(0) powder and 0.276 g (2 mmol) of K_2CO_3 dispersed in a solution of 2 mL PEG-300. The flask was kept in an oil bath at 110 ^{o}C for 5 hours under constant magnetic stirring. The vial was capped, and the reaction was done in air. After the reaction, the mixture was separated into a supernatant and a precipitate by centrifugation at 5000 rpm for 5 minutes, and the supernatant and precipitate were then placed in two separate vials for future reactions.

Reactions with the precipitate: The precipitate was cleaned with 2 mL of ethyl acetate and then with 2 mL of water by centrifuging at 5000 rpm for 5 minutes twice and later dried under nitrogen flow for half an hour. The nitrogen-dried precipitate was used as a catalyst for the first reaction at 110 ^{o}C for 5 hours and with 0.2 g (1 mmol) of 4-iodotoluene, 0.146 g (1.2 mmol) of phenylboronic acid, and 0.276 g (2 mmol) of K_2CO_3 in a solution of 2 mL PEG-300. The reaction vial was capped, and the reaction was done in air. After the reaction, the reaction mixture was again separated into a supernatant and a precipitate by centrifugation at 5000 rpm for 5 minutes. Because any coupling product would be in the solution phase, the solution was injected into the GC-MS for product identification. A flowchart of the reaction experiment is shown in Figure S5.4.

Reactions with the supernatant: The supernatant was extracted with ethyl acetate and water three times resulting in clearly separated organic and inorganic phases. The organic phase was discarded, whereas the inorganic phase was used for further reactions and characterizations. The inorganic layer was then added with 2 mL of PEG-300, 0.2 g (1 mmol) of 4-iodotoluene, 0.146 g (1.2 mmol) of phenylboronic acid, and 0.276 g (2 mmol) of K_2CO_3 to perform the reaction at 110 °C for 5 hours. After the reaction, the reaction product, 4-phenyltoluene, was measured with the GC-MS analysis. The reaction mixture was also extracted three times with ethyl acetate and water to collect the organic and inorganic layers. The organic layer was discarded, and the inorganic layer was again added with fresh PEG-300, 4-iodotoluene, phenylboronic acid, and K_2CO_3 to perform the reaction at 110 °C for 5 hours. The procedure was repeated for additional runs until no product was detected.

5.2.2.2 Catalyst preparation with substrates and SM reactions

In a reaction vial, 2.93 mg (0.05 mmol) of Ni(0) powder, 0.2 g (1 mmol) of 4-iodotoluene, 0.146 g (1.2 mmol) of phenylboronic acid, and 0.276 g (2 mmol) of K_2CO_3 were dispersed in a solution of 2 mL PEG-300. The flask was kept in an oil bath at 110 °C for 5 hours under constant magnetic stirring. The vial was capped, and the reaction was done in air. After the reaction, the mixture was separated into a supernatant and a precipitate by centrifugation at 5000 rpm for 5 minutes, and the supernatant and precipitate were then placed in two separate vials for future reactions. The coupling product, 4-phenyltoluene, in the supernatant was measured through GC-MS analysis.

Reactions with the precipitate: The precipitate was cleaned with 2 mL of ethyl acetate and then with 2 mL of water by centrifuging at 5000 rpm for 5 minutes twice and then dried under nitrogen flow for half an hour. The nitrogen-dried precipitate was used as a catalyst for the next run also at 110 ºC for 5 hours and with the same amount of fresh 4-iodotoluene, phenylboronic acid, K_2CO_3, and PEG-300. The procedure was repeated for additional runs until no product was detected. A flowchart of the reaction experiment is shown in Figure S5.5.

Reactions with the supernatant: After the extraction of the organic layer in the supernatant, the inorganic layer was collected and extracted three times with ethyl acetate and water to remove any remaining organic compounds. The inorganic layer was then added with fresh PEG-300, 4-iodotoluene, phenylboronic acid, and K_2CO_3 to perform the reaction at 110 ºC for 5 hours. The procedure was repeated for additional runs until no product was detected.

5.2.3 Characterization

5.2.3.1 GC-MS

GC-MS analysis of the reaction product was performed using an Agilent Technologies 6890N GC with split injection and 5973 Mass Selective Detector (MSD). Ultra-high purity He gas (99.999%) was used as the carrier gas at 0.5 mL/min after passing through an oxygen and moisture trap. Samples for the GC-MS analysis were prepared at a concentration of 1 mg/mL in an ethyl acetate solvent. Following automated injection of 0.1 mL, the oven was held at 70 °C for 3 minutes, then ramped at 10 °C/min to 280 °C, where it was held for 22 minutes to complete the run.

5.2.3.2 ^{1}H NMR

^{1}H NMR experiments were collected on a 400 MHz Bruker AVANCE NEO (Billerica, MA, USA) equipped with a 5 mm smart probe. The solvents used was deuterated chloroform ($CDCl_3$).

5.2.3.3 UV-Vis

UV-Vis absorption spectra were collected using an Evolution™ 201 UV-Vis spectrophotometer. Data were obtained using a baseline flatness of 200 to 700 nm, a data interval of 1 nm, a spectral bandwidth of 1.0 nm, and an integration time of 2.5 seconds. The blanks were performed using water. UV-Vis samples were prepared using 10 µL of the sample and 2 mL of water as the solvent. UV-Vis was measured for the inorganic layer of the supernatant phase for each run so as to avoid any interference from the organics (reactants, solvent, or products).

5.2.3.4 XPS

XPS data was collected X was collected using a Thermo VG Scientific Sigma Probe system with an Al K_α X-ray source (1486.3 eV) at an energy resolution of 0.47 eV full width at half maximum (FWHM) under ultrahigh vacuum (10^{-8} Torr). The samples for XPS measurements were prepared using the drop-casting method. First, 1µL of the Ni-containing suspension in water was drop casted on a silicon (Si) wafer. Then, it was dried in the oven for 10 minutes. This drop-casting method was repeated several times to ensure uniform spreading of the sample on the Si wafer. Ni 2p XPS spectra were obtained with 10 scans in the range 845 to 885 eV, with a spot size of 400 µm. Deconvolution of the XPS spectra was performed using Thermo Avantage software with a FWHM of 1.50 eV for each peak and a 30% Lorentzian/Gaussian mixed convolution.

5.2.3.5 XAS

XAS spectra were collected at 20-BM beamline of the Argonne National Laboratory. A Si (111) double-crystal monochromator beam was focused by toroidal mirror. Harmonic rejection was facilitated by using a sRh-coated mirror (4 mrad) as well as a 15% detuning of the beam intensity at 9300 eV. 100% N_2 gas was used for all ionization chambers. Details on the beamline optics and instruments can be found elsewhere.[101] The solid samples were measured on the Kapton tape in transmission mode at room temperature. Several spectra were collected for each sample to ensure the reproducibility of the spectra and good signal-to-noise ratios. Samples were scanned at energies near the Ni K absorption edge (8,332.8 eV). The standard Ni foil was scanned simultaneously, between the transmission and reference ionization chambers and used for calibration. Extended X-ray absorption fine structure (EXAFS) at the Ni K-edge was recorded at room temperature and the Ni local coordination environment was determined using the EXAFS data. EXAFS oscillations were extracted using Athena code and analyzed using Artemis software.[102] The Ni foil was analyzed first and used to determine the amplitude reduction factor (S_0^2), which was fixed. The photoelectron energy origin correction (ΔE_0), coordination numbers (N), distances (R), and Debye-Waller factor (σ^2) were treated as adjustable parameters during the fitting process. The EXAFS fitting were done within the R range of 1.0 - 3.0 Å, and the k range of 3.0 -10.0 $Å^{-1}$ under the k^2-weighted $\chi(k)$ functions with Hanning windows (dk=1.0$Å^{-1}$).

5.2.3.6 TEM

TEM images were obtained using FEI Talos F200X. The energy of the field emission gun was maintained at 200 keV. The resolution was kept at 0.16 nm. A high-speed Ceta camera of 16 megapixel with 40 frames per second was operated at 4K resolution. TEM samples were prepared by dispersing a small amount of the isolated Ni-containing precipitate in ethanol and by sonicating the mixture for 30 minutes. Then, 10 μL of the diluted solution mixture was drop-cast onto a 300 mesh Au grid with a lacey carbon film.

5.3 Results and Discussion

5.3.1 SM Coupling is Catalyzed by Homogeneous Catalytic Mechanism

Two sets of experiments were performed independently to investigate if the reaction proceeded with a homogeneous or heterogenous catalytic mechanism, one with water-soluble Ni species and the other with the Ni-containing precipitates. The soluble Ni species and Ni precipitates were isolated from catalytical mixtures that were prepared at 110 °C in two batches: one with the 4-iodotoluene and phenylboronic acid substrates (batch A) and the other without them (batch B), both in the presence of Ni(0) powder, potassium carbonate, and polyethylene glycol (PEG-300). After the separation of the two layers, the soluble Ni species were present in the light-yellow inorganic layer of the supernatant after aqueous extraction, while the solid Ni particles resided in the black precipitate. These supernatant and precipitate layers were then used to perform the reactions at 110 °C for five hours with fresh reactants, base, and solvent. The details of the chemicals used, the SM reactions, the separation of the two layers are presented in Figures S5.4 and S5.5, and the results are summarized in Table 5.1. The yields of the coupling product, 4-phenyltoluene, were measured by GC-MS (Figure S5.6). 4-phenyltoluene was also characterized with ^{1}H NMR spectroscopy (Figure S5.7). As shown in the table, both the soluble and solid Ni prepared from batch A exhibit a higher 4-phenyltoluene yield than that with batch B.

Table 5.1. SM coupling of 4-iodotoluene and phenylboronic acid catalyzed by soluble Ni species and solid Ni particles isolated from catalytical mixtures.

Mixture[a]	Yield (%) with soluble Ni species[b]	Yield (%) with solid Ni particles[b]
With substrates (batch A)	84	37
Without substrates (batch B)	46	23

[a] In both cases, the mixtures consisting of Ni(0) powder (0.05 mmol), K_2CO_3 (2.0 mmol) and 2 mL of PEG-300 were stirred in air at 110°C for 5 h. The amounts of 4-iodotoluene and phenylboronic acid were 1.0 and 1.2 mmol, respectively.
[b] Yields of 4-phenyltoluene were measured with GC-MS. SM coupling reactions of 4-iodotoluene and phenylboronic acid were carried out with stir in air at 110°C for 5 h in the solution of K_2CO_3 (2.0 mmol) and 2 mL of PEG-300.

5.3.1 Reusability and stability of the water-soluble Ni catalyst

We then investigated the reusability and stability of the water-soluble Ni catalyst. Figure 5.2a and 5.2b present the yields of 4-phenyltoluene obtained from several runs by using the soluble and solid Ni isolated from the mixture with and without the substrates, respectively. Each run was carried out in triplicate. The higher yield observed in the reactions with the substrates is consistent with previous studies Pd and Cu.[106, 136] To test the stability of the soluble Ni species in the solution, we performed the SM coupling after the fresh inorganic supernatant was stored at room temperature for 14 weeks and found the reaction generated 4-phenyltoluene with 35% yield. This observation shows the water-soluble Ni species is reasonably stable under ambient conditions, a clearly desirable property for any catalysts.

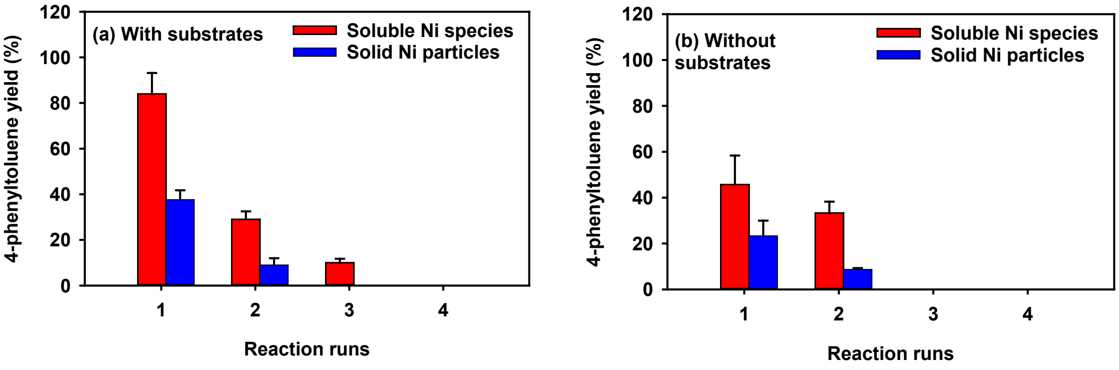

Figure 5.2. Comparison of 4-phenyltoluene yields of the SM reaction catalyzed with (a) and without the substrates (b) with soluble Ni species (red) and Ni(0) particles (blue). The yields were measured with GC-MS.

5.3.2 Ni is Generated Through Leaching of the Ni-Containing Precipitate

Presumably the active Ni(0) catalyst could be formed directly in the solution or through leaching of Ni-containing precipitates. Because we observed the significant SM product by using the Ni particles prepared with the substrates (Table 5.1), the active Ni(0) catalyst is unlikely produced directly from reactions in the solution. Instead, active Ni(0) catalyst is most likely generated through the leaching of the Ni particles under our experimental conditions, and the leaching is enhanced by the presence of the substrates and by increasing temperatures. To investigate which substrate enhanced the leaching process, we performed the SM reaction using the soluble Ni species prepared with only 4-iodotoluene or phenylboronic acid and obtained a yield of 28% with 4-iodotoluene and 0% with phenylboronic acid. These observations indicate the presence of both substrates has a larger effect on the leaching (with 84% yield) than a single substrate, which are in contrast to a previous study that reported phenylboronic acid contributed more to the Pd leaching than the aryl halide.[106] Our temperature-dependent experiments showed that the 4-phenyltoluene yield increased from 0% at room temperature to 55% at 60 ^{0}C to 70% at 80 ºC to 84% at 110 ºC with the presence of both substrates but 0% at the ambient temperature and 60 ºC, 18% at 80 ºC, and 46% at 110 ºC without substrates. This temperature effect on the leaching of Ni species is consistent with previous reports on leaching of other Ni particles[164], Cu particles[53, 181] or Pd nanoparticles.[97-98]

5.3.3 Ni(0) Nanoparticles in the Precipitates Serve as the Reservoir for the Ni Catalyst

5.3.3.1 XPS

Because the precipitates serve as a reservoir for the water-soluble active Ni(0) catalyst, we conducted experiments to characterize the Ni particles using XPS. XPS were used to determine the oxidation state of Ni. We measured the Ni 2p photoelectron spectra in the binding energy region of 845-885 eV. (Figure 5.3). For Ni(0) foil (Figure 5.3a), the Ni 2p electron binding energies are observed at 852.7, 856.0, 861.5, 869.9, 873.7, and 880.1 eV. The peaks at 852.7 and 869.9 eV are characteristic of Ni(0) $2p_{3/2}$ and $2p_{1/2}$ spin-orbit terms, respectively.[182-187] The other peaks of Ni(0) powder correspond to Ni(II), possibly to the oxidation of the sample. The peaks at 856.0 and 873.7 eV correspond to the Ni(II) $2p_{3/2}$ and $2p_{1/2}$ spin-orbit terms, respectively.[188-190] Similarly, the peaks at 861.5 and 880.1 eV correspond to the $2p_{3/2}$ and $2p_{1/2}$ satellite peaks, respectively.[190-191] The energy ordering of the two spin-orbit terms arising from the $2p^5$ configuration upon ionization is consistent with Hund's rules, where for a more than half-filled subshell, the state with a larger total angular momentum J has a lower binding energy. The relative intensity of the $2p_{3/2}$ to $2p_{1/2}$ bands is governed by the (2J+1) degeneracy of each term, where J = 3/2 and 1/2. There is a weak satellite band at the higher energy side of the Ni(II) peaks, and these weak bands arise from a shake-up process where the outgoing 2p electron interacts with a valence electron and excite it to a higher energy level. Similarly, for Ni (II) oxide dissolved in water (Figure 5.3b), the Ni 2p electron binding energies are observed at 854.2, 856.2, 861.4, 872.3, and 879.6 eV. Here, we observe the loss of the Ni(0) peak from the previous sample, and an additional Ni (II) $2p_{3/2}$ satellite peak.[183, 189, 192] This doublet structure of Ni (II) from multiplet interaction is a characteristic of NiO.[189, 191-199] The multiplet interaction occurs because of the unpaired valence electrons in the $3d^8$ orbital. Ejection of a core electron from the 2p orbital can create multiple final states. In other words, the $2p^63d^8$ configuration of NiO rearranges to $2p^53d^8$ configuration upon the ejection of an electron in $2p^5$. This can be represented as $2p^53d^9L$, where L represents a hole in the O 2p level. [192, 194-195] Thus, the two configurations arise due to $2p_{3/2}$ (the $2p^53d^9L$ mechanism) and $2p_{3/2}$ satellite ($2p^53d^8$ configuration). Figure 5.3(c, d, and e) presents the Ni 2p XPS spectra of the fresh precipitates prepared with and without the presence of the substrates [Figure 5.3(c,d)] and the spent precipitates prepared with the presence of the substrates (Figure 5.3e). The fresh precipitates are those with catalytical activity (i.e., 37% and 23% 4-phenyltoluene yields with and without the substrates, respectively), while the spent precipitate shows no catalytical reactivity. We also attempted to perform the XPS measurements for the fresh supernatant but were unable to obtain a clean spectrum. The XPS spectra for the fresh precipitates with the substrates (Figure 5.3 c) depicts a peak at 851.8 eV, which is most likely the Ni(0) band. Similarly, for the fresh precipitates without the substrates (Figure 5.3d), a peak is observed at 852.5 eV, which is also corresponds to Ni(0).[182-186] However, for the spent precipitates prepared with the presence of the substrates, all the peaks correspond to the Ni(II) bands (Figure 5.3e). These preliminary observations support the argument that the decrease in catalytic cycles is likely due to the formation of oxidized Ni (II). Table 5.2 shows the binding energies of the samples and their assignments.

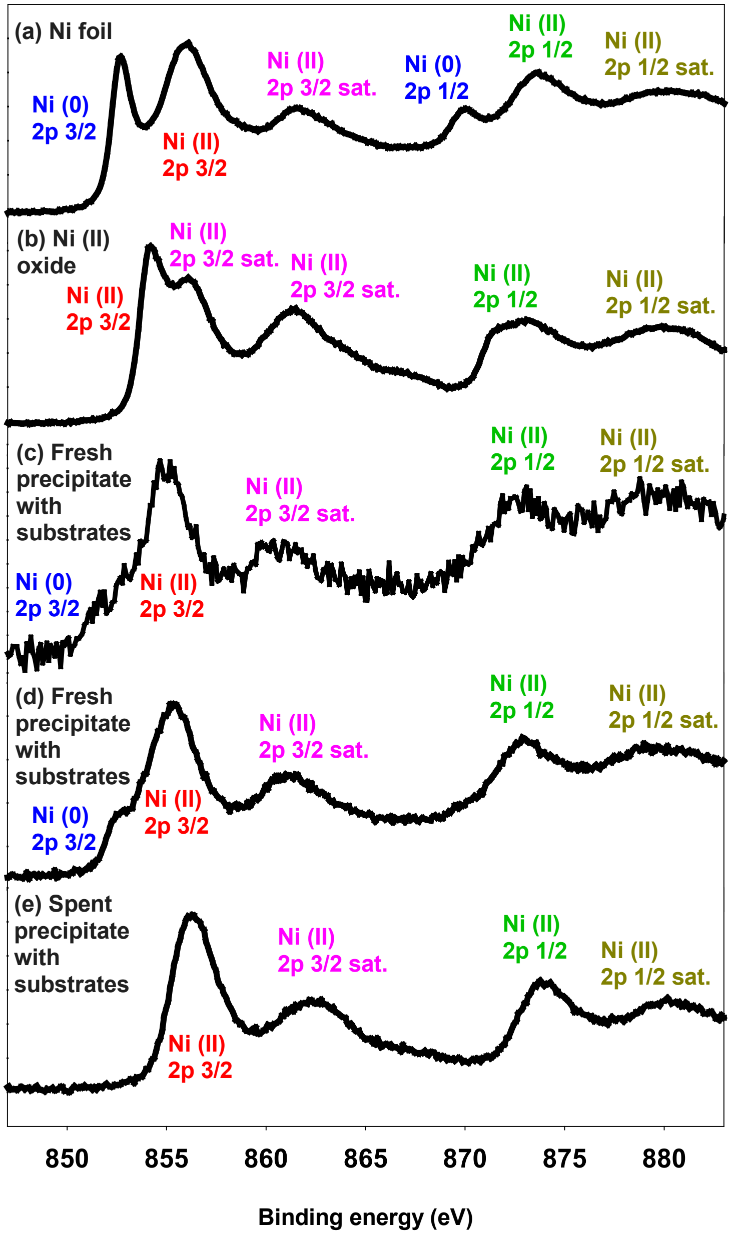

Figure 5.3. XPS spectra of Ni 2p for the aqueous solutions of metallic Ni foil (a), Ni (II) oxide (b), fresh precipitates with (c) and without the substrates (d), and the spent precipitate (e).

Table 5.2. Binding energies for the Ni samples measured by XPS analysis.

				Binding energy (eV)			
		Ni(0)		Ni(II)			
Entry	Sample	$2p_{3/2}$	$2p_{1/2}$	$2p_{3/2}$	$2p_{3/2}$ sat.	$2p_{1/2}$	$2p_{1/2}$ sat.
a	Ni foil	852.7	869.9	856.0	861.5	873.7	880.1
b	Ni (II) oxide	-	-	854.2	856.2 861.4	872.3	879.6
c	Fresh precipitate with substrates	851.8	-	855.0	860.6	872.9	879.4
d	Fresh precipitate without substrates	852.5	-	855.3	861.0	873.0	879.4
e	Spent precipitate	-	-	856.2	862.3	873.9	880.1

Conditions: [a]Ni foil; [b]Ni (II) oxide: 0.05 mmol in 1.5 mL water; [c, e]Ni(0) powder (0.05 mmol), 4-iodotoluene (1.0 mmol), phenylboronic acid (1.2 mmol), K_2CO_3 (2.0 mmol), 2 mL of PEG-300; [d]Ni(0) powder (0.05 mmol), K_2CO_3 (2.0 mmol), 2 mL of PEG-300.

5.3.3.2 XAS

Figure 5.4 presents the Ni-K-edge EXAFS fits in the R-space for the Ni foil (Figure 5.4a), fresh and spent precipitates [Figure 5.4(b,c)], and fresh supernatant (Figure 5.4d) prepared with the substrates. Figure S5.8 presents the XANES data for the same samples. The spectrum for the spent supernatant was too weak to be measured. The overall conclusion we obtained from these graphs is that we only observed Ni-Ni bond as the first shell, and that no clear Ni-O bond was obtained.

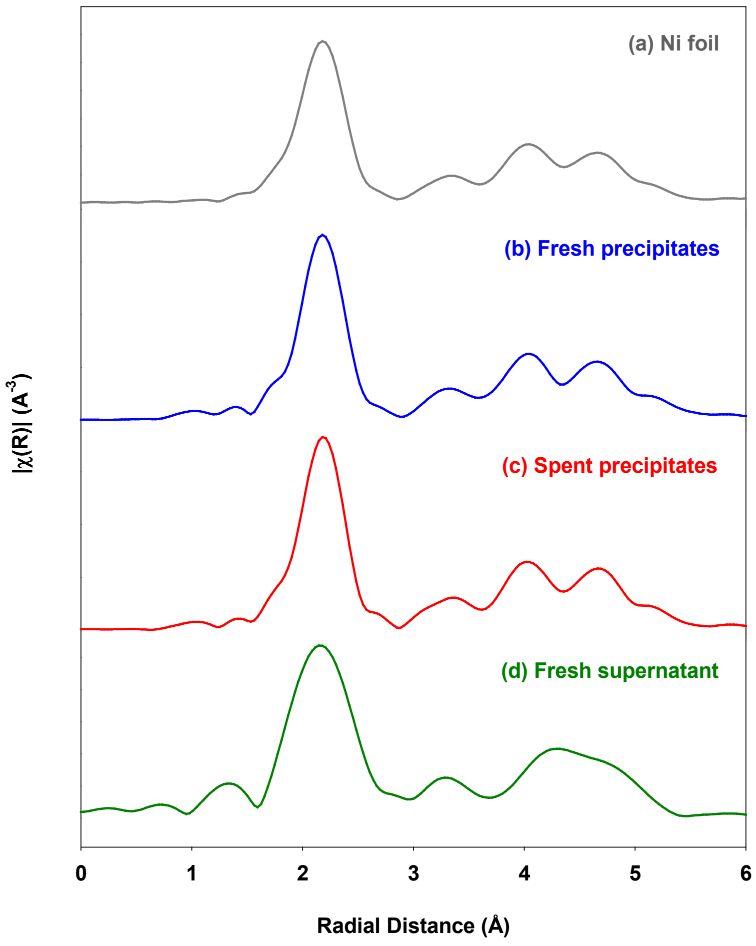

Figure 5.4. Ni K-edge EXAFS single-shell fits in the R-space for the Ni foil (a), fresh precipitates (b), spent precipitates (c), and fresh supernatant (d) prepared with the substrates.

5.3.3.3 TEM

Figure 5.5 shows the TEM images of the fresh and spent precipitate prepared with the substrates. Most of the Ni(0) particles are observed to have a spherical shape in the fresh precipitate sample, where the average diameter is estimated to be 15 ± 3 nm, whereas for the spent precipitate sample, the Ni(0) particles are observed to have a cylindrical shape, where the average semi-major axis diameter is estimated to be 15 ± 3 nm, while that of the semi-minor axis is 8 ± 3 nm.

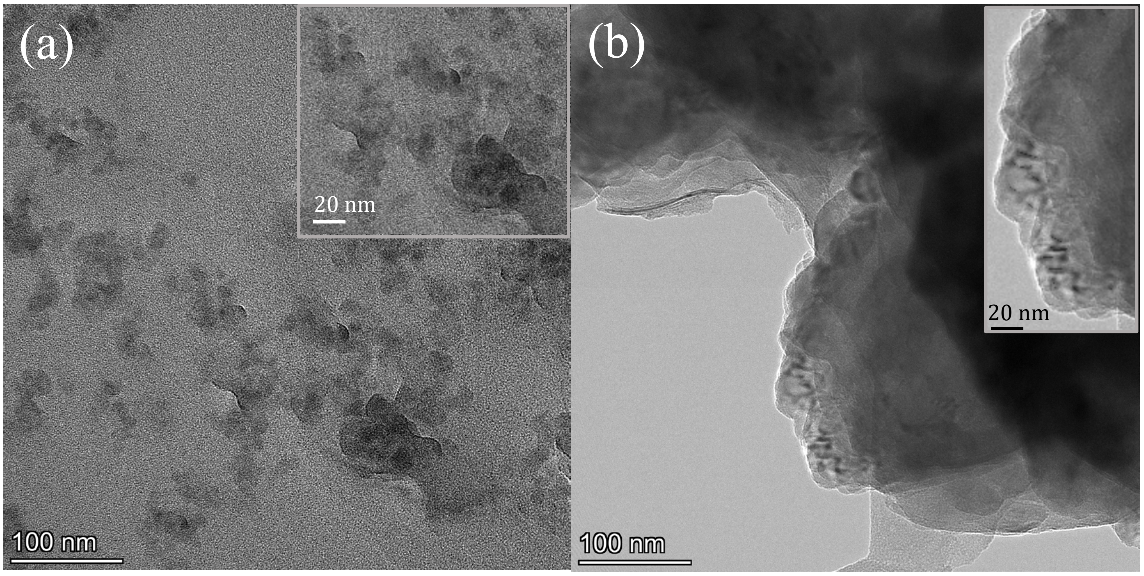

Figure 5.5. TEM image of the fresh and spent precipitate prepared with the substrates. The insets show the magnified region of the images. The scale bar for the larger images is 100 nm, and the scale bar for the insets is 20 nm.

5.4 Conclusions

In summary, we report a Ni(0) catalyst and its formation in the SM coupling reaction between 4-iodotoluene and phenylboronic acid with Ni(0) powder as a precatalyst. The SM coupling is homogenous in nature without any stabilizing organic ligands. Although the chemical identity of the water-soluble active Ni(0) catalyst remains to be characterized by experimental and theoretical UV-Vis spectroscopy, preliminary results suggest that the water-soluble active Ni(0) catalyst is generated through the leaching of Ni(0) nanoparticles on the solid surface at elevated temperatures, and the leaching is enhanced by the presence of the reaction substrates. The Ni(0) catalysts is stable in aqueous solutions for at least fourteen weeks at the room temperature. Although this work is conducted with Ni(0) powder as the precatalyst, we envision that the conclusions arrived in this study about the active catalyst will likely be valid for SM reactions with other inorganic Ni salts in aqueous solutions and also for Ni dispersed on support as heterogenous catalysts.

5.5 Supporting Information

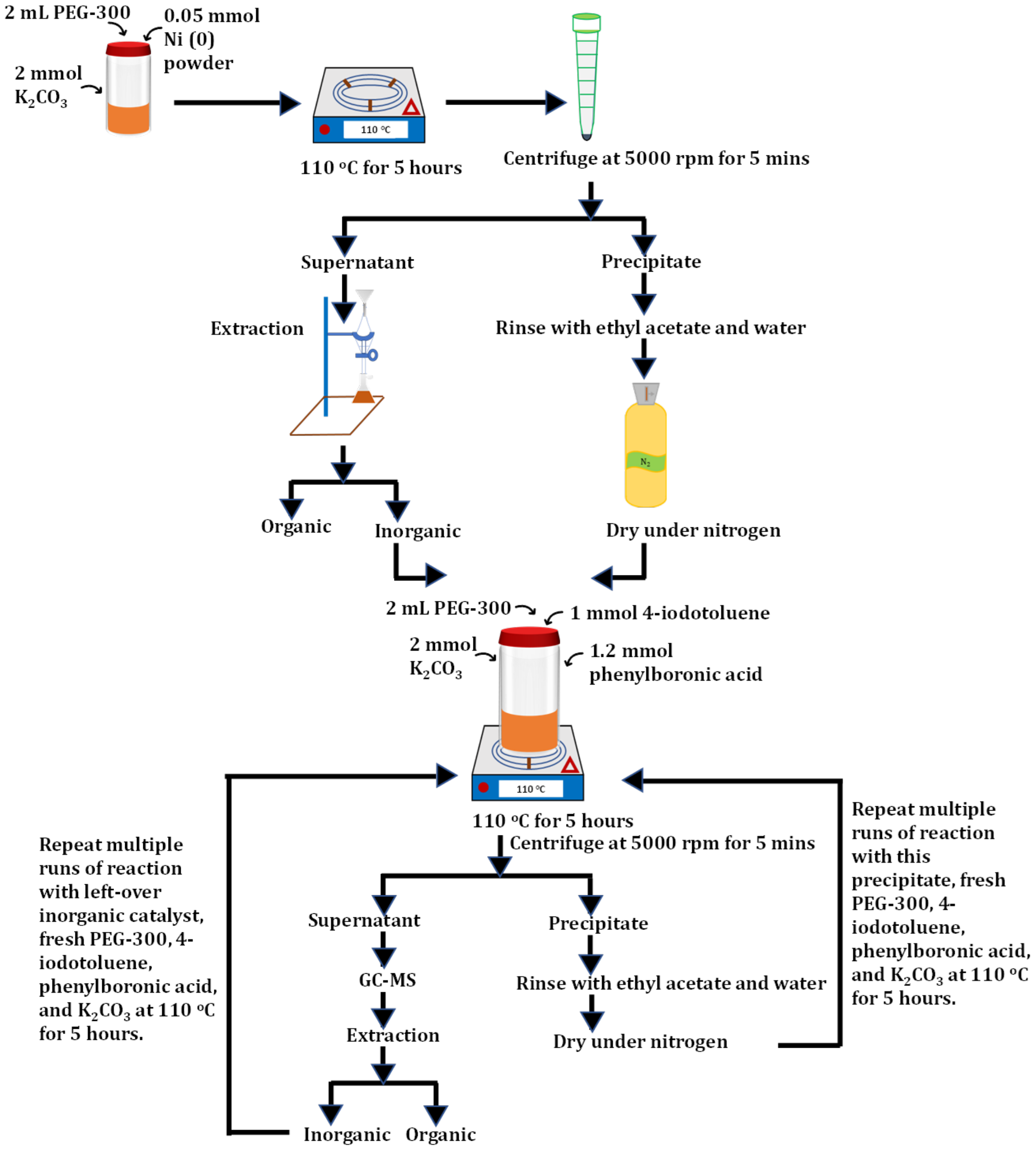

Figure S5.6. Experimental flowchart depicting catalyst preparation, reaction conditions, steps for the purification of the crude product, and recyclability of the precipitate and soluble catalysts. The catalyst was prepared without the 4-iodotoluene and phenylboronic acid substrates.

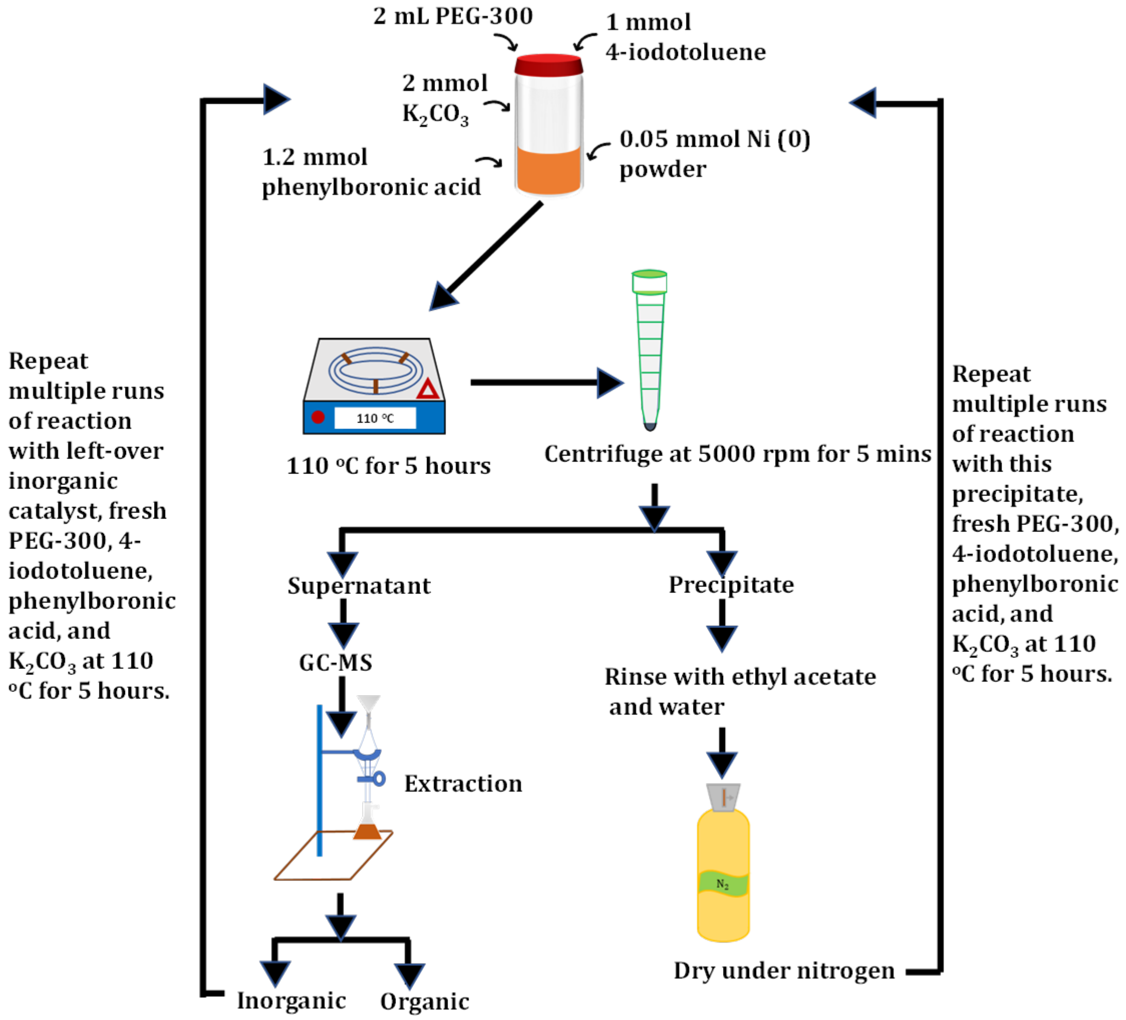

Figure S5.7. Experimental flowchart depicting reaction conditions, steps for the purification of the crude product, and recyclability of the precipitate and soluble catalysts. The catalyst was prepared with the 4-iodotoluene and phenylboronic acid substrates.

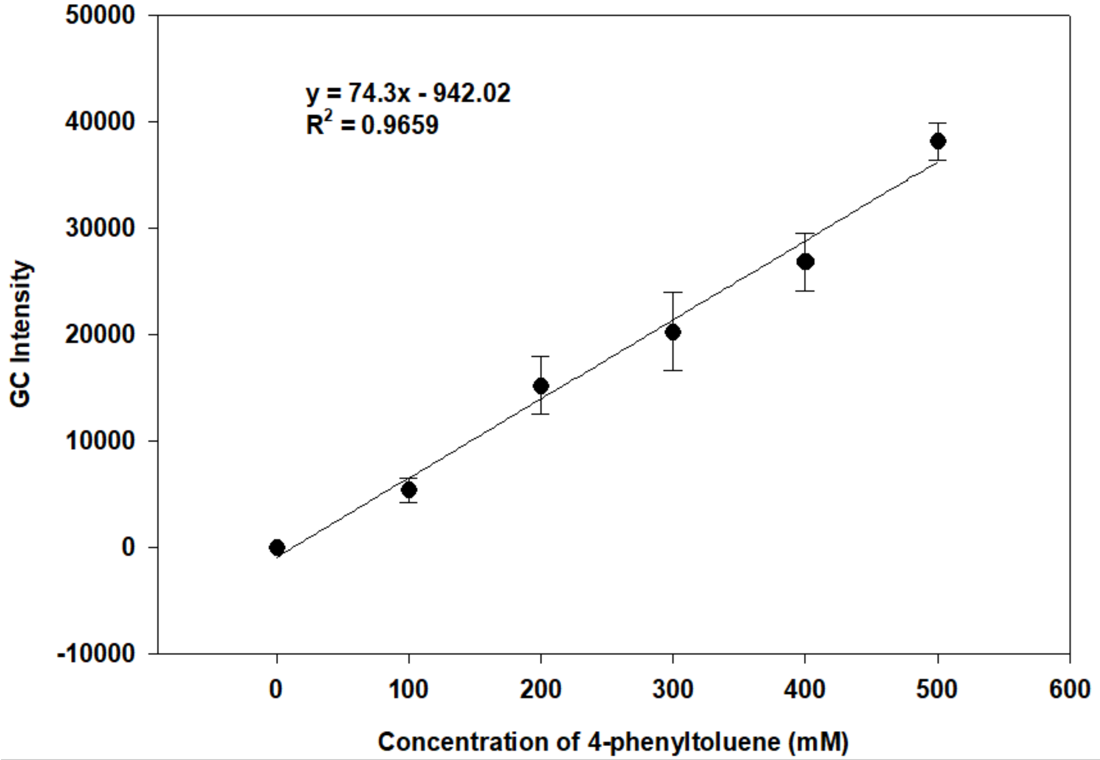

Figure S5.8. Calibration curve of pure 4-phenyltoluene for determining the yields of 4-phenyltoluene produced in SM reactions. Triplicates of 500-, 400-, 300-, 200-, and 100-mM solutions were prepared from a stock solution of 1000 mM. Each sample was injected into the GC-MS instrument to yield a certain GC intensity. The error bars correspond to the GC intensities of three samples at each concentration.

.

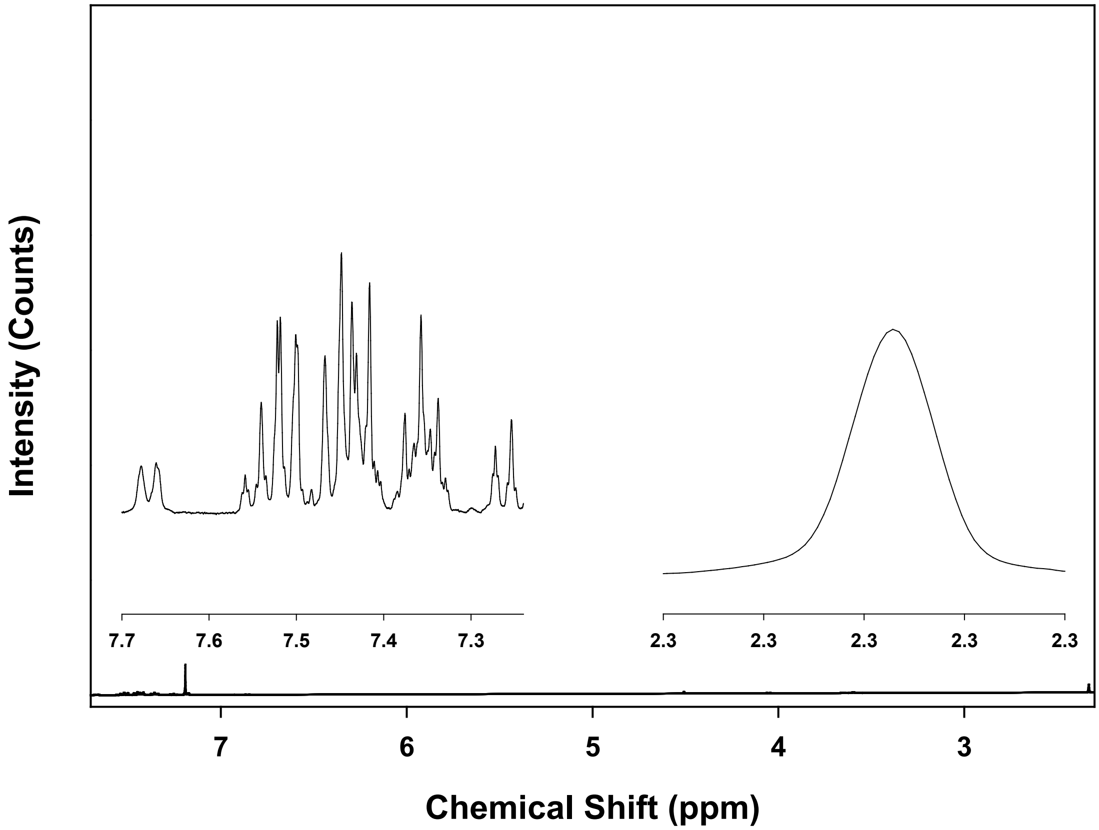

Figure S5.9. ^{1}H NMR (400 MHz, $CDCl_3$) of 4-phenyltoluene: δ (ppm) 7.67 (d, J = 8.0Hz, 2H), 7.56 – 7.40 (m, 4H), 7.36 (t, J = 8.0 Hz, 1H), 7.26 (d, J = 8.0 Hz, 2H), 2.33 (s, 3H).[200-203]

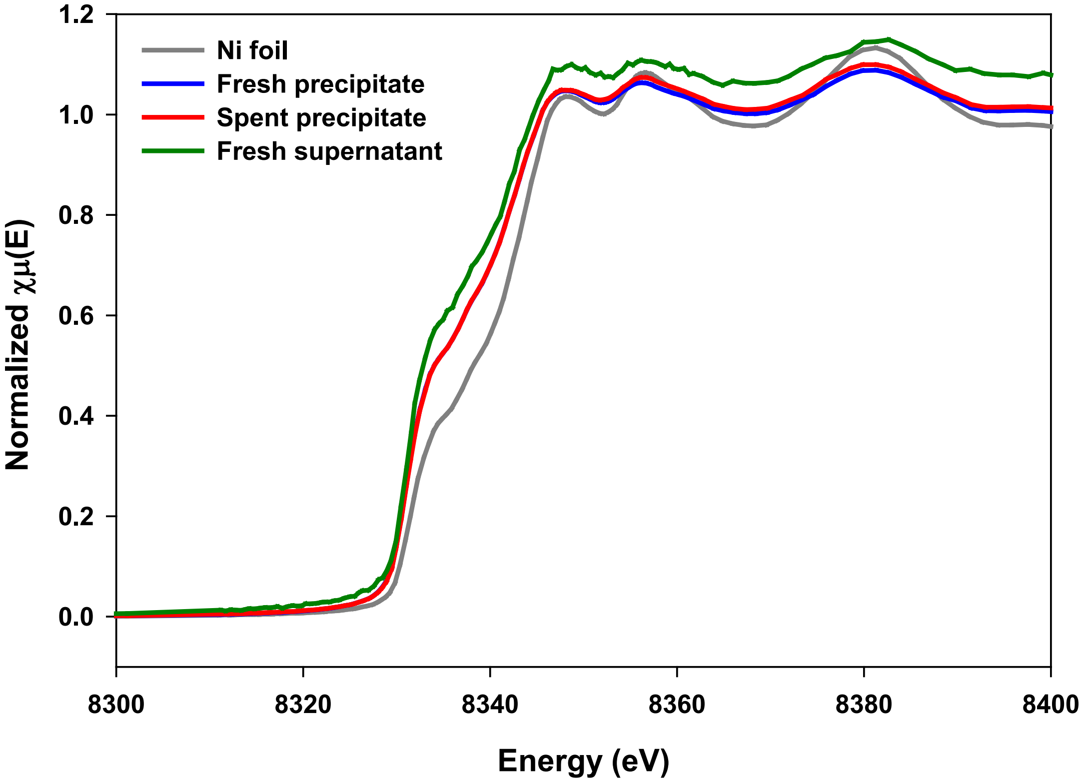

Figure S5.10. Cu XANES spectra after normalization. Only the Ni-Ni bond was observed as the first shell, and no clear Ni-O bond was obtained.

CHAPTER 6. CONCLUSIONS AND FUTURE PERSPECTIVES

This work showcases the nature of catalysis and the identity of catalytically active species in ligand-free SM reactions catalyzed by Pd, Cu, and Ni transition metals. For Pd-catalyzed ligand-free SM reaction, this work reports the Pd-nanocluster catalysts and their formation in the SM coupling reaction between benzene bromide and phenylboronic acid with palladium nitrate as a precatalyst. SM coupling is homogenous in nature without any stabilizing organic ligands. The Pd catalyst consists of mainly neutral Pd tetramers with secondary Pd trimers in their singlet electronic states. The Pd nanoclusters are generated by leaching of the Pd(0) nanoparticles and stable in aqueous solutions for at least three months at the room temperature with the product yield of 40%. The morphology of the solid Pd particles that serve as the reservoir of the Pd clusters was also addressed using TEM. Before the SM reaction, most of the Pd nanoparticles have a spherical shape, and the average diameter of fifty-five nanoparticles is estimated to be 2.99 ± 1.32 nm. After the final run of the SM reaction, the shape of most Pd nanoparticles becomes roughly cylindrical with the average dimension of 2.71 ± 1.18 nm in diameter and 7.42 ± 0.97 nm in length. The local coordination of the Pd nanoparticles using Pd-K-edge EXAFS single-shell fits in the R-space indicate that the local coordination number of Pd-Pd is 4.3 ± 0.9 for the sample before the reaction and reduces slightly to 3.4 ± 0.6 for the sample after the final run of the reaction. The Pd(0) nanoparticles are formed by reducing Pd(II) nitrate, and the reduction is induced by ethanol and enhanced by potassium hydroxide. Without the base, the extent of the Pd(II) nitrate reduction is not sufficient for the SM coupling.

Similarly, for Cu-catalyzed ligand-free SM reaction, this work reports the water-soluble cuprous hydroxide, Cu(OH), as the active catalyst in its singlet electronic state in the reaction between iodobenzene and phenylboronic acid with CuI as a precatalyst. The ligand-free SM coupling is homogeneous in nature. The homogeneous catalyst is identified as Cu(OH) in in its singlet electronic state using UV-Vis spectroscopy. The stability of the water-soluble Cu(OH) catalyst was investigated by storing the fresh inorganic supernatant at room temperature for four weeks and found that the SM coupling with the four-week-old supernatant generated biphenyl with 31% yield. Cu(OH) is generated through leaching of the Cu-containing precipitate, and the leaching is enhanced by the presence of the substrates and increasing temperatures. The precipitates serve as a reservoir for the molecular catalyst, and therefore, they were characterized based on morphology and local coordination environment. The EXAFS and XANES measurements show that the spectrum of the fresh sample is close to that of Cu_2O, while the spent sample largely overlaps with that of CuO. Most of the Cu(I) particles are observed to have an oval shape, where the average semi-major axis diameter of thirty-three nanoparticles is estimated to be 15 ± 3 nm, while that of the semi-minor axis is 9 ± 4 nm. The TEM images of the spent precipitate show that the particles are highly agglomerated; hence, their sizes and shape are not measurable.

Moreover, for Ni-catalyzed ligand-free SM reaction, this work reports the reaction between 4-iodotoluene and phenylboronic acid with Ni(0) powder as a precatalyst. The ligand-free SM coupling is homogeneous in nature. The chemical identity of the Ni(0) catalyst is yet to be determined by the experimental and computational UV-Vis spectroscopy. The stability of the water-soluble active Ni(0) catalyst was investigated by storing the fresh inorganic supernatant at room temperature for fourteen weeks and found that the SM coupling with the eight-week-old supernatant generated biphenyl with 35% yield. The water-soluble active Ni(0) catalyst is most likely generated through leaching of the Ni-containing precipitate, and the leaching is enhanced by the presence of the substrates and increasing temperatures. The precipitates serve as a reservoir for the water-soluble active Ni(0) catalyst. Only the Ni-Ni bond was observed as the first shell, and no clear Ni-O bond was obtained from the EXAFS and XANES measurements. The TEM images of the fresh and spent precipitate prepared with the substrates suggest that most of the Ni(0) particles are observed to have a spherical shape in the fresh precipitate sample, where the average diameter is estimated to be 15 ± 3 nm. For the spent precipitate sample, the Ni(0) particles are observed to have a cylindrical shape, where the average semi-major axis diameter is estimated to be 15 ± 3 nm, while that of the semi-minor axis is 8 ± 3 nm.

The work in this dissertation can further be expanded by exploring other transition metals commonly used in the SM cross-coupling reactions, such as Fe and Co. Identifying the chemical identity of the catalyst and the nature of catalysis in the reaction can be useful to design novel catalysts for use in the pharmaceutical, agrichemical, and natural product synthesis industries. Although the work in this dissertation only explores the unsupported precatalysts that catalyze the ligand-free SM cross-coupling reactions, the studies presented in this dissertation can be used to design future experiments to investigate the precatalysts dispersed on some form of solid support. From a synthetic point of view, using such support may increase the turnover frequency of the catalyst, increase the stability of the catalyst under ambient conditions, and make the catalyst easy to recover. From a physical chemistry point of view, it would be interesting to observe how the active catalyst and nature of catalysis would behave in precatalysts on the solid support-catalyzed SM cross-coupling reactions. Thus, there are many possible directions that the findings based on this dissertation can lead to, and further help the future of chemical catalysis.

REFERENCES

1. Biffis, A.; Centomo, P.; Del Zotto, A.; Zeccal, M., Pd Metal Catalysts for Cross-Couplings and Related Reactions in the 21st Century: A Critical Review. *Chem. Rev.* **2018,** *118* (4), 2249-2295.
2. Sun, J.; Fu, Y.; He, G.; Sun, X.; Wang, X., Green Suzuki–Miyaura coupling reaction catalyzed by palladium nanoparticles supported on graphitic carbon nitride. *Appl. Catal. B: Environ.* **2015,** *165*, 661-667.

3. Wang, S.-B.; Zhu, W.; Ke, J.; Lin, M.; Zhang, Y.-W., Pd–Rh Nanocrystals with Tunable Morphologies and Compositions as Efficient Catalysts toward Suzuki Cross-Coupling Reactions. *ACS Catal.* **2014,** *4* (7), 2298-2306.
4. Wang, Y.; Qi, X.; Ma, Q.; Liu, P.; Tsui, G. C., Stereoselective Palladium-Catalyzed Base-Free Suzuki–Miyaura Cross-Coupling of Tetrasubstituted gem-Difluoroalkenes: An Experimental and Computational Study. *ACS Catal.* **2021,** *11* (8), 4799-4809.
5. Hong, K.; Sajjadi, M.; Suh, J. M.; Zhang, K.; Nasrollahzadeh, M.; Jang, H. W.; Varma, R. S.; Shokouhimehr, M., Palladium Nanoparticles on Assorted Nanostructured Supports: Applications for Suzuki, Heck, and Sonogashira Cross-Coupling Reactions. *ACS Appl. Nano Mater.* **2020,** *3* (3), 2070-2103.
6. Itami, K.; Tonogaki, K.; Ohashi, Y.; Yoshida, J.-i., Rapid Construction of Multisubstituted Olefin Structures Using Vinylboronate Ester Platform Leading to Highly Fluorescent Materials. *Org. Lett.* **2004,** *6* (22), 4093-4096.
7. Ruiz-Castillo, P.; Buchwald, S. L., Applications of Palladium-Catalyzed C–N Cross-Coupling Reactions. *Chem. Rev.* **2016,** *116* (19), 12564-12649.
8. Vitaku, E.; Smith, D. T.; Njardarson, J. T., Analysis of the Structural Diversity, Substitution Patterns, and Frequency of Nitrogen Heterocycles among U.S. FDA Approved Pharmaceuticals. *J. Med. Chem.* **2014,** *57* (24), 10257-10274.
9. Bringmann, G.; Gulder, T.; Hertlein, B.; Hemberger, Y.; Meyer, F., Total Synthesis of the N,C-Coupled Naphthylisoquinoline Alkaloids Ancistrocladinium A and B and Related Analogues. *J. Am. Chem. Soc.* **2010,** *132* (3), 1151-1158.
10. Meyers, C.; Rombouts, G.; Loones, K. T. J.; Coelho, A.; Maes, B. U. W., Auto-Tandem Catalysis: Synthesis of Substituted 11H-Indolo[3,2-c]quinolines via Palladium-Catalyzed Intermolecular C-N and Intramolecular C-C Bond Formation. *Adv. Synth. Catal* **2008,** *350* (3), 465-470.
11. Campeau, L.-C.; Parisien, M.; Jean, A.; Fagnou, K., Catalytic Direct Arylation with Aryl Chlorides, Bromides, and Iodides: Intramolecular Studies Leading to New Intermolecular Reactions. *J. Am. Chem. Soc.* **2006,** *128* (2), 581-590.
12. Ackermann, L.; Althammer, A., Domino N□H/C□H Bond Activation: Palladium-Catalyzed Synthesis of Annulated Heterocycles Using Dichloro(hetero)arenes. *Angew. Chem., Int. Ed.* **2007,** *46* (10), 1627-1629.
13. Guyonnet, M.; Baudoin, O., Synthesis of Tricyclic Nitrogen Heterocycles by a Sequence of Palladium-Catalyzed N–H and C(sp3)–H Arylations. *Org. Lett.* **2012,** *14* (1), 398-401.
14. Lebel, H.; Ladjel, C.; Bréthous, L., Palladium-Catalyzed Cross-Coupling Reactions in One-Pot Multicatalytic Processes. *J. Am. Chem. Soc.* **2007,** *129* (43), 13321-13326.

15. Mpungose, P. P.; Vundla, Z. P.; Maguire, G. E. M.; Friedrich, H. B., The Current Status of Heterogeneous Palladium Catalysed Heck and Suzuki Cross-Coupling Reactions. *Molecules* **2018,** *23* (7).
16. Fringuelli, F.; Girotti, R.; Piermatti, O.; Pizzo, F.; Vaccaro, L., Uncatalyzed and Solvent-Free Multicomponent Process for the Synthesis of Biphenyl-2-carbonitrile Derivatives. *Org. Lett.* **2006,** *8* (25), 5741-5744.
17. Tanitame, A.; Oyamada, Y.; Ofuji, K.; Fujimoto, M.; Iwai, N.; Hiyama, Y.; Suzuki, K.; Ito, H.; Terauchi, H.; Kawasaki, M.; Nagai, K.; Wachi, M.; Yamagishi, J.-i., Synthesis and Antibacterial Activity of a Novel Series of Potent DNA Gyrase Inhibitors. Pyrazole Derivatives. *J. Med. Chem.* **2004,** *47* (14), 3693-3696.
18. Tollefson, E. J.; Hanna, L. E.; Jarvo, E. R., Stereospecific Nickel-Catalyzed Cross-Coupling Reactions of Benzylic Ethers and Esters. *Acc. Chem. Res.* **2015,** *48* (8), 2344-2353.
19. Nauš, P.; Pohl, R.; Votruba, I.; Džubák, P.; Hajdúch, M.; Ameral, R.; Birkuš, G.; Wang, T.; Ray, A. S.; Mackman, R.; Cihlar, T.; Hocek, M., 6-(Het)aryl-7-Deazapurine Ribonucleosides as Novel Potent Cytostatic Agents. *J. Med. Chem.* **2010,** *53* (1), 460-470.
20. Balcells, S.; Haughey, M. B.; Walker, J. C. L.; Josa-Culleré, L.; Towers, C.; Donohoe, T. J., Asymmetric Total Synthesis of (−)-(3R)-Inthomycin C. *Org. Lett.* **2018,** *20* (12), 3583-3586.
21. Fleuti, M.; Bártová, K.; Slavětínská, L. P.; Tloušt’ová, E.; Tichý, M.; Gurská, S.; Pavliš, P.; Džubák, P.; Hajdúch, M.; Hocek, M., Synthesis and Biological Profiling of Pyrazolo-Fused 7-Deazapurine Nucleosides. *J. Org. Chem.* **2020,** *85* (16), 10539-10551.
22. Gildner, P. G.; Colacot, T. J., Reactions of the 21st Century: Two Decades of Innovative Catalyst Design for Palladium-Catalyzed Cross-Couplings. *Organometallics* **2015,** *34* (23), 5497-5508.
23. Campeau, L.-C.; Hazari, N., Cross-Coupling and Related Reactions: Connecting Past Success to the Development of New Reactions for the Future. *Organometallics* **2019,** *38* (1), 3-35.
24. Heck, R. F., Acylation, methylation, and carboxyalkylation of olefins by Group VIII metal derivatives. *J. Am. Chem. Soc.* **1968,** *90* (20), 5518-5526.
25. Miyaura, N.; Yanagi, T.; Suzuki, A., The Palladium-Catalyzed Cross-Coupling Reaction of Phenylboronic Acid with Haloarenes in the Presence of Bases. *Synth. Commun.* **1981,** *11* (7), 513-519.
26. Negishi, E.; King, A. O.; Okukado, N., Selective carbon-carbon bond formation via transition metal catalysis. 3. A highly selective synthesis of unsymmetrical biaryls and diarylmethanes by the nickel- or palladium-catalyzed reaction of aryl- and benzylzinc derivatives with aryl halides. *J. Org. Chem.* **1977,** *42* (10), 1821-1823.
27. Haas, D.; Hammann, J. M.; Greiner, R.; Knochel, P., Recent Developments in Negishi Cross-Coupling Reactions. *ACS Catal.* **2016,** *6* (3), 1540-1552.
28. Albaneze-Walker, J.; Raju, R.; Vance, J. A.; Goodman, A. J.; Reeder, M. R.; Liao, J.; Maust, M. T.; Irish, P. A.; Espino, P.; Andrews, D. R., Imidazolylsulfonates: Electrophilic Partners in Cross-Coupling Reactions. *Org. Lett.* **2009,** *11* (7), 1463-1466.
29. Adams, C. J.; Bedford, R. B.; Carter, E.; Gower, N. J.; Haddow, M. F.; Harvey, J. N.; Huwe, M.; Cartes, M. Á.; Mansell, S. M.; Mendoza, C.; Murphy, D. M.; Neeve, E. C.; Nunn, J., Iron(I) in Negishi Cross-Coupling Reactions. *J. Am. Chem. Soc.* **2012,** *134* (25), 10333-10336.

30. Kashihara, M.; Nakao, Y., Cross-Coupling Reactions of Nitroarenes. *Acc. Chem. Res.* **2021,** *54* (14), 2928-2935.

31. Poremba, K. E.; Dibrell, S. E.; Reisman, S. E., Nickel-Catalyzed Enantioselective Reductive Cross-Coupling Reactions. *ACS Catal.* **2020,** *10* (15), 8237-8246.

32. Tamao, K.; Sumitani, K.; Kumada, M., Selective carbon-carbon bond formation by cross-coupling of Grignard reagents with organic halides. Catalysis by nickel-phosphine complexes. *J. Am. Chem. Soc.* **1972,** *94* (12), 4374-4376.

33. Milstein, D.; Stille, J. K., A general, selective, and facile method for ketone synthesis from acid chlorides and organotin compounds catalyzed by palladium. *J. Am. Chem. Soc.* **1978,** *100* (11), 3636-3638.

34. Gu, N.; Liu, Y.; Liu, P.; Ma, X.; Liu, Y., Synthesis of symmetrical terphenyl derivatives by PdCl2-catalyzed Suzuki–Miyaura reaction of dibromobenzene using 3-(diphenylphosphino)propanoic acid as a ligand. *Synth. Commun.* **2016,** *46* (2), 154-159.

35. Jensen, J. F.; Johannsen, M., New Air-Stable Planar Chiral Ferrocenyl Monophosphine Ligands: Suzuki Cross-Coupling of Aryl Chlorides and Bromides. *Org. Lett.* **2003,** *5* (17), 3025-3028.

36. Meng, G.; Szostak, R.; Szostak, M., Suzuki–Miyaura Cross-Coupling of N-Acylpyrroles and Pyrazoles: Planar, Electronically Activated Amides in Catalytic N–C Cleavage. *Org. Lett.* **2017,** *19* (13), 3596-3599.

37. Lima, C. F.; Rodrigues, A. S.; Silva, V. L.; Silva, A. M.; Santos, L., Role of the Base and Control of Selectivity in the Suzuki–Miyaura Cross-Coupling Reaction. *ChemCatChem* **2014,** *6* (5), 1291-1302.

38. Sherwood, J.; Clark, J. H.; Fairlamb, I. J.; Slattery, J. M., Solvent effects in palladium catalysed cross-coupling reactions. *Green Chem.* **2019,** *21* (9), 2164-2213.

39. MacQuarrie, S.; Horton, J. H.; Barnes, J.; McEleney, K.; Loock, H. P.; Crudden, C. M., Visual observation of redistribution and dissolution of Palladium during the Suzuki–Miyaura Reaction. *Angew. Chem., Int. Ed.* **2008,** *47* (17), 3279-3282.

40. Amoroso, F.; Cersosimo, U.; Del Zotto, A., Studies on the catalytic ability of palladium wire, foil and sponge in the Suzuki–Miyaura cross-coupling. *Inorganica Chim. Acta* **2011,** *375* (1), 256-262.

41. Len, C.; Bruniaux, S.; Delbecq, F.; Parmar, V. S., Palladium-Catalyzed Suzuki–Miyaura Cross-Coupling in Continuous Flow. *Catalysts* **2017,** *7* (5), 146.

42. Leyva-Pérez, A.; Oliver-Meseguer, J.; Rubio-Marqués, P.; Corma, A., Water-Stabilized Three- and Four-Atom Palladium Clusters as Highly Active Catalytic Species in Ligand-Free C-C Cross-Coupling Reactions. *Angew. Chem. Int. Ed.* **2013,** *52* (44), 11554-11559.

43. Narita, H.; Morisaku, K.; Tamura, K.; Tanaka, M.; Shiwaku, H.; Okamoto, Y.; Suzuki, S.; Yaita, T., Extraction Properties of Palladium(II) in HCl Solution with Sulfide-Containing Monoamide Compounds. *Ind. Eng. Chem. Res.* **2014,** *53* (9), 3636-3640.

44. Johansson Seechurn, C. C. C.; Sperger, T.; Scrase, T. G.; Schoenebeck, F.; Colacot, T. J., Understanding the Unusual Reduction Mechanism of Pd(II) to Pd(I): Uncovering Hidden Species and Implications in Catalytic Cross-Coupling Reactions. *J. Am. Chem. Soc.* **2017,** *139* (14), 5194-5200.

45. Waghmode, S. B.; Arbuj, S. S.; Wani, B. N., Heterogeneous photocatalysed Heck reaction over PdCl 2/TiO 2. *New J. Chem.* **2013,** *37* (9), 2911-2916.

46. Cristoforetti, G.; Pitzalis, E.; Spiniello, R.; Ishak, R.; Muniz-Miranda, M., Production of Palladium Nanoparticles by Pulsed Laser Ablation in Water and Their Characterization. *J. Phys. Chem. C* **2011,** *115* (12), 5073-5083.
47. Shao, L.; Zhang, B.; Zhang, W.; Hong, S. Y.; Schlögl, R.; Su, D. S., The role of palladium dynamics in the surface catalysis of coupling reactions. *Angew. Chem. Int. Ed.* **2013,** *52* (7), 2114-2117.
48. Moussa, S.; Siamaki, A. R.; Gupton, B. F.; El-Shall, M. S., Pd-Partially Reduced Graphene Oxide Catalysts (Pd/PRGO): Laser Synthesis of Pd Nanoparticles Supported on PRGO Nanosheets for Carbon–Carbon Cross Coupling Reactions. *ACS Catal.* **2012,** *2* (1), 145-154.
49. Slavinskaya, E.; Kardash, T. Y.; Stonkus, O.; Gulyaev, R.; Lapin, I.; Svetlichnyi, V.; Boronin, A., Metal–support interaction in Pd/CeO 2 model catalysts for CO oxidation: from pulsed laser-ablated nanoparticles to highly active state of the catalyst. *Catal. Sci. Technol.* **2016,** *6* (17), 6650-6666.

50. Ritter, S. K. Chemists introduce a user’s guide for palladium acetate 2016.
51. Ye, Y.-M.; Wang, B.-B.; Ma, D.; Shao, L.-X.; Lu, J.-M., CuO-2,2′-Diamino-6,6′-Dimethylbiphenyl Catalyzed Suzuki–Miyaura Coupling Reactions of Arylboronic Acids with Aryl Iodides and Bromides. *Catal. Lett.* **2010,** *139* (3), 141-144.
52. Thapa, S.; Shrestha, B.; Gurung, S. K.; Giri, R., Copper-catalysed cross-coupling: an untapped potential. *Org. Biomol. Chem.* **2015,** *13* (17), 4816-4827.
53. Panova, Y. S.; Kashin, A. S.; Vorobev, M. G.; Degtyareva, E. S.; Ananikov, V. P., Nature of the Copper-Oxide-Mediated C–S Cross-Coupling Reaction: Leaching of Catalytically Active Species from the Metal Oxide Surface. *ACS Catal.* **2016,** *6* (6), 3637-3643.
54. Rajalakshmi, C.; Krishnan, A.; Saranya, S.; Anilkumar, G.; Thomas, V. I., A detailed theoretical investigation to unravel the molecular mechanism of the ligand-free copper-catalyzed Suzuki cross-coupling reaction. *Org. Biomol. Chem.* **2022,** *20* (22), 4539-4552.
55. Kadu, B. S., Suzuki–Miyaura cross coupling reaction: recent advancements in catalysis and organic synthesis. *Catal. Sci. Technol.* **2021,** *11* (4), 1186-1221.
56. Evano, G.; Blanchard, N.; Toumi, M., Copper-Mediated Coupling Reactions and Their Applications in Natural Products and Designed Biomolecules Synthesis. *Chem. Rev.* **2008,** *108* (8), 3054-3131.
57. Miyaura, N.; Suzuki, A., Palladium-Catalyzed Cross-Coupling Reactions of Organoboron Compounds. *Chem. Rev.* **1995,** *95* (7), 2457-2483.
58. Zhu, G.; Tong, X.; Cheng, J.; Sun, Y.; Li, D.; Zhang, Z., Palladium-Catalyzed Tandem Cyclization/Suzuki Coupling of 1,6-Enynes: Reaction Scope and Mechanism. *J. Org. Chem.* **2005,** *70* (5), 1712-1717.
59. Kim, Y. M.; Yu, S., Palladium(0)-Catalyzed Amination, Stille Coupling, and Suzuki Coupling of Electron-Deficient Aryl Fluorides. *J. Am. Chem. Soc.* **2003,** *125* (7), 1696-1697.
60. Collins, G.; Schmidt, M.; O’Dwyer, C.; McGlacken, G.; Holmes, J. D., Enhanced Catalytic Activity of High-Index Faceted Palladium Nanoparticles in Suzuki–Miyaura Coupling Due to Efficient Leaching Mechanism. *ACS Catal.* **2014,** *4* (9), 3105-3111.

61. Shao, Y.; Zeng, H. C., Nanowire Networks of Metal–Organosilicates as Reversible Pd(II) Reservoirs for Suzuki Coupling Reactions. *ACS Appl. Nano Mater.* **2021,** *4* (10), 10886-10901.
62. Molina, R.; Gómez-Ruiz, S.; Montilla, F.; Salinas-Castillo, A.; Fernández-Arroyo, S.; Ramos, M. d. M.; Micol, V.; Mallavia, R., Progress in the Synthesis of Poly(2,7-Fluorene-alt-1,4-Phenylene), PFP, via Suzuki Coupling. *Macromolecules* **2009,** *42* (15), 5471-5477.
63. Zhu, G.; Zhang, Z., Palladium-Catalyzed Tandem Cyclization/Suzuki Coupling Reaction of 1,2,7-Trienes. *Org. Lett.* **2004,** *6* (22), 4041-4044.
64. Chen, Q.; Wu, S.; Yan, S.; Li, C.; Abduhulam, H.; Shi, Y.; Dang, Y.; Cao, C., Suzuki–Miyaura Cross-Coupling of Sulfoxides. *ACS Catal.* **2020,** *10* (15), 8168-8176.
65. Jana, R.; Pathak, T. P.; Sigman, M. S., Advances in Transition Metal (Pd,Ni,Fe)-Catalyzed Cross-Coupling Reactions Using Alkyl-organometallics as Reaction Partners. *Chem. Rev.* **2011,** *111* (3), 1417-1492.
66. Goossen, L. J.; Koley, D.; Hermann, H. L.; Thiel, W., Palladium Monophosphine Intermediates in Catalytic Cross-Coupling Reactions: A DFT Study. *Organometallics* **2006,** *25* (1), 54-67.
67. García-Melchor, M.; Braga, A. A. C.; Lledós, A.; Ujaque, G.; Maseras, F., Computational Perspective on Pd-Catalyzed C–C Cross-Coupling Reaction Mechanisms. *Acc. Chem. Res.* **2013,** *46* (11), 2626-2634.
68. Moreno-Mañas, M.; Pérez, M.; Pleixats, R., Palladium-Catalyzed Suzuki-Type Self-Coupling of Arylboronic Acids. A Mechanistic Study. *J. Org. Chem.* **1996,** *61* (7), 2346-2351.
69. Braga, A. A. C.; Ujaque, G.; Maseras, F., A DFT Study of the Full Catalytic Cycle of the Suzuki−Miyaura Cross-Coupling on a Model System. *Organometallics* **2006,** *25* (15), 3647-3658.
70. Zhao, T.; Ghosh, P.; Martinez, Z.; Liu, X.; Meng, X.; Darensbourg, M. Y., Discrete Air-Stable Nickel(II)–Palladium(II) Complexes as Catalysts for Suzuki–Miyaura Reactions. *Organometallics* **2017,** *36* (9), 1822-1827.
71. Kumar, A.; Rao, G. K.; Kumar, S.; Singh, A. K., Formation and Role of Palladium Chalcogenide and Other Species in Suzuki–Miyaura and Heck C–C Coupling Reactions Catalyzed with Palladium(II) Complexes of Organochalcogen Ligands: Realities and Speculations. *Organometallics* **2014,** *33* (12), 2921-2943.
72. Wang, Z. J.; Ghasimi, S.; Landfester, K.; Zhang, K. A. I., Photocatalytic Suzuki Coupling Reaction Using Conjugated Microporous Polymer with Immobilized Palladium Nanoparticles under Visible Light. *Chem. Mater.* **2015,** *27* (6), 1921-1924.
73. Ridgway, B. H.; Woerpel, K. A., Transmetalation of Alkylboranes to Palladium in the Suzuki Coupling Reaction Proceeds with Retention of Stereochemistry. *J. Org. Chem.* **1998,** *63* (3), 458-460.
74. Ben Halima, T.; Zhang, W.; Yalaoui, I.; Hong, X.; Yang, Y.-F.; Houk, K. N.; Newman, S. G., Palladium-Catalyzed Suzuki–Miyaura Coupling of Aryl Esters. *J. Am. Chem. Soc.* **2017,** *139* (3), 1311-1318.
75. Song, Z.; Huang, X.; Jiang, S.; He, C.; Tang, L.; Ni, Q.; Ma, M.; Chen, B.; Ma, Y., C(sp2)–C(sp2) Reductive Cross-Coupling of Triarylphosphines with Aryl Halides by Palladium/Nickel Co-catalysis. *Org. Lett.* **2022,** *24* (30), 5573-5578.
76. Turner, D. GC-MS Principle, Instrument and Analyses and GC-MS/MS 2022.

77. Donald L. Pavia, G. M. L., George S. Kriz, James A. Vyvyan *Introduction to Spectroscopy*. 5 ed.; Cengage Learning: Stamford, 2014.

78. Kolasinski, K. W., *Surface Science: Foundations of Catalysis and Nanoscience*. 2 ed.; Wiley: Chichester, 2008.

79. Buddy D. Ratner, D. G. C., *Surface Analysis – The Principal Techniques*. 2nd ed.; John Wiley & Sons Ltd: Chichester, 2009.

80. Lucas, C. A., *Surface Analysis – The Principal Techniques*. 2nd ed.; John Wiley & Sons Ltd: Chichester, 2009.

81. David B. Williams , C. B. C., *Transmission Electron Microscopy*. 2 ed.; Springer: New York, 2009.

82. Jensen, F., *Introduction to Computational Chemistry*. 2 ed.; John Wiley & Sons Ltd: Chichester, 2007.

83. Becke, A. D., Density-functional thermochemistry. III. The role of exact exchange. *J. Chem. Phys.* **1993,** *98* (7), 5648-5652.

84. Lee, C. T.; Yang, W. T.; Parr, R. G., Development of the Colle-Salvetti correlation-energy formula into a functional of the electron density. *Phys. Rev. B* **1988,** *37* (2), 785-789.

85. Davidson, E. R., Comment on "Comment on Dunning's correlation-consistent basis sets". *Chem. Phys. Lett.* **1996,** *260* (3), 514-518.

86. Hazari, N.; Melvin, P. R.; Beromi, M. M., Well-defined nickel and palladium precatalysts for cross-coupling. *Nat. Rev. Chem.* **2017,** *1* (3), 1-16.

87. Devendar, P.; Qu, R. Y.; Kang, W. M.; He, B.; Yang, G. F., Palladium-Catalyzed Cross-Coupling Reactions: A Powerful Tool for the Synthesis of Agrochemicals. *J. Agric. Food Chem.* **2018,** *66* (34), 8914-8934.

88. Choi, J.; Fu, G. C., Transition metal-catalyzed alkyl-alkyl bond formation: Another dimension in cross-coupling chemistry. *Science* **2017,** *356* (6334), eaaf7230.

89. Uehling, M. R.; King, R. P.; Krska, S. W.; Cernak, T.; Buchwald, S. L., Pharmaceutical diversification via palladium oxidative addition complexes. *Science* **2019,** *363* (6425), 405-408.

90. Hooshmand, S. E.; Heidari, B.; Sedghi, R.; Varma, R. S., Recent advances in the Suzuki-Miyaura cross-coupling reaction using efficient catalysts in eco-friendly media. *Green Chem.* **2019,** *21* (3), 381-405.

91. Fu, F. Y.; Xiang, J.; Cheng, H.; Cheng, L. J.; Chong, H. B.; Wang, S. X.; Li, P.; Wei, S. Q.; Zhu, M. Z.; Li, Y. D., A Robust and Efficient Pd_3 Cluster Catalyst for the Suzuki Reaction and Its Odd Mechanism. *ACS Catal.* **2017,** *7* (3), 1860-1867.

92. Proutiere, F.; Aufiero, M.; Schoenebeck, F., Reactivity and Stability of Dinuclear Pd(I) Complexes: Studies on the Active Catalytic Species, Insights into Precatalyst Activation and Deactivation, and Application in Highly Selective Cross-Coupling Reactions. *J. Am. Chem. Soc.* **2012,** *134* (1), 606-612.

93. Chen, Z.; Vorobyeva, E.; Mitchell, S.; Fako, E.; Ortuño, M. A.; López, N.; Collins, S. M.; Midgley, P. A.; Richard, S.; Vilé, G.; Pérez-Ramírez, J., A heterogeneous single-atom palladium catalyst surpassing homogeneous systems for Suzuki coupling. *Nat. Nanotechnol.* **2018,** *13* (8), 702-707.

94. Zhao, Y.; Du, L.; Li, H.; Xie, W.; Chen, J., Is the Suzuki–Miyaura Cross-Coupling Reaction in the Presence of Pd Nanoparticles Heterogeneously or Homogeneously

Catalyzed? An Interfacial Surface-Enhanced Raman Spectroscopy Study. *J. Phys. Chem. Lett.* **2019,** *10* (6), 1286-1291.

95. Thomas, A. A.; Denmark, S. E., Pre-transmetalation intermediates in the Suzuki-Miyaura reaction revealed: The missing link. *Science* **2016,** *352* (6283), 329-332.

96. Del Zotto, A.; Zuccaccia, D., Metallic palladium, PdO, and palladium supported on metal oxides for the Suzuki-Miyaura cross-coupling reaction: a unified view of the process of formation of the catalytically active species in solution. *Catal. Sci. Technol.* **2017,** *7* (18), 3934-3951.

97. Elias, W. C.; Signori, A. M.; Zaramello, L.; Albuquerque, B. L.; de Oliveira, D. C.; Domingos, J. B., Mechanism of a Suzuki-Type Homocoupling Reaction Catalyzed by Palladium Nanocubes. *ACS Catal.* **2017,** *7* (2), 1462-1469.

98. Thathagar, M. B.; ten Elshof, J. E.; Rothenberg, G., Pd nanoclusters in C-C coupling reactions: Proof of leaching. *Angew. Chem. Int. Ed.* **2006,** *45* (18), 2886-2890.

99. Ye, T.-N.; Lu, Y.; Xiao, Z.; Li, J.; Nakao, T.; Abe, H.; Niwa, Y.; Kitano, M.; Tada, T.; Hosono, H. J. N. c., Palladium-bearing intermetallic electride as an efficient and stable catalyst for Suzuki cross-coupling reactions. *Nat. Commun.* **2019,** *10* (1), 1-10.

100. Sun, J.; Fu, Y.; He, G.; Sun, X.; Wang, X., Green Suzuki–Miyaura coupling reaction catalyzed by palladium nanoparticles supported on graphitic carbon nitride. *Appl. Catal. B* **2015,** *165*, 661-667.

101. Heald, S. M. C., J. O.; Brewe, D. L.; Gordon, R. A. , The PNC/XOR X-ray microprobe station at APS sector 20. *Nucl. Instrum. Methods Phys. Res.* **2007,** *582* (1), 215-217.

102. Ravel, B.; Newville, M., ATHENA, ARTEMIS, HEPHAESTUS: data analysis for X-ray absorption spectroscopy using IFEFFIT. *J. Synchrotron Radiat.* **2005,** *12* (4), 537-541.

103. Dolg, M.; Stoll, H.; Preuss, H., Energy-Adjusted Abinitio Pseudopotentials for the Rare-Earth Elements. *J. Chem. Phys.* **1989,** *90* (3), 1730-1734.

104. Tomasi, J.; Mennucci, B.; Cammi, R., Quantum Mechanical Continuum Solvation Models. *Chem. Rev.* **2005,** *105* (8), 2999-3094.

105. Frisch, M. J. T., G. W.; Schlegel, H. B.; Scuseria, G. E.; Robb, M. A.; Cheeseman, J. R.; Scalmani, G.; Barone, V.; Mennucci, B.; Petersson, G. A.; Nakatsuji, H.; Caricato, M.; Li, X.; Hratchian, H. P.; Izmaylov, A. F.; Bloino, J.; Zheng, G.; Sonnenberg, J. L.; Hada, M.; Ehara, M.; Toyota, K.; Fukuda, R.; Hasegawa, J.; Ishida, M.; Nakajima, T.; Honda, Y.; Kitao, O.; Nakai, H.; Vreven, T.; Montgomery, Jr., J. A.; Peralta, J. E.; Ogliaro, F.; Bearpark, M.; Heyd, J. J.; Brothers, E.; Kudin, K. N.; Staroverov, V. N.; Kobayashi, R.; Normand, J.; Raghavachari, K.; Rendell, A.; Burant, J. C.; Iyengar, S. S.; Tomasi, J.; Cossi, M.; Rega, N.; Millam, N. J.; Klene, M.; Knox, J. E.; Cross, J. B.; Bakken, V.; Adamo, C.; Jaramillo, J.; Gomperts, R.; Stratmann, R. E.; Yazyev, O.; Austin, A. J.; Cammi, R.; Pomelli, C.; Ochterski, J. W.; Martin, R. L.; Morokuma, K.; Zakrzewski, V. G.; Voth, G. A.; Salvador, P.; Dannenberg, J. J.; Dapprich, S.; Daniels, A. D.; Farkas, Ö.; Foresman, J. B.; Ortiz, J. V.; Cioslowski, J.; Fox, D. J. *Gaussian 09, Revision A.1*, Wallingford, CT. , 2009.

106. Soomro, S. S.; Ansari, F. L.; Chatziapostolou, K.; Köhler, K., Palladium leaching dependent on reaction parameters in Suzuki–Miyaura coupling reactions catalyzed by palladium supported on alumina under mild reaction conditions. *J. Catal.* **2010,** *273* (2), 138-146.

107. Gnad, C.; Abram, A.; Urstöger, A.; Weigl, F.; Schuster, M.; Köhler, K., Leaching Mechanism of Different Palladium Surface Species in Heck Reactions of Aryl Bromides and Chlorides. *ACS Catal.* **2020,** *10* (11), 6030-6041.

108. Tomasi, J.; Mennucci, B.; Cammi, R., Quantum mechanical continuum solvation models. *Chem. Rev.* **2005,** *105*, 2999-3093.

109. Svanqvist, M.; Hansen, K., Non-jellium scaling of metal cluster ionization energies andelectron affinities. *Eur. Phys. J. D* **2010,** *56* (2), 199-203.

110. Muzart, J., Palladium-catalyzed oxidation of primary and secondary alcohols. *Tetrahedron* **2003,** *59*, 5789-5816.

111. Deitrich, R.; Zimatkin, S.; Pronko, S., Oxidation of ethanol in the brain and its consequences. *Alcohol Res. Health* **2006,** *29*, 266-273.

112. Amatore, C.; Le Duc, G.; Jutand, A., Mechanism of Palladium-Catalyzed Suzuki-Miyaura Reactions: Multiple and Antagonistic Roles of Anionic "Bases" and Their Countercations. *Chem. Eur. J.* **2013,** *19* (31), 10082-10093.

113. Amatore, C.; Jutand, A.; Due, G. L., Kinetic Data for the Transmetalation/Reductive Elimination in Palladium-Catalyzed Suzuki-Miyaura Reactions: Unexpected Triple Role of Hydroxide Ions Used as Base. *Chem. Eur. J* **2011,** *17*, 2492-2503.

114. Miyaura, N.; Suzuki, A., Stereoselective synthesis of arylated (E)-alkenes by the reaction of alk-1-enylboranes with aryl halides in the presence of palladium catalyst. *J. Chem. Soc. Chem. Commun.* **1979,** (19), 866-867.

115. Ansari, T. N.; Sharma, S.; Hazra, S.; Jasinski, J. B.; Wilson, A. J.; Hicks, F.; Leahy, D. K.; Handa, S., Shielding Effect of Nanomicelles: Stable and Catalytically Active Oxidizable Pd(0) Nanoparticle Catalyst Compatible for Cross-Couplings of Water-Sensitive Acid Chlorides in Water. *JACS Au* **2021,** *1* (9), 1506-1513.

116. Ansari, T. N.; Jasinski, J. B.; Leahy, D. K.; Handa, S., Metal–Micelle Cooperativity: Phosphine Ligand-Free Ultrasmall Palladium(II) Nanoparticles for Oxidative Mizoroki–Heck-type Couplings in Water at Room Temperature. *JACS Au* **2021,** *1* (3), 308-315.

117. Sharma, S.; Parmar, S.; Ibrahim, F.; Clark, A. H.; Nachtegaal, M.; Jasinski, J. B.; Gallou, F.; Kozlowski, P. M.; Handa, S., Sustainable and Bench-Stable Photoactive Aqueous Nanoaggregates of Cu(II) for ppm Level Cu(I) Catalysis in Water. *Adv. Funct. Mater.* **2022,** *32* (36), 2204459.

118. Cahiez, G.; Gager, O.; Buendia, J., Copper-Catalyzed Cross-Coupling of Alkyl and Aryl Grignard Reagents with Alkynyl Halides. *Angew. Chem., Int. Ed.* **2010,** *49* (7), 1278-1281.

119. Wang, X.; Song, Y.; Qu, J.; Luo, Y., Mechanistic Insights into the Copper-Cocatalyzed Sonogashira Cross-Coupling Reaction: Key Role of an Anion. *Organometallics* **2017,** *36* (5), 1042-1048.

120. Lefèvre, G.; Franc, G.; Tlili, A.; Adamo, C.; Taillefer, M.; Ciofini, I.; Jutand, A., Contribution to the Mechanism of Copper-Catalyzed C–N and C–O Bond Formation. *Organometallics* **2012,** *31* (22), 7694-7707.

121. Soria-Castro, S. M.; Andrada, D. M.; Caminos, D. A.; Argüello, J. E.; Robert, M.; Peñéñory, A. B., Mechanistic Insight into the Cu-Catalyzed C–S Cross-Coupling of Thioacetate with Aryl Halides: A Joint Experimental–Computational Study. *J. Org. Chem.* **2017,** *82* (21), 11464-11473.

122. He, C.; Zhang, G.; Ke, J.; Zhang, H.; Miller, J. T.; Kropf, A. J.; Lei, A., Labile Cu(I) Catalyst/Spectator Cu(II) Species in Copper-Catalyzed C–C Coupling Reaction: Operando IR, in Situ XANES/EXAFS Evidence and Kinetic Investigations. *J. Am. Chem. Soc.* **2013,** *135* (1), 488-493.

123. Zhang, S.; Ding, Y., Theoretical Study on Mechanism of Copper(I)-Catalyzed Cross-Coupling between Aryl Halides and Alkylamines. *Organometallics* **2011,** *30* (3), 633-641.

124. Wang, T.; Wang, M.; Fang, S.; Liu, J.-y., DFT Studies on Cu-Catalyzed Cross-Coupling of Diazo Compounds with Trimethylsilylethyne and tert-Butylethyne: Formation of Alkynes for Trimethylsilylethyne while Allenes for tert-Butylethyne. *Organometallics* **2014,** *33* (15), 3941-3949.

125. Li, J.-H.; Li, J.-L.; Wang, D.-P.; Pi, S.-F.; Xie, Y.-X.; Zhang, M.-B.; Hu, X.-C., CuI-Catalyzed Suzuki−Miyaura and Sonogashira Cross-Coupling Reactions Using DABCO as Ligand. *J. Org. Chem.* **2007,** *72* (6), 2053-2057.

126. Gurung, S. K.; Thapa, S.; Kafle, A.; Dickie, D. A.; Giri, R., Copper-Catalyzed Suzuki–Miyaura Coupling of Arylboronate Esters: Transmetalation with (PN)CuF and Identification of Intermediates. *Org. Lett.* **2014,** *16* (4), 1264-1267.

127. Mao, J.; Guo, J.; Fang, F.; Ji, S.-J., Highly efficient copper(0)-catalyzed Suzuki–Miyaura cross-coupling reactions in reusable PEG-400. *Tetrahedron* **2008,** *64* (18), 3905-3911.

128. Jiao, J.; Zhang, X.-R.; Chang, N.-H.; Wang, J.; Wei, J.-F.; Shi, X.-Y.; Chen, Z.-G., A Facile and Practical Copper Powder-Catalyzed, Organic Solvent- and Ligand-Free Ullmann Amination of Aryl Halides. *J. Org. Chem.* **2011,** *76* (4), 1180-1183.

129. Oliver-Messeguer, J.; Liu, L.; García-García, S.; Canós-Giménez, C.; Domínguez, I.; Gavara, R.; Doménech-Carbó, A.; Concepción, P.; Leyva-Pérez, A.; Corma, A., Stabilized Naked Sub-nanometric Cu Clusters within a Polymeric Film Catalyze C–N, C–C, C–O, C–S, and C–P Bond-Forming Reactions. *J. Am. Chem. Soc.* **2015,** *137* (11), 3894-3900.

130. Woo, H.; Mohan, B.; Heo, E.; Park, J. C.; Song, H.; Park, K. H., CuO hollow nanosphere-catalyzed cross-coupling of aryl iodides with thiols. *Nanoscale Res. Lett.* **2013,** *8* (1), 1-7.

131. Jammi, S.; Sakthivel, S.; Rout, L.; Mukherjee, T.; Mandal, S.; Mitra, R.; Saha, P.; Punniyamurthy, T., CuO Nanoparticles Catalyzed C−N, C−O, and C−S Cross-Coupling Reactions: Scope and Mechanism. *J. Org. Chem.* **2009,** *74* (5), 1971-1976.

132. Ranu, B. C.; Dey, R.; Chatterjee, T.; Ahammed, S., Copper Nanoparticle-Catalyzed Carbon-Carbon and Carbon-Heteroatom Bond Formation with a Greener Perspective. *ChemSusChem* **2012,** *5* (1), 22-44.

133. Thathagar, M. B.; Beckers, J.; Rothenberg, G., Copper-Catalyzed Suzuki Cross-Coupling Using Mixed Nanocluster Catalysts. *J. Am. Chem. Soc.* **2002,** *124* (40), 11858-11859.

134. Babu, S. A.; Saranya, S.; Rohit, K. R.; Anilkumar, G., Ligand-Free Cu-Catalyzed Suzuki Coupling of Alkynyl Bromides with Boronic Acids in Ethanol Under Microwave Irradiation. *ChemistrySelect* **2019,** *4* (3), 1019-1022.

135. Kidwai, M.; Mishra, N. K.; Bhardwaj, S.; Jahan, A.; Kumar, A.; Mozumdar, S., Cu Nanoparticles in PEG: A New Recyclable Catalytic System for N-Arylation of Amines with Aryl Halides. *ChemCatChem* **2010,** *2* (10), 1312-1317.

136. Karna, P.; Okeke, M.; Meira, D. M.; Finfrock, Z.; Yang, D.-S., Water-Soluble Palladium Nanoclusters as Catalysts in Ligand-Free Suzuki–Miyaura Cross-Coupling Reactions. *ACS Appl. Nano Mater.* **2022,** *5* (3), 3188-3193.

137. Fehér, P. P.; Stirling, A., Assessment of reactivities with explicit and implicit solvent models: QM/MM and gas-phase evaluation of three different Ag-catalysed furan ring formation routes. *New J. Chem.* **2019,** *43* (39), 15706-15713.

138. Tomasi, J.; Persico, M., Molecular Interactions in Solution: An Overview of Methods Based on Continuous Distributions of the Solvent. *Chem. Rev.* **1994,** *94* (7), 2027-2094.

139. Korzhavyi, P. A.; Soroka, I. L.; Isaev, E. I.; Lilja, C.; Johansson, B., Exploring monovalent copper compounds with oxygen and hydrogen. *Proc. Natl. Acad. Sci.* **2012,** *109* (3), 686-689.

140. Devamani, H.; Alagar, M., Synthesis and Characterisation of Copper II Hydroxide Nano Particles. *Nano Biomed. Eng.* **2013,** *5* (3), 116-120.

141. Köhler, K.; Heidenreich, R. G.; Soomro, S. S.; Pröckl, S. S., Supported Palladium Catalysts for Suzuki Reactions: Structure-Property Relationships, Optimized Reaction Protocol and Control of Palladium Leaching. *Adv. Synth. Catal.* **2008,** *350* (18), 2930-2936.

142. Illas, F.; Rubio, J.; Centellas, F.; Virgili, J., Molecular structure of copper(I) hydroxide and copper hydroxide(1-) ($Cu(OH)_2^-$). An ab initio study. *J. Phys. Chem.* **1984,** *88* (22), 5225-5228.

143. Martin, L.; Martinez, H.; Poinot, D.; Pecquenard, B.; Le Cras, F., Comprehensive X-ray Photoelectron Spectroscopy Study of the Conversion Reaction Mechanism of CuO in Lithiated Thin Film Electrodes. *J. Phys. Chem. C* **2013,** *117* (9), 4421-4430.

144. Tariq, M.; Koch, M. D.; Andrews, J. W.; Knowles, K. E., Correlation between Surface Chemistry and Optical Properties in Colloidal Cu_2O Nanoparticles. *J. Phys. Chem. C* **2020,** *124* (8), 4810-4819.

145. Diaz Leon, J. J.; Fryauf, D. M.; Cormia, R. D.; Zhang, M.-X. M.; Samuels, K.; Williams, R. S.; Kobayashi, N. P., Reflectometry–Ellipsometry Reveals Thickness, Growth Rate, and Phase Composition in Oxidation of Copper. *ACS Appl. Mater. Interfaces* **2016,** *8* (34), 22337-22344.

146. Wang, J.; Lu, D.; Li, C.; Zhu, Y.; Boscoboinik, J. A.; Zhou, G., Measuring Charge Transfer between Adsorbate and Metal Surfaces. *J. Phys. Chem. Lett.* **2020,** *11* (16), 6827-6834.

147. Wang, S.; Kou, T.; Varley, J. B.; Akhade, S. A.; Weitzner, S. E.; Baker, S. E.; Duoss, E. B.; Li, Y., Cu_2O/CuS Nanocomposites Show Excellent Selectivity and Stability for Formate Generation via Electrochemical Reduction of Carbon Dioxide. *ACS Mater. Lett.* **2021,** *3* (1), 100-109.

148. Platzman, I.; Brener, R.; Haick, H.; Tannenbaum, R., Oxidation of Polycrystalline Copper Thin Films at Ambient Conditions. *J. Phys. Chem. C* **2008,** *112* (4), 1101-1108.

149. Dubot, P.; Jousset, D.; Pinet, V.; Pellerin, F.; Langeron, J. P., Simulation of the LMM auger spectra of copper. *Surf. Interface Anal.* **1988,** *12* (2), 99-104.

150. Antonides, E.; Janse, E. C.; Sawatzky, G. A., LMM Auger spectra of Cu, Zn, Ga, and Ge, II. Relationship with the L_{23} photoelectron spectra via the $L_2L_3M_{45}$ Coster-Kronig process. *Phys. Rev. B* **1977,** *15* (10), 4596-4601.

151. Haak, H. W.; Sawatzky, G. A.; Thomas, T. D., Auger-Photoelectron Coincidence Measurements in Copper. *Phys. Rev. Lett.* **1978,** *41* (26), 1825-1827.

152. Zhang, G.; Luan, Y.; Han, X.; Wang, Y.; Wen, X.; Ding, C.; Gao, J., A palladium complex with functionalized β-cyclodextrin: a promising catalyst featuring recognition abilities for Suzuki–Miyaura coupling reactions in water. *Green Chem.* **2013,** *15* (8), 2081-2085.
153. Han, W.; Liu, C.; Jin, Z., Aerobic Ligand-Free Suzuki Coupling Reaction of Aryl Chlorides Catalyzed by In Situ Generated Palladium Nanoparticles at Room Temperature. *Adv. Synth. & Catal.* **2008,** *350* (3), 501-508.
154. Kogan, V.; Aizenshtat, Z.; Popovitz-Biro, R.; Neumann, R., Carbon−Carbon and Carbon−Nitrogen Coupling Reactions Catalyzed by Palladium Nanoparticles Derived from a Palladium Substituted Keggin-Type Polyoxometalate. *Org. Lett.* **2002,** *4* (20), 3529-3532.
155. Zim, D.; Lando, V. R.; Dupont, J.; Monteiro, A. L., NiCl2(PCy3)2: A Simple and Efficient Catalyst Precursor for the Suzuki Cross-Coupling of Aryl Tosylates and Arylboronic Acids. *Org. Lett.* **2001,** *3* (19), 3049-3051.
156. Handa, S.; Slack, E. D.; Lipshutz, B. H., Nanonickel-Catalyzed Suzuki–Miyaura Cross-Couplings in Water. *Angew Chem. Int. Ed.* **2015,** *54* (41), 11994-11998.
157. Payard, P.-A.; Perego, L. A.; Ciofini, I.; Grimaud, L., Taming Nickel-Catalyzed Suzuki-Miyaura Coupling: A Mechanistic Focus on Boron-to-Nickel Transmetalation. *ACS Catal.* **2018,** *8* (6), 4812-4823.
158. Singh, S.; Sunoj, R. B., Mechanism and Origin of Enantioselectivity in Nickel-Catalyzed Alkyl–Alkyl Suzuki Coupling Reaction. *J. Phys. Chem. A* **2019,** *123* (31), 6701-6710.
159. Li, Y.; Wang, K.; Ping, Y.; Wang, Y.; Kong, W., Nickel-Catalyzed Domino Heck Cyclization/Suzuki Coupling for the Synthesis of 3,3-Disubstituted Oxindoles. *Org. Lett.* **2018,** *20* (4), 921-924.
160. Inamoto, K.; Kuroda, J.-i.; Hiroya, K.; Noda, Y.; Watanabe, M.; Sakamoto, T., Synthesis and Catalytic Activity of a Pincer-Type Bis(imidazolin-2-ylidene) Nickel(II) Complex. *Organometallics* **2006,** *25* (12), 3095-3098.
161. Hanley, P. S.; Ober, M. S.; Krasovskiy, A. L.; Whiteker, G. T.; Kruper, W. J., Nickel- and Palladium-Catalyzed Coupling of Aryl Fluorosulfonates with Aryl Boronic Acids Enabled by Sulfuryl Fluoride. *ACS Catal.* **2015,** *5* (9), 5041-5046.
162. Mohadjer Beromi, M.; Nova, A.; Balcells, D.; Brasacchio, A. M.; Brudvig, G. W.; Guard, L. M.; Hazari, N.; Vinyard, D. J., Mechanistic Study of an Improved Ni Precatalyst for Suzuki–Miyaura Reactions of Aryl Sulfamates: Understanding the Role of Ni(I) Species. *J. Am. Chem. Soc.* **2017,** *139* (2), 922-936.
163. Muto, K.; Yamaguchi, J.; Musaev, D. G.; Itami, K., Decarbonylative organoboron cross-coupling of esters by nickel catalysis. *Nat. Commun.* **2015,** *6* (1), 7508.
164. Dong, Y.; Jv, J.-J.; Li, Y.; Li, W.-H.; Chen, Y.-Q.; Sun, Q.; Ma, J.-P.; Dong, Y.-B., Nickel-metalated porous organic polymer for Suzuki–Miyaura cross-coupling reaction. *RSC Adv.,* **2019,** *9* (35), 20266-20272.
165. Zhang, K.; Conda-Sheridan, M.; R. Cooke, S.; Louie, J., N-Heterocyclic Carbene Bound Nickel(I) Complexes and Their Roles in Catalysis. *Organometallics* **2011,** *30* (9), 2546-2552.
166. Talukder, M. M.; Cue, J. M. O.; Miller, J. T.; Gamage, P. L.; Aslam, A.; McCandless, G. T.; Biewer, M. C.; Stefan, M. C., Ligand Steric Effects of α-Diimine

Nickel(II) and Palladium(II) Complexes in the Suzuki–Miyaura Cross-Coupling Reaction. *ACS Omega* **2020,** *5* (37), 24018-24032.

167. Elumalai, P.; Mamlouk, H.; Yiming, W.; Feng, L.; Yuan, S.; Zhou, H.-C.; Madrahimov, S. T., Recyclable and Reusable Heteroleptic Nickel Catalyst Immobilized on Metal–Organic Framework for Suzuki–Miyaura Coupling. *ACS Appl. Mater. Interfaces* **2018,** *10* (48), 41431-41438.

168. Tailor, S. B.; Manzotti, M.; Asghar, S.; Rowsell, B. J. S.; Luckham, S. L. J.; Sparkes, H. A.; Bedford, R. B., Revisiting Claims of the Iron-, Cobalt-, Nickel-, and Copper-Catalyzed Suzuki Biaryl Cross-Coupling of Aryl Halides with Aryl Boronic Acids. *Organometallics* **2019,** *38* (8), 1770-1777.

169. Domin, D.; Benito-Garagorri, D.; Mereiter, K.; Fröhlich, J.; Kirchner, K., Synthesis and Reactivity of Palladium and Nickel β-Diimine Complexes: Application as Catalysts for Heck, Suzuki, and Hiyama Coupling Reactions. *Organometallics* **2005,** *24* (16), 3957-3965.

170. Chen, L.; Yang, J.-C.; Xu, P.; Zhang, J.-J.; Duan, X.-H.; Guo, L. N., Nickel-catalyzed Suzuki Coupling of Cycloalkyl Silyl Peroxides with Boronic Acids. *J. Org. Chem.* **2020,** *85* (11), 7515-7525.

171. Lin, X.; Phillips, D. L., Density Functional Theory Studies of Negishi Alkyl–Alkyl Cross-Coupling Reactions Catalyzed by a Methylterpyridyl-Ni(I) Complex. *J. Org. Chem.* **2008,** *73* (10), 3680-3688.

172. Clevenger, A. L.; Stolley, R. M.; Aderibigbe, J.; Louie, J., Trends in the Usage of Bidentate Phosphines as Ligands in Nickel Catalysis. *Chem. Rev.* **2020,** *120* (13), 6124-6196.

173. Guard, L. M.; Mohadjer Beromi, M.; Brudvig, G. W.; Hazari, N.; Vinyard, D. J., Comparison of dppf-Supported Nickel Precatalysts for the Suzuki–Miyaura Reaction: The Observation and Activity of Nickel(I). *Angew. Chem. Int. Ed. 2* **2015,** *54* (45), 13352-13356.

174. Xi, Z.; Zhang, X.; Chen, W.; Fu, S.; Wang, D., Synthesis and Structural Characterization of Nickel(II) Complexes Supported by Pyridine-Functionalized N-Heterocyclic Carbene Ligands and Their Catalytic Acitivities for Suzuki Coupling. *Organometallics* **2007,** *26* (26), 6636-6642.

175. Tang, Z.-Y.; Hu, Q.-S., Triphenylphosphine as a Ligand for Room-Temperature Ni(0)-Catalyzed Cross-Coupling Reactions of Aryl Chlorides with Arylboronic Acids. *J. Org. Chem.* **2006,** *71* (5), 2167-2169.

176. Key, R. J.; Tengco, J. M. M.; Smith, M. D.; Vannucci, A. K., A Molecular/Heterogeneous Nickel Catalyst for Suzuki–Miyaura Coupling. *Organometallics* **2019,** *38* (9), 2007-2014.

177. Zim, D.; Monteiro, A. L., Suzuki cross-coupling of aryl halides with aryl boronic acids catalyzed by phosphine-free $NiCl_2 \cdot 6H_2O$. *Tetrahedron Lett.* **2002,** *43* (22), 4009-4011.

178. Islam, K.; Arora, V.; Vikas; Nag, B.; Kumar, A., Nickel Bromide Catalyzed Ligand-Free and Activator-less Suzuki Coupling Reactions. *ChemCatChem* **2022,** *14* (16), e202200440.

179. Cho, C. S.; Tran, N. T., Nickel(0) powder catalysis in Suzuki–Miyaura cross-coupling reaction. *Catal. Commun.* **2009,** *11* (3), 191-195.

180. Murugan, K.; Nainamalai, D.; Kanagaraj, P.; Nagappan, S. G.; Palaniswamy, S., Green-Synthesized Nickel Nanoparticles on Reduced Graphene Oxide as an Active and Selective Catalyst for Suzuki and Glaser-Hay Coupling Reactions. *Appl. Organomet. Chem.* **2020,** *34* (9), e5778.
181. Karna, P.; Finfrock, Z.; Li, J.; Hu, Y.; Yang, D.-S., Water-Soluble Copper(I) Hydroxide Catalyst and Its Formation in Ligand-Free Suzuki–Miyaura Cross-Coupling Reactions. *J. Phys. Chem. C* **2023,** *127* (12), 5791-5799.
182. Luo, P. F.; Kuwana, T.; Paul, D. K.; Sherwood, P. M. A., Electrochemical and XPS Study of the Nickel−Titanium Electrode Surface. *Anal. Chem.* **1996,** *68* (19), 3330-3337.
183. Li, C. P.; Proctor, A.; Hercules, D. M., Curve Fitting Analysis of ESCA Ni 2p Spectra of Nickel-Oxygen Compounds and Ni/Al2O3 Catalysts. *Appl. Spectrosc.* **1984,** *38* (6), 880-886.
184. Lebugle, A.; Axelsson, U.; Nyholm, R.; Mårtensson, N., Experimental L and M Core Level Binding Energies for the Metals 22Ti to 30Zn. *Phys. Scr.* **1981,** *23* (5A), 825.
185. Venezia, A. M.; Bertoncello, R.; Deganello, G., X-ray photoelectron spectroscopy investigation of pumice-supported nickel catalysts. *Surf. Interface Anal.* **1995,** *23* (4), 239-247.
186. Powell, C. J., Recommended Auger parameters for 42 elemental solids. *J. Electron Spectrosc. Relat. Phenom.* **2012,** *185* (1), 1-3.
187. Miller, A. C.; Simmons, G. W., Nickel by XPS. *Surf. Sci. Spectra* **1992,** *1* (3), 312-317.
188. Schreifels, J. A.; Maybury, P. C.; Swartz, W. E., X-Ray photoelectron spectroscopy of nickel boride catalysts: Correlation of surface states with reaction products in the hydrogenation of acrylonitrile. *J. Catal.* **1980,** *65* (1), 195-206.
189. McIntyre, N. S.; Chan, T. C.; Chen, C., Characterization of oxide structures formed on nickel-chromium alloy during low pressure oxidation at 500–600°C. *Oxid. Met.* **1990,** *33* (5), 457-479.
190. Mansour, A. N., Characterization of β-Ni(OH)2 by XPS. *Surf. Sci. Spectra* **1994,** *3* (3), 239-246.
191. Christopher E. Dubé, B. W., Samuel P. Kounaves, Albert Robbat Jr., M. Levant Aksub and Geoffrey Davies, Electrodeposition of Metal Alloy and Mixed Oxide Films Using a Single-Precursor Tetranuclear Copper-Nickel Complex. *J. Electrochem. Soc.* **1995,** *142* (10), 3357-3365.
192. Grosvenor, A. P.; Biesinger, M. C.; Smart, R. S. C.; McIntyre, N. S., New interpretations of XPS spectra of nickel metal and oxides. *Surf. Sci.* **2006,** *600* (9), 1771-1779.
193. Carver, J. C.; Schweitzer, G. K.; Carlson, T. A., Use of X-Ray Photoelectron Spectroscopy to Study Bonding in Cr, Mn, Fe, and Co Compounds. *J. Chem. Phys.* **1972,** *57* (2), 973-982.
194. Biju, V., Ni 2p X-ray photoelectron spectroscopy study of nanostructured nickel oxide. *Mater. Res. Bull.* **2007,** *42* (5), 791-796.
195. Peck, M. A.; Langell, M. A., Comparison of Nanoscaled and Bulk NiO Structural and Environmental Characteristics by XRD, XAFS, and XPS. *Chem. Mater.* **2012,** *24* (23), 4483-4490.
196. Gupta, R. P.; Sen, S. K., Calculation of multiplet structure of core p -vacancy levels. II. *Phys. Rev. B* **1975,** *12* (1), 15-19.

197. Taguchi, M.; Matsunami, M.; Ishida, Y.; Eguchi, R.; Chainani, A.; Takata, Y.; Yabashi, M.; Tamasaku, K.; Nishino, Y.; Ishikawa, T.; Senba, Y.; Ohashi, H.; Shin, S., Revisiting the Valence-Band and Core-Level Photoemission Spectra of NiO. *Phys. Rev. Lett.* **2008,** *100* (20), 206401.

198. Bagus, P. S.; Pacchioni, G.; Parmigiani, F., Final state effects for the core-level XPS spectra of NiO. *Chem. Phys. Lett.* **1993,** *207* (4), 569-574.

199. Altieri, S.; Tjeng, L. H.; Tanaka, A.; Sawatzky, G. A., Core-level x-ray photoemission on NiO in the impurity limit. *Phys. Rev. B* **2000,** *61* (20), 13403-13409.

200. Li, L.; Wang, J.; Zhou, C.; Wang, R.; Hong, M., pH-Responsive chelating N-heterocyclic dicarbene palladium(ii) complexes: recoverable precatalysts for Suzuki–Miyaura reaction in pure water. *Green Chem.* **2011,** *13* (8), 2071-2077.

201. Lai, Y.; Zong, Z.; Tang, Y.; Mo, W.; Sun, N.; Hu, B.; Shen, Z.; Jin, L.; Sun, W.-h.; Hu, X., Highly bulky and stable geometry-constrained iminopyridines: Synthesis, structure and application in Pd-catalyzed Suzuki coupling of aryl chlorides. *Beilstein J. Org. Chem.* **2017,** *13*, 213-221.

202. Tang, Y.; Zeng, Y.; Hu, Q.; Huang, F.; Jin, L.; Mo, W.; Sun, N.; Hu, B.; Shen, Z.; Hu, X.; Sun, W.-H., Efficient Catalyst for Both Suzuki and Heck Cross-Coupling Reactions: Synthesis and Catalytic Behaviour of Geometry- Constrained Iminopyridylpalladium Chlorides. *Adv. Synth. Catal.* **2016,** *358* (16), 2642-2651.

203. Chua, Y.-Y.; Duong, H. A., Selective Kumada biaryl cross-coupling reaction enabled by an iron(III) alkoxide–N-heterocyclic carbene catalyst system. *Chem. Commun.* **2014,** *50* (61), 8424-8427.

VITA

Education:

Doctor of Philosophy, Chemistry | University of Kentucky | Lexington, KY
Research Advisor: Dr. Dong-Sheng Yang
August 2017 to Present

Bachelor of Science, Biology | Union College | Barbourville, KY
Minor: Chemistry, *magna cum laude*
Degree Awarded: May 2017

Awards:

- Nathan Vanderford Award for Excellence in Research on Graduate and Professional Students (2023) | University of Kentucky Graduate School
- Academic Success Pillar Awards (2023) | University of Kentucky Student Government Association
- ACS Journals Diversity & Inclusion Cover Art (2023) | American Chemical Society
- Graduate Student Congress Research Awards (2022, 2021) | University of Kentucky Graduate Student Association
- Gabriela Jiskrova Outstanding Service Award (2022) | University of Kentucky Graduate School
- Belonging and Engagement Pillar Awards (2022) | University of Kentucky Student Government Association
- Leadership Legacy Award (2022) | University of Kentucky Student Government Association
- Arts & Sciences Outstanding Teaching Assistant Award (2022) | University of Kentucky Graduate School
- Graduate Student Congress Conference Awards (2022, 2021) | University of Kentucky Graduate Student Association
- GradResearch Live! Top 3 Finalist (2021) | University of Kentucky Graduate School
- Graduate Student Congress Professional Development Awards (2021) | University of Kentucky Graduate Student Association
- GradTeach Live! Top 3 Finalist (2021) | University of Kentucky Graduate School
- Max Steckler Fellowship (2020) | University of Kentucky Graduate School

Publications:

1) **Karna, Priya**; DuBravac, P.; Zhang, Y.; Chen, Y.; Meira, D.M.; and Yang, D.S. "Water-Soluble Nickel (0) Catalyst and its Formation in Ligand-Free Suzuki-Miyaura Cross-Coupling Reactions." Manuscript in preparation.

2) **Karna, Priya**. **(2023)**. "Women in Science: From Country to Chemistry." *Journal of Physical Chemistry Letters*, 14, 8, 2222. DOI: 10.1021/acs.jpclett.3c00385

3) **Karna, Priya**; Finfrock, Z.; Li, Junjie; Hu, Yongfeng; and Yang, D.S. **(2023)**. "Water-Soluble Copper (I) Hydroxide Catalyst and its Formation in Ligand-Free Suzuki-Miyaura Cross-Coupling Reactions." *Journal of Physical Chemistry C,* 127, 12, 5791–5799. DOI: 10.1021/acs.jpcc.3c00268

4) **Karna, Priya**; Okeke, M.; Meira, D.M.; Finfrock, Z.; and Yang, D.S. **(2022)**. "Water-Soluble Palladium Clusters as a Catalyst in Ligand-Free Suzuki-Miyaura Cross-Coupling Reactions." *ACS Applied Nano Materials*, 5, 3, 3188–3193. DOI: 10.1021/acsanm.2c00389

5) Calabro, Rosemary; **Karna, P**.; Kim, D.Y.; and Yang, D.S. **(2020)**. "Controlled synthesis and characterization of $NaYF_4$:Yb/Er upconverting nanoparticles produced by laser ablation in liquid." *Journal of Chemical Physics*, 153, 6. DOI: 10.1063/5.0021011

Conference Proceedings:

1) **Karna, Priya**; Finfrock, Z.; Li, Junjie; Hu, Yongfeng; and Yang, D.S. Water-Soluble Copper (I) Hydroxide Catalysts in Ligand-Free Suzuki-Miyaura Cross-Coupling Reactions." Oral Presentation. *Materials Research Society Fall 2022.* Boston, MA. December 1, 2022. Abstract ID: 3778544.

2) **Karna, Priya**; Okeke, M.; and Yang, D.S. (2022). "Ligand-free Suzuki-Miyaura cross-coupling reactions catalyzed by water-soluble and stabilized Cu species." *American Chemical Society Spring 2022*. San Diego, CA. Abstract ID: 3649377. Oral Presentation.

3) **Karna, Priya**; Okeke, M.; Meira, D.M.; Finfrock, Z.; and Yang, D.S. (2021). "Understanding the mechanism of the Pd (II) to Pd (0) reduction in Suzuki-Miyaura cross-coupling reactions by investigating the active species and its characterization." *American Chemical Society National Meeting Spring 2021*. Virtual. DOI: 10.1021/scimeetings.1c00162. Poster Presentation.

4) Calabro, Rosemary; **Karna, P.**; Yang, D.S.; and Kim, Doo-Young. (2019). "Synthesis and photoluminescence properties of upconverting nanomaterials produced through laser ablation in liquid." *2019 MRS Fall Meeting and Exhibit*. Boston, MA. Oral Presentation.

5) Nyambo, Silver; Kim, J.H.; **Karna, P.**; Zhang, Y.; and Yang, D.S. (2019). "Mati spectroscopy of $Ln(OH)_2$ (Ln = La and Ce) formed by O-H bond activation of water." *74th International Symposium on Molecular Spectroscopy*. Urbana, IL. Poster Presentation.

Service to the University:

- Chemistry Graduate Student Association (ChemGSA) - Media Officer (2022 – 2023)
- Chemistry Graduate Student Association (ChemGSA) - Representative for the Diversity, Equity, and Inclusion Committee (2021 – 2022)
- ChemCamp Instructor for High School Students (2022)

- Department of Chemistry Graduate Recruitment Speaker (2021 – 2023)
- Nepalese Student Organization (NSO) - Event Manager/Social Coordinator (2021-2023)
- Graduate Microteaching Leader (2019)
- Graduate Connections Team Member (2019)
- Kentucky State Science Olympiad Judge (2019)